MOLYBDENUM PEROXO SPECIES IN VARIOUS STRUCTURAL ENVIRNOMENT FOR OXIDATION REACTIONS

A THESIS

SUBMITTED TO THE

UNIVERSITY OF PUNE

FOR THE DEGREE OF

DOCTOR OF PHILOSOPHY

IN
CHEMISTRY

BY
PRAKASH CHANDRA

RESEARCH GUIDE

Dr. SHUBHANGI B. UMBARKAR

CATALYSIS DIVISION

CSIR - NATIONAL CHEMICAL LABORATORY

PUNE - 411008, INDIA

JULY - 2014

Certificate of the Guide

Certified that the work incorporated in the thesis entitled *"Molybdenum Peroxo Species in Various Structural Environment for Oxidation Reactions"* submitted by *Prakash Chandra* for the Degree of **Doctor of Philosophy,** in **Chemistry** was carried out by the candidate under my supervision in the Catalysis Division, National Chemical Laboratory, Pune-411008, India. Materials obtained from other sources have been duly acknowledged in the thesis.

Date :   Dr. Shubhangi B. Umbarkar

                                                                            (Research Supervisor)

DECLARATION

I hereby declare that the thesis entitled **"*Molybdenum Peroxo Species in Various Structural Environments for Oxidation Reactions*"** submitted for my ***Ph.D. degree*** to the University of Pune has been carried out at National Chemical Laboratory, under the guidance of **Dr. Shubhangi B. Umbarkar.** The work is original and has not been submitted in part or full by me for any degree or diploma to this or any other University.

Date: **Prakash Chandra**

                                                                                                             (Research Student)

Never cut a tree down in the winter time. Never make a negative decision in the low time. Never make your most important decisions when you are in your worst moods. Wait. Be patient. The storm will pass. The spring will come.

-*Robert H. Schuller*

Dedicated to my Parents, Teachers and Elder Sister

Acknowledgments

Table of Contents

ABBREVIATIONS

Cp	Cyclopentadienyl anion
EDAX	Energy Dispersive X-ray spectroscopy
FID	Flame Ionized Detector
FT-IR	Fourier-Transform Infrared
GC	Gas Chromatography
GC-MS	Gas Chromatography-Mass Spectrometry
NMR	Nuclear Magnetic Resonance
TBHP	*tert-* Butyl Hydrogen Peroxide
tmtacn	1,4,7-trimethyl-1,4,7-triazacyclononane
TON	Turn Over Number
TOF	Turn Over Frequency
UV-Vis	Ultra Violet-Visible
XRD	X-ray Diffraction
NMO	*N-* Methymorpholine *N*-oxide
THF	Tetrahydrofuran
δ	Chemical Shift
ν	Wave Number
TEM	Transmission Electron Microscopy
SEM	Scanning Electron Microscopy
SDS	sodiumdodecylsulphate
CTAB	Cetyltrimethylammonium bromide
TEOS	Tetra Ethyl Ortho Silicate
TZVP	Triple Zeta Valence with Polarization
DFT	Density functional theory
BP86	Becke-Perdew -86

PBE	Perdew, Burke, and Ernzerhof
B3LYP	Becke, three-parameters, Lee-Yang-Parr
ΔG	Gibbs-free energy
ΔH	Change in enthalpy
COSMO	COnductor like Screening MOdel
marij	Multipole Accelerated RI-J

1

Introduction: Catalytic Applications of Molybdenum Peroxo in Various Structural Environments for Oxidation Reactions

This chapter deals with literature review on the use of various molybdenum based homogeneous and heterogeneous catalysts, their advantages and disadvantages. Detailed literature review for synthesis and characterization using various physicochemical techniques done previously by various groups of researchers on supported molybdena catalyst as well as catalytic activity in olefin oxidation reactions. This chapter also deals with experimental as well as theoretical studies done in the past by various group of workers for investigating the mechanism for olefin epoxidation and cis-dihydroxylation. Significance of such studies will helps us to understand the role of ligand environment and oxidant in altering the mechanism of a catalytic reaction. Theoretical methodology used in elucidating the comparative study of olefin epoxidation as well as cis-dihydroxylation will be discussed in this chapter.

1.1. History of Catalysis

Catalysis has been applied by mankind since thousands of years in process such as fermentation. An interesting example for catalytic process is sulphuric acid synthesis by burning sulphur in presence of HNO_3 in glass vessel under hot and humid air. In 1746 lead was used in reaction chamber for large scale production. At the end of 18th and beginning of 19th century influence of metal oxides such as iron, copper etc. on the decomposition of several substances like ethanol to carbon. Ethanol decomposition on pumice stone (mixed metal oxide) on the other hand led to formation of ethane and water, in other words selectivity was demonstrated for the first time. Thènard first observed dissociation of NH_3 and H_2O_2 over hot metal surface. Humphry Davy discovered that on heating platinum and palladium were effective in catalyzing oxidation of coal, whereas copper, silver and gold were ineffective in catalyzing such reaction. Later studies found that finally ground Pt or Pd were effective in coal oxidation at room temperature. [1-3]

In 1834 Faraday proposed that reactants have to absorb on catalyst surface, but he did not explain any catalytic action. It was Berzelius who for the first time coined the term catalysis in 1836 and, concluded that besides 'affinity' there is a new force operating, i.e. 'Catalytic Force'. The term catalysis originated from Greek, having the sense of 'down' or 'loosen'. He too did not give any explanation, but gave simplified description of many of results which were not easy to explain previously. Later, Ostwald gave proper definition that catalyst does not influence the thermodynamic equilibrium of reactant and products but affects the rate of chemical reaction.

1.2. Some Basic Concepts of Catalysis

Catalysis is a chemical reaction brought by catalyst. A catalyst as discussed in previous section alters the rate of chemical reaction without altering the thermodynamic equilibrium. It is like a chemical version of 'matchmaker', because it physically brings down two chemicals in such a way that their chance of reacting is maximized. The catalyst itself is not consumed during the chemical process. It provides a pathway of lower free energy of activation (reaction kinetics).[4-5] As shown in Fig. 1.1 (a), (b) and (c) uncatalyzed reaction has higher energy barrier as compared to catalyzed reaction, indicating role played by the catalyst in lowering the energy barrier by altering the pathway of the reaction. New pathway can be single

step process or multistep process, but barrier to climb is always lower than uncatalyzed reaction. [6-8]
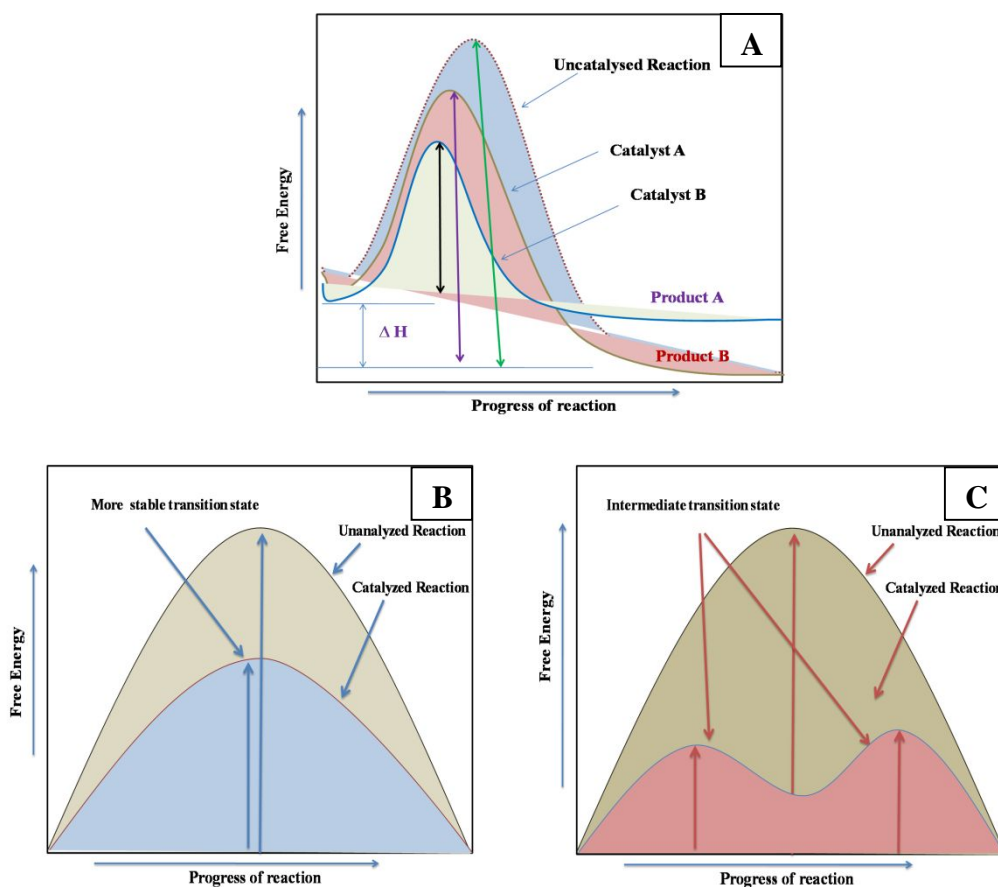
Fig. 1.1: (A) The free energy diagram for catalytic reaction giving same product as uncatalysed reaction and different product using catalyst B; (B) The free energy versus progress of reaction curve for catalyzed and uncatalyzed reaction; (C) represents one step two step catalytic process with low energy barrier.

Catalysis is ubiquitous to life as well as society. Catalytic processes are omnipresent, i.e. in production of food, clothes, energy via which we thrive and enzymatic biotransformation occurring via biological processes within our body. Catalysts are used in 60% of chemicals synthesized and 90% of chemical processes occurring in industry. This accounts for 20% of gross GDP of USA per annum. Catalyst manufacture alone accounts $10 billion in sale worldwide and spread out in four major sectors: refinery, chemicals, polymerization and exhaust emission catalyst. The overall impact of catalysts is $10 trillion per year. The intermediates synthesized by catalyst find applications in production of materials, chemicals and control devices

for various industries including chemical, petroleum, pharmaceuticals, automotives, electronic materials, food and energy. [9]

1.3. Types of Catalysis

Catalysis has applications in many fields, which includes energy, industry, environment and life sciences. Whether it is homogeneous or heterogeneous (or even enzymatic), catalysis primarily is a molecular phenomenon since it involves the chemical transformation of molecules into other molecules. This distinction is related to the fact that when catalyst operates in same phase where the reaction occurs is called homogeneous catalysis, whereas when it operations under distinct phases is called heterogeneous catalysis. At the beginning of 21st century even though many attempts have been made to bring close these two important fields of chemistry, they still belong to different scientific communities: homogeneous catalysis is more closely related to molecular organometallic chemistry, and heterogeneous catalysis is closer to surface science and solid-state chemistry. [10-11]

Inspite of many modern analytical techniques the level of understanding of the heterogeneous catalysis still limited, especially when compared to molecular organometallic chemistry and homogeneous catalysis. A concept was introduced in 1926 by H. S. Taylor in heterogeneous catalysis with small number of active sites to solve the problem in difficulty in obtaining structure-activity relationship. To the date none of the physicochemical characterization techniques either give clear insight about the structure of active sight and role played by it or any description of mechanistic aspects of reactions occurring at active site. Mechanistic aspects here mean bond breaking and bond making at so called active site. Homogeneous catalysis offers advantage over heterogeneous counterparts as discussed in the table 1.1 that all active sites are accessible because catalyst is dissolved metal complex and it is possible to tune more chemo-selectivity, regio-selectivity and/or stereo-selectivity of the catalyst. [12-13]

Inspite of so many advantages many homogeneous catalysts have not been commercialized because separation of catalyst from reactants, products and solvent is difficult. This problem arises because the most commonly used separation method, distillation, requires elevated temperatures unless the product is very volatile. Homogeneous catalysts suffer from the drawback that they are thermally sensitive and mostly decompose above 423 K. Product distillation elevates thermal stress even at

reduced pressure resulting into decomposition of expensive catalyst. Other conventional processes such as chromatography or extraction also lead to catalyst loss. The homogeneous reactions that have been commercialized either involve volatile substrates and products or do not contain thermally sensitive organic ligands. [14-17]

Table 1.1: The major features of homogeneous and heterogeneous catalysis are given in the table.

Homogeneous	Heterogeneous
• High and controllable chemo-, regio-, and stereo-selectivity.	• Low and uncontrollable chemo-, regio-, and stereo-selectivity
• Separation methods are quite complicated and products are difficult to separate from reaction mixture.	• Separation methods are quite simple such as decantation, filtration, centrifugation, etc.
• Very high catalytic activity in terms of TON and TOF	• Catalyst can be recycled several times.
• All active sites are accessible and no mass transfer limitations and pressure drop.	▪ Only surface atoms are active, bulk phase is not accessible. To overcome this drawback, materials with high surface are and surface to volume ratio are required.
• Organic ligand systems alter the catalytic activity and product selectivity.	• Supports such as Al_2O_3, SiO_2, zeolites, TiO_2 helps in modifying the catalytic activity and product selectivity. Resistant to drastic operational conditions.

1.4. Transition Metals in Catalysis

Transition metals are those which form one or more stable ions and have incompletely filled d-orbital. Transition metals act as efficient catalyst because they show multiple oxidation state with vacant d-orbital which can absorb reactant

molecules on to its surface and activate them in this process. [18-20] There are also reports of these transition metals used in the form of clusters and nanoparticles synthesized by transition metal salt reduction, thermal and photochemical decomposition, ligand reduction and displacement from organometallics and finally metal vapor deposition. Transition metal nanoparticles and clusters are nothing but combination of 10-1000 metal atoms stabilized by surfactants, ligands and polymers or dendrimers protecting their surface. [21-22] The success of transition metal catalysts lies in the relative ease of catalyst modification by changing the structural environment. Influenced the rate of the reaction and the selectivity to certain products is pivotal point of the catalyst modification. The following types of selectivity can be distinguished in a chemical reaction:

(a) *Chemo-selectivity.* In the same molecule when two functional groups are present, the preferential attack at one of the functional group is determined by chemo-electivity. A good example for chemo-selective reaction is oxidation of –OH group and double bond in an allylic alcohol depends very much on the transition metal involved during oxidation process.[23]

(b) *Regio-selectivity.* When the same functional group is present at two different position, for example –OH group present on primary or secondary, then the relative preference of –OH group getting oxidized first is determined by regeio-selectivity.

(c) *Stereo-selectivity.* The substrate contains a stereogenic centre and this together with the catalyst can direct the addition to form major product sterioselectively. For example H_2O_2 addition to cyclohexene results in two diastereomers *cis*-1, 2-cyclohexanediol or *trans*-1, 2-cyclohexanediol, the selectivity for either one is called the stereo-selectivity. [24]

Transition metals are employed for synthesis of bulk and fine chemicals either catalytically or stoichiometrically. Catalytic routes are preferred over stoichiometric ones whenever it is possible. Vast varieties of reactions catalyzed by transition metal are hydrogenation reaction, C-C coupling, asymmetric catalysis, isomerization, oxidation reaction.(See Fig. 1.3) Present research work mainly focuses on molybdenum in homogeneous and heterogeneous environments and its catalytic applications in oxidation reactions.
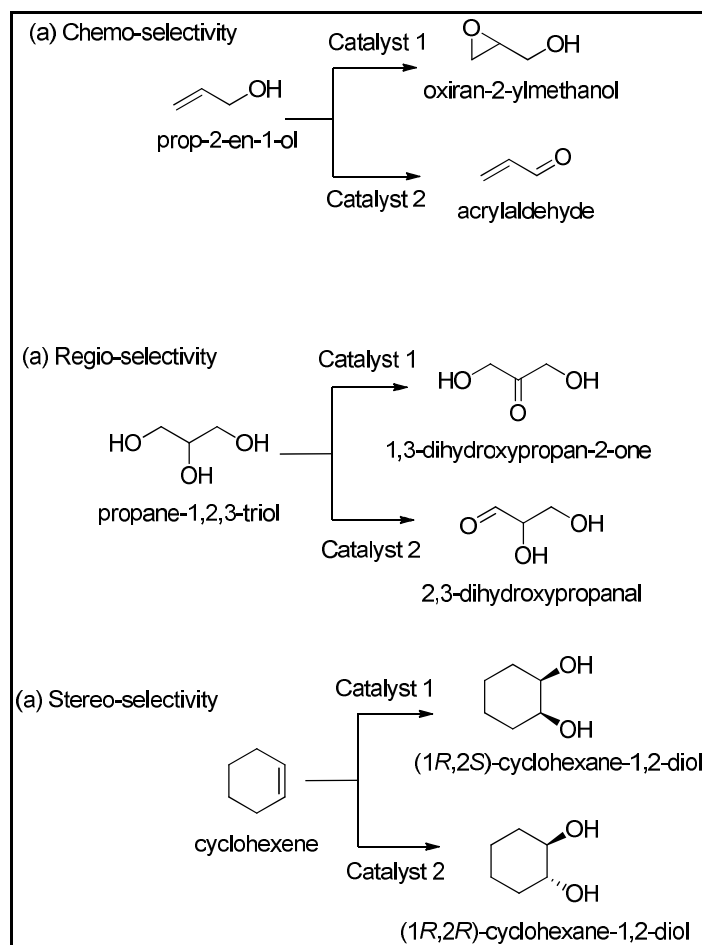
Fig. 1.2: Various examples of chemo-, regio- and stereo selective reactions

Catalytic oxidation reaction continues to be significant class of reactions and still makes a major contribution in modern chemical industry.[25] These reactions are significant as they convert petroleum based feed stock into useful chemicals such as alcohols, carbonyls and epoxides. [26] Million tons of these chemicals are synthesized and transported worldwide and find applications in chemical industries from fine chemical manufacturers such as pharmaceutical to large scale commodity chemical industry. The success of oxidation lies mainly on the choice of transition metal used for the oxidation reaction. Some very significant commercial processes for transition metal catalyzed oxidation reactions using molecular oxygen are oxidation of xylene to terephthalic acid in the presence of manganese and cobalt salts, [27] synthesis of ethylene oxide from ethylene using molecular oxygen as oxidant and silver oxide as catalyst, [28] Wacker's process for oxidation of alkenes to carbonyl process with the help of Pd salts. (See Scheme 1.1) [29]
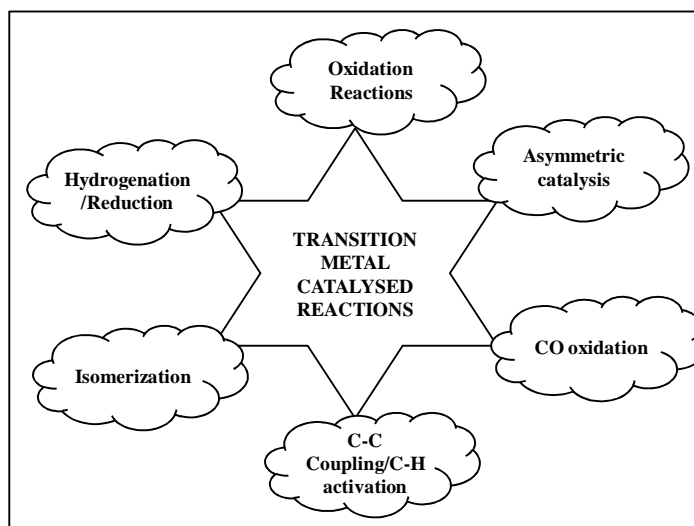
Fig. 1.3: Schematics for various transition metal catalyzed reaction. (Referred from Transition Metal for Fine: Synthesis Willey VHC: Matthias Beller and Carsten Bolm)
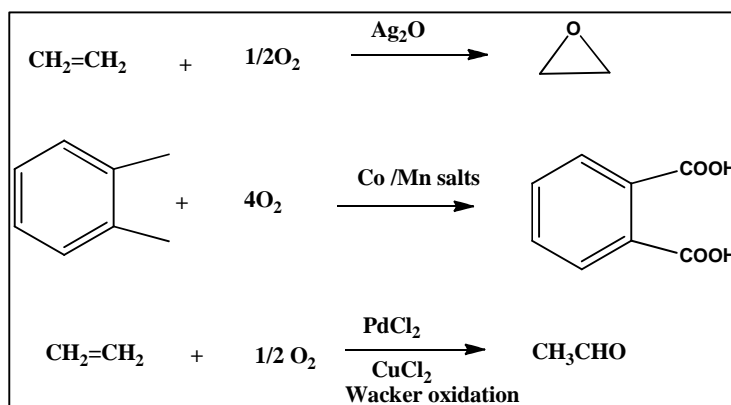
Scheme 1.1: Few examples of commercial process for oxidation of petrochemicals using transition metal based catalyst.

Oxidation reactions are the pivotal reactions in organic synthesis. Catalytic oxidation reactions are important reactions in context of Green chemistry because fine chemical industries have been performing oxidation reaction via employing stochiometric amount of inorganic oxidants such as chromium(VI) reagents, permanganate, and manganese dioxide, resulting in generation of copious amount of inorganic waste from chemical industry. Governments worldwide have imposed stringent laws to render such methods prohibitive and generate greener and environmentally safer methods of by using dioxygen, H_2O_2 as oxidizing agents. Catalytic oxidation reactions are categorized under three groups. [30]

(a) *Free Radical Autoxidation.* Free radical oxidation involves initiation, propagation, and termination steps. The reaction is started by an initiator which undergoes

homolytic thermolysis at the reaction temperature to produce chain initiating radicals. These chain initiators can be generated either at high temperature (> 100 $^{\circ}$C) or by addition of variable valence transition metals such as Co, Fe, Ce, etc., these radicals can be generated at low temperatures. A good example for this is work done by Ishii *et al.* [31-33] for oxidation of cyclohexylbenzene using N- hydroxyphthalimide (NHPI) as initiator in the presence of molecular oxygen and transition metal ions such as Co(II) or Mn(II). The transition metal ions not only act as an initiator for autoxidation reaction, but also catalyze the decomposition of intermediate hydroperoxide (See scheme 1.2.).
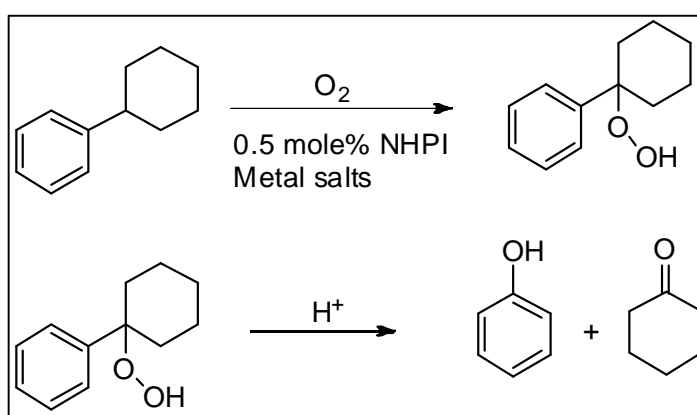
Scheme 1.2: Shows the schematic representation of oxidation of cyclohexylbenzene in the presence of oxygen, NHPI and transition metal ions

(b) *Direct Oxidation of Substrate by the (metal) Oxidant or Mars-van Krevelen Mechanism.* Many gas phase reactions involve direct incorporation of oxygen from metal oxide lattice to the substrate by metal oxo species present on the metal surface, followed by re-oxidation of the reduced form of the catalyst by metal catalyst. Fe=O of monoxygenase presents a excellent example for alkene oxidation, in which Fe^V is reduced to Fe^{IV}–OH species which further reacts with the entrapped radical generated during the first step, and does not diffuses out and further incorporates the molecular oxygen to give the desired product. The reduced catalyst is regenerated further by reacting with molecular oxygen present in the surrounding atmosphere. [34-35]

$$Fe^V=O + RH \longrightarrow Fe^{IV}\text{-}OH + R^{\cdot} \longrightarrow Fe^{III} + ROH \qquad (1)$$

$$Fe^{III} + \tfrac{1}{2} O_2 \longrightarrow Fe=O \qquad (2)$$
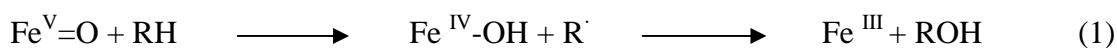
(c) *Oxygen Atom Transfer Reactions.* Catalytic oxygen transfer is widely employed for organic synthesis, example, olefin epoxidation, dihydroxylation, aminohydroxylation, alcohol oxidation, heteroatom addition, Baeyer-Villiger oxidations, etc. Almost all the transition metal elements and several main group elements are known to catalyze oxygen atom transfer reaction. Generalized mechanism for oxygen atom transfer is given in the table below. A variety of single atom donors are known to catalyze the oxygen atom transfer process, list of which is given in table 2. [36], [30]

$$\text{Cyclohexene} + H_2O_2 \xrightarrow{\text{Catalyst}} \text{cyclohexene oxide} + H_2O \qquad (3)$$

Out of various classes of oxidation reactions catalyzed by transition metals, olefin epoxidation and *cis*-dihydroxylation reactions are quiet significant and have been   discussed in the present chapter of the thesis. Taken for our studies here more details of literature been discussed here.

The Olefin Epoxidation. Olefin epoxidation is a major industrial reaction for the production of a wide variety of chemicals. [37-38] The oxirane group being highly reactive makes them important organic intermediates. Some epoxides play important role in the development of epoxy resins, paints, surfactants, drugs, agrochemicals, food additives and has important role in biological activity. [39-41]

Catalytic process includes the use of peroxides and peracids such as H_2O_2, TBHP, urea-H_2O_2 etc. (See table 1.2). Amongst the most significant catalytic processes HALCON-ARCO process, using peroxides of group 4-7 metals have been used for olefin epoxidation. [42-44] Titanium containing silicates, including amorphous titania–silica materials and Ti-substituted molecular sieves are the most efficient heterogeneous catalysts for epoxidation reactions. [45-47] The main drawback of this catalyst is small pore diameter which makes it accessible to small reactants. To overcome this difficulty mesoporous and macroporous materials have been developed such as titanium containing beta-zeolytic material.[48-49] Manganese and iron[50] complexes have been found to be effective in olefin epoxidation. Metal porphyrins and salen complexes lead to the formation of porphyrin based catalysts which have been used for the enantioselective epoxidation of alkenes. [51, 52] Kamanta *et al.*[53] have reported heteropoly acids as efficient epoxidation catalyst with epoxide selectivity > 99 % using H_2O_2 as oxidant.

Mimoun type complexes $Mo(O)_2L_1L_2$ (M= Mo, W; L_1, L_2 = hmf, dmpa etc.) are the most extensively investigated complexes in the literature for olefin epoxidation.[54-56]   Methyl-rhenium trioxide (MTO)/hydrogen peroxide oxidant system, has also been employed in the past for olefin epoxidation. However MTO is expensive as compared to MoO_3. The other major drawbacks are cleavage of Re-C bond during prolonged usage and inefficient recycling of the catalyst. Peroxo-molybdic acid synthesized by dissolving MoO_3 in H_2O_2, result in the formation of $MoO(O)_2(H_2O)_2$ species. In hydrophilic phase this species is found to be inactive for olefin epoxidation. The peroxomolybdic species shows poor catalytic activity for olefin in the presence of ligands such as pyridine, pyridine-N-oxide, pyrazole, $OPPh_3$, dmf, hmpa, etc. However in the presence of long chain trialkyl amine, trialky phosphine or trialky arsinite (C > 10) these catalyst become very active. These long chain hydrocarbons make the catalyst biphasic, hence organic phase remains in chloroform and peroxomlybdic phase remains in aqueous phase. Detailed kinetics and mechanism for such type of biphasic systems are studied systematically before. [57]

Table 1.2: Showing various types of oxidants employed for olefin oxidation

Oxidant	Active oxygen content (%)	Waste product
Oxygen (O_2)	100	Nil
Oxygen (O_2)/reductor	50	H_2O
O_3	33.3	O_2
H_2O_2	47.0	H_2O
HNO_3	25.4	NOx
NaOBr	13.4	NaBr
NaOCl	21.6	NaCl
CH_3CO_3H	21.1	CH_3CO_2H
t-BuOOH (TBHP)	17.8	*t*-BuOH
$KHSO_5$	10.5	$KHSO_4$
PhIO	7.3	PhI
$NaIO_4$	7.5	$NaIO_3$
$C_5H_{11}NO_2$	13.7	$C_5H_{11}NO$

The Olefin cis-Dihydroxylation. The other conspicuous product of olefin oxidation, i.e., *cis*-1, 2-diols is important organic reagent in organic synthesis.[58-61] The *cis*-1, 2-diols are a group of chiral synthons valuable in the synthesis of a diverse range of natural products and molecules of biological interest as well as in the development of general methodologies for organic molecules.[62] Sharpless method employing osmium tetra oxide (OsO_4) is well known for *vicinal* - dihydroxylation of olefins and provide structured route for olefin oxidation.[63-65] To increase the productivity of the process complexation of OsO_4 was done with organic ligands, which were hetergenised on soluble and insoluble polymers,[66-68] silica gel,[69-70] ion-exchange resins[71] or dendrimers.[72-73] The major drawback of this process is high cost, toxicity and contamination. Another disadvantage of this process was the addition of co-oxidants such as N-methyl morpholine N-oxide (NMO), $K_3Fe(CN)_6$.[74-75] Hydrogen peroxide has been used as terminal oxidant for recycle of Os(VI) to Os(VIII) along with NMO and biomimetic flavin.[76-77] Beller *et al.* have used molecular oxygen or air for osmium catalyzed dihydroxylation with good to excellent chemo-selectivity under optimized pH conditions.[78] For α-methyl styrene as model substrate, under slightly elevated oxygen pressure very high yields of diols are obtained even at very low catalyst concentrations.[78] In order to overcome the problem of toxicity, cost and also to have environmentally benign process for dihydroxylation of olefins, there is a need to search for an alternative metal catalyst system for the production of vicinal diols. There are few reports on Os/Re [79] catalytic systems for dihydroxylation, however addition of co-oxidant and/or addition of various carboxylic acids for maintaining acidic medium is essential for dihydroxylation. Feringa *et al.* [80] have used manganese complexes as catalysts for dihydroxylation using hydrogen peroxide as oxidant. However they have shown that the use of various carboxylic acids as co-catalysts is essential in this case, and epoxide was obtained as a major product along with *cis* - diol in many cases. There are several reports in the literature for *cis*- dihydroxylation of olefin using iron complexes of a macrocyclic tetraaza ligand[81] and bio-inspired N,N,O- ligand.[82] Feringa *et al.*[80] have reported olefin epoxidation as well as *cis*- dihydroxylation using $Mn_2O(RCO)_2(tmtacn)_2$ catalyst and H_2O_2 as an oxidant. They have also extended this to asymmetric epoxidation using chiral N containing ligands with excellent yields and *ee* up to 97%.

1.5. Catalytic Activity Study and Applications of Molybdenum: Heterogeneous Catalysis

Seeing efficient olefin epoxidation properties of MoO_3, various researchers have tried to heterogenise MoO_3 and its complexes on various supports such as MCM-41, SBA-15, ZrO_2, TiO_2 and Al_2O_3 etc. [83]

Apart from oxidation MoO_3 being supported on SiO_2 used as catalyst for esterification, [84] Beckmann rearrangement, [85] olefin metathesis [86] etc. Simplest method for synthesis procedure used for MoO_3/SiO_2 is impregnation of ammonium heptamolybdate (AHM) over silica surface. But the major drawback of the process was limited dispersion of molybdena species over silica surface. Thermal treatment is another useful method for dispersing molybdena over silica under anhydrous condition. Gao *et al.* [87] synthesized MoO_3/SiO_2 by mechanically dispersing via hand grinding MoO_3 over pre-calcined silica MCM-41 followed by thermal treatment. The advantage of thermal treatment over wet impregnation method is that it is performed under anhydrous condition without employing water or any solvent. Balkar *et al.* [88] used "thermal spreading method" for $MoO_3/MCM-41$ for olefin metathesis.

Another useful approach employed was sol-gel synthesis of silica supported molybdenum oxide catalyst using tetraethyl orthosilicate (TEOS), n-octylamine as template molecules on hexagonal mesoporous silica for efficient olefin metathesis. One-step template free sol-gel synthesis of mesoporous MoO_3/SiO_2 was employed by Dongare *et al.* by using ethyl silicate (ES-40) for various acid catalyzed reactions such as glycerol acetalization,[89] aromatic nitration[90] esetrification of ethanol with acetic acid,[91] transesterification of diethyl oxalate with phenol to form di-phenyl oxalate.[92] Alternatively using precursors such as $MoCl_5$, $Mo_2(OAc)_4$, $Mo(\eta^3-C_3H_5)_4$ $MoO_2(acac)_2$ resulted in better interaction of MoO_3 with surface Si-OH species. To overcome this drawback MoO_3/SiO_2 was synthesized by using $MoO_2(acac)_2$, resulting into the formation of uniformly dispersed molybdena particles even at higher concentration. This method is also called molecular design dispersion (MDD) because the interaction between the complex organic ligand and the surface hydroxyl group causes uniform dispersion of molybdena particles. Gedanken *et al.* [93-94] used sonochemical synthesis of MoO_3/SiO_2 by deposition of $Mo(CO)_6$ on Stöber silica particles. Another significant approach used to enhance the interaction between MoO_3 and SiO_2 was utilizing less acidic Mo^{3+} species. [95]

Present thesis work mainly focuses on utilization of novel nanotechnology methods for synthesis of MoO_3/SiO_2 and their catalytic application in olefin epoxidation reaction and theoretical calculations for mode of action of molybdenum acetylide complex, $CpMo(CO)_3(C \equiv CPh)$; $Cp = \eta^5\text{-}C_5H_5$ in cyclohexene epoxidation. Herein we have briefly discussed various novel nanotechnology methods used for MoO_3/SiO_2 synthesized by various group of researchers.

Starting with the work done by Hyeon *et al.* [96a] for synthesis of magnetically separable hematite coated MoO_3/SiO_2 for efficient olefin epoxidation. Magnetic separation provides a convenient method for removing and recycling magnetized species by applying magnetic field. This approach helps in separation of catalyst from the reaction mixture without being agglomerated. Hematite (α-Fe_2O_3) particles of uniform size and shape of about 400 nm were pre-synthesized. These nanoparticles were stabilized by PVP and coated with dense silica particles using conventional hydrolysis condensation method used for Stöber silica synthesis. These dense silica coated particles were further uniformly dispersed in mixture of ammonia and ethanol. To provide a mesoporous silica shell simultaneous sol–gel polymerization of a mixture of TEOS and n-octadecyltrimethoxysilane (C18TMS) with a molar ratio of 4:7 for 2 h at room temperature. These mesoporous silica coated hematite particles were thermally treated, followed by impregnation of these silica spheres with ammonium heptamolybdate (AHM) solution (weight ratio 1:10). Finally these AHM coated silica particles were reduced with H_2/N_2 (1:1) molar ratio to form black coloured MoO_3/SiO_2 particles giving very good catalytic activity for epoxides.

Zang *et al.* [96b] synthesized mesoporous core@shell and hollow core@shell $MoO_3@SiO_2$ for alkylation reactions using *inside-out* preinstallation-infusion-hydration method. In this process discrete molybdenum dioxde (MoO_2) nanoparticles of 25 to 60 nm were formed via one-pot hydrothermal synthesis route in water/ethanol mixed solvent at 180 °C, utilized as core with silica shell synthesized with the help of tetra-ethylortho silicate (TEOS) and cetyltrimethylammonium chloride (CTACl) in an alkaline solution. By thermal treatment of as-synthesized $MoO_2@SiO_2$ core-shell spheres, the organic templates were burned off releasing mesoporous shell. The Mo^{4+} particles were oxidized to Mo^{6+} particles, forming heptamolybdate species $Mo_7O_{24}^{6-}$. Hollow core@shell particles were synthesised by etching core@shell particles with KOH solution. Resulting catalysts gave very good catalytic activity of alkylation reactions, which were 2.5 times better than Amberlyst-15 catalyst.

Alternative procedure used for synthesis of MoO_3/SiO_2 was reverse micelle microemultion. Nanoparticles synthesised in a microemultion has been a hot topic of research since 1980 when first colloidal solution of Pd, Pt and Rh metal nanoparticles were synthesized. Microemultion is thermodynamically stable dispersion of two immiscible fluids, which is stabilized by addition of surfactant(s), which are amphiphilic molecules such as cetyltrimethylammonium bromide (CTAB), bis(2-ethylhexyl) sulfosuccinate (AOT), sodiumdodecylsulphate (SDS), Brij, Triton-X, large block copolymers or fatty acid molecules.[96c-100] Different type of emulsions are well known such as water in oil (w/o), oil in water (o/w), water in super critical carbon dioxide (w/scCO$_2$). Water in oil microemultion is formed when water is dispersed in hydrocarbon based continuous phase. Added polar or ionic component gets compartmentalized resulting into the centre core of this reverse micelle hence affording uniform dispersion of inorganic materials in oil. Micelles so formed are in the state of continuous motion via random Brownian motion. While in a continuous state of motion, these spherical micelles tend to collide with each other, resulting into exchange of materials and mixing up of inorganic materials trapped in the capsules. These nanoparticles act as "nanoreactors" providing suitable environment for controlled nucleation and growth. Steric stabilization provided by the surfactant molecules further prevents the nanoparicles from getting aggregated.

1.6. Catalytic Activity Study and Applications of Molybdenum - Homogeneous Catalysis.

Since W. R. Thiel first time reported homogeneous molybdenum complexes as efficient olefin epoxidation catalysts,[101] there has been a lot of work done on molybdenum as epoxidation catalyst.[102-103] Molybdenum complexes form basis of industrially important process such as ARCO-HALCON process for olefin epoxidation.[53, 104] Mo(VI) oxo–peroxo or oxo–diperoxo complexes with various ligands and successfully used these complexes for oxidation of alcohols to carbonyl compounds,[105] epoxidation of alkenes,[106] further oxidation of epoxides to dioxetanes or fragmentation products,[107] sulphides to sulfoxides and sulfoxides to sulphones.[108-109] High-valent molybdenum species are most studied and have preponderance over other catalyst for olefin epoxidation in the presence of H_2O_2 or alkyperoxides as oxidants. [39], [110-111]

Over the past few years there has been growing interest in the synthesis and characterization of molybdenum carbonyl complexes for olefin oxidation reaction. Molybdenum carbonyl complexes have been widely explored oxidation catalysts because of their high activity for selective oxidation with TBHP or H_2O_2. Molybdenum carbonyl complexes can be converted to dioxo molecules and oxo-peroxo via different methods like irradiation of carbonyl complexes in presence of oxygen or treating it with hydrogen peroxide or organic peroxides. Cousin and Green in 1964 reported the synthesis of dioxomolybdenum complex by direct irradiation of molybdenum carbonyl complex in oxygen.[112-113] But such species are further used along with the oxidants for the catalytic reactions to obtain the real catalytically active species i.e. oxo-peroxo molecule. But the direct *in-situ* treatment of molybdenum carbonyl complexes with hydrogen peroxide or organic peroxides gives the molybdenum oxo-peroxo species, which is the active species for the oxidation reactions and can be used for oxygen transfer reactions. Molybdenum carbonyl complex as a catalyst is the well set model for the epoxidation of olefins. During last decade much of the research on molybdenum carbonyl complexes was concentrated on epoxidation of olefins.

Molybdenum carbonyl complexes have proven to be a versatile oxidation catalyst for various selective oxidation reactions. $[MoCl(\eta^5-C_5R_5)(CO)_3]$[114-115] has been used for cyclooctene epoxidation. Molybdenum carbonyl complexes with different ligands like halides, N-containing and cyclopentadienyl;[116-117] η^5-C_5R_5; R=H, Me, Ph are mainly used for epoxidation of variety of olefins.[115] Kuehn *et al.* [114] as well as Goncalves *et al.* [118] have reported use of $CpMo(CO)_3Cl$ as catalyst for olefin oxidation with very high selectivity for epoxide.[119] Yamamoto *et al.* have synthesized molybdenum chiral bishydroxamic acid of molybdenum for asymmetric olefin epoxidation.[120] Tungsten acetylide complexes are reported to form oxo–peroxo complexes on treatment with H_2O_2 in acidic medium.[121] Hence similar molybdenum complexes are expected to be good oxidation catalysts.

1.7. Homogeneous Catalysis and Computational Catalysis

Homogeneous catalysis is an area of catalysis where modeling can have major impact. Reaction cycles in this case are complicated, multistep, short lived intermediates as well as transition states are difficult and most of the times impossible to characterize. Computational chemistry is the only tool left to access to detail

knowledge of reaction mechanism, which can guide us to design a new process and catalysis. [122] The applications of computer based models using analytical potential functions within the frame work of classical mechanics have proven to be interestingly powerful tool for chemical, organic and biochemical and organic chemical interest. Molecular modeling employs molecular mechanics or quantum mechanics. A typical molecular modeling job is done by geometry optimization of guess structure generated hypothetically using software such as Molden, Gauss view, PyMol (for biological molecules) etc and an energy minima is obtained during optimization process. [122-124] Structure is saved in xyz format (that contains Cartesian coordinates of the atom) or the z-matrix, providing the details of each atom in molecule such as bond angle bond length, dihedral angle, atomic number and so-called internal co-ordinates. The use of z-matrix format reduces the computational cost because chemical structures are highly coupled systems. [125] Mathematical calculations are employed in such a manner that overall energy is minimized. Lower the energy, higher the stability, as nature prefers minimum energy configuration. [122], [126-127]

Molecular Mechanics (MM). Molecular mechanics (MM) describes molecule in terms of "bonded atoms", which have been distorted from idealized geometry due to non-bonding van der Waals and Columbic interactions. Molecular mechanics employs Newtonian or classical mechanics to molecular systems. Molecular mechanics (MM) or force field methods use classical method to predict the energy of molecule in terms of conformation. This allows predictions of

A. Equilibrium geometries and transition states.

B. Relative energy between conformers or between different molecules.

In case of MM molecule is assumed to be a ball and spring model, where ball represents the atom and spring represents the bond between the atoms. The force constant of the spring is derived from a database called force field, which is calculated experimentally for example FT-IR spectroscopy and theoretically i.e., quantum mechanical calculations (discussed in later sections) The success of molecular mechanics model lies in providing quiet accurate guess of torsion angles, bond length and bond angles, provided that molecule has been represented in terms of a particular valence structure. Overall in molecular mechanics the total contribution in energy comes from bond stretching, bending, and torsion angle. Addition to these there are

contributions due to non-bonding, i.e. van der Waals and Columbic interactions. All these energies when combined together are called "strain energy". [128-129]

$$E = \sum_{A}^{bonds} E_A^{Stretch} + \sum_{A}^{bond\ angles} E_A^{Bend} + \sum_{A}^{torsion\ angles} E_A^{Tosion} + \sum_{A}^{torsion\ angles} \sum_{A}^{non-bonded\ atoms} E_A^{Tosion}$$

(1)

The first three summations in equation 1 are overall "bonds", "bond angles" and "torsion angles" respectively present in a molecule. The last summation in equation one is for "non-bonded" atoms. There are too many approximations involved in MM therefore it is called "empirical". There are two classes of force field methods available

I.   *Class I Methods.* Higher order terms and cross terms. Higher accuracy is used for small and medium sized molecules. Examples Alligner's, MM 1-4, EFF and CFF. [130-133]

II. *Class II Methods.* These methods are effective for large molecules such as proteins. Made cheap by using Taylor expansions and neglecting cross terms. Example AMBER, CHARAM, GROMOS etc. [134]

Advantages and Limitations of Molecular Mechanics. The chief advantage of MM is their simplicity. Except for very small systems computational costs are completely dominated by evaluation of non-bonded van der Waals and Columbic terms. Molecular mechanics calculations may easily be performed on molecules comprising several thousand atoms. Additionally, molecular mechanics calculations are very fast permuting extensive conformational searching on molecules containing upwards of 100-200 atoms. Conformational analysis is perhaps the single most important application of molecular mechanics.

The major disadvantages associated with MM are

I.   MM calculations are limited to description of equilibrium geometries and equilibrium conformations. As discussed in previous sections "Strain energy" (how much molecule deviates from its "ideal arrangement") is specific to a molecule and cannot be used in thermochemical calculation.

II. MM calculations do not reveal anything about bonding and electron distributions in molecules. Electron distribution study holds key in study

of reaction mechanism, reactivity and selectivity. In some cases where steric effects are involved in trends in reactivity and selectivity, MM calculations are significant.

III.   Molecular mechanics (MM) requires parameters $R_o{}^{AB}$, k_{AB}, $V_n{}^{ABCD}$, etc. Suppose we take an example of 30 atoms molecule will have $30^4/2$ torsion parameters or more than 1.25 million parameters are present, out of which 2466 useful parameters are present in MM2, i.e. certain parameters cannot be described. Lack of parameters is serious drawback of all force field methods. Automatic guessing of some parameters, sometimes leads to misleading results.

IV.   Molecular mechanics is an interpolation scheme, which not only depends on good parameters, but also on systematic amongst related molecules. Molecular mechanics would not be able to describe the structure and conformation of unfamiliar molecules outside parameterization range.

Quantum Mechanics (QM). Quantum mechanics provides mathematical description of duel particles like and wave like behavior and interaction of energy and matter. Quantum mechanics (QM) also describes molecule in terms of nuclei and electrons, and molecular geometry in terms of minimum energy arrangements of nuclei. All quantum mechanical methods date back to Schrödinger equation which for the specific case of hydrogen atom may be represented as

$$-\frac{1}{2}\,\nabla^2 - \frac{Z}{r} = E\psi(r)$$

(2)

In the above equation Z represents charge, E is electronic energy in atomic units and ψ the function of electron coordinates, r, is wave function describing the motion electron in three dimensional space. The square of the wave function gives the probability of finding an electron inside this volume defined as electron density. The major drawback of Schrödinger equation is that it is not applicable to many electron systems or even for two electron systems such as He atom or hydrogen molecule. Approximation need to be introduced to provide practical method. Born-Oppenheimer approximation a simplified version of Schrödinger equation for molecular system assumed that nuclear motion is negligible as compared to electronic motion. In other words we can say that nuclear wave functions are separated and then the electrons are treated as quantum mechanical objects and the nuclei are treated as classical objects.

Schrödinger equation was still intractable and further approximations were employed. The most important of the later was Hartree-Fock (H-F) approximation, which when applied to many electrons Schrödinger equation, not only leads to an important class of molecular orbital models or Hartree–Fock (H-F) molecular orbitals or simply molecular models. The (H-F) approximation replaces the "correct" description of electron motions by a picture in which the electrons behave essentially as independent particles. H-F model was first put to test in 1950, soon after the invention of first digital computer became available. Except for the case of transition metals, H-F models provided good description of equilibrium geometries and conformations. However, H-F failed in explaining thermochemistry of reactions involving explicit bond making or bond breaking. The main reason for the failure of Hartree-Fock models was due to incomplete description of "electron correlation" or, simply stated, the way in which the motion of one electron affects the motions of all the other electrons. Failure of H-F models lead to new approach to construct more flexible models for description of electron motion. Few of them are discussed here [129], [135]

Density Functional Theory (DFT). The Density Functional Theory (DFT) uses a completely different approach to recover the electron correlation energy. Currently it is most popular method applied to real life chemistry problems. Using this theory the properties of a many-electron system can be determined by using functional, i.e. functions of another function, which in this case is the spatially dependent electron density. Hence the name density functional comes, i.e. functional of electron density. The density functional theory of Hohenberg, Kohn and Sham was based on the fact that that the sum of the exchange and correlation energies of a uniform electron gas can be calculated exactly knowing only its density. [136]

$$E = E_T + E_V + E_J + E_{XC} \qquad (3)$$

The equation mentioned above is Kohn-Sham formalism, and the terms ground-state electronic energy, E, is written as a sum of the kinetic energy, E_T, the electronuclear interaction energy, E_V, the Coulomb energy, E_J, and the exchange or correlation energy, Exc. Except for E_T all are dependent on density.

Density functional models are well-defined and yield unique results. Density functional models, like Hartree-Fock models are applicable to molecules of moderate size (50-100 atoms). For carrying out DFT calculations an initial guess structure is required, the functional to be used for the calculation and the "basis set". Basis set is

nothing but definition of an atom as input in the calculations. There are different qualities of basis sets available such as SVP (split valence with polarization), DZVP (Double Zeta Valance with Polarization), TZVP (Triple Zeta Valence with Polarization) and there are numerous such basis set available depending on problem. The higher the quality of basis sets, higher is the computational cost and higher the accuracy.

Problems Faced in Molecular Modeling and Transition State Search. Homogeneous catalysis occurs through a sequence of reactions which constitute the catalytic cycle. Within the transition state based approach, the theoretical study of the field requires geometries and energies of all the reactants, products and all the relevant intermediates and transition states. Optimization of the geometries is usually done through gradient technique. The characterization of the stationary points involves differentiation between local minima (intermediates, reactants and products), and the saddle point (the transition state), by computing matrix second order derivative of the energy with respect to molecular coordinates. Here stationary phase is a geometry such that the derivative of energy with respect to all the displacement of the nuclei is zero, whereas a local minima is a stationary point where all the displacement lead to an increase in energy, that is, a stable molecule. In case of local minima all the eigen values or molecular coordinates are positive, where as in the case of saddle point (See Fig.1.4) (transition state), there one and only one negative eigen value. The activation energy of the reaction is calculated by finding the difference in the energy of reactants and transition state. Determination of perfect transition state is the hardest part for a computational chemistry and it is regarded more of art than science. The reaction profile of a typical catalytic reaction consists of many transition states and intermediates. Based on this information it is possible to determine the activity and the selectivity determining step of the catalytic process and evaluating different energies and energy barriers. The analysis of rate determining transition state provides information about the factors governing the catalytic activity. For a multistep process, (See Fig.1.5) with several transition states and intermediates of comparable energies could contribute to catalytic turnover. In such a case, it is not straightforward to calculate efficiency of catalytic cycle, that is, its turnover frequency (TOF) from theoretically obtained energy profile. To obtain catalytic turnover frequency (TOF) from a theoretically obtained energy profile, Kozuch and Shaik proposed a more sophisticated methodology, the energy span model, which is based on *Energetic Span*

Model, based on Erying's transition state theory (TST) and corresponding steady state regime.[137]
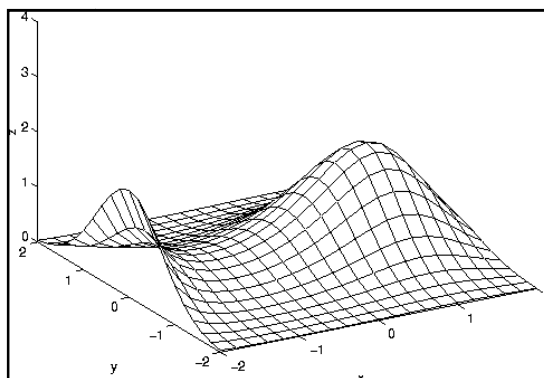
Fig. 1.4: The potential energy surface for "saddle point" the transition state.

Hybrid Force Field Models and Truncated Models: While tackling large molecules such as protein molecules, there is a hybrid method applied to tackle such problem. "Uninteresting" part is calculated using force field model and the "interesting" part is calculated using electronic structure method or quantum mechanical method. A good example for truncated model is considering ethylene molecule for computational calculations, instead of taking cyclohexene, styrene, etc. Another example is replacing triphenyl phospine group with a small group such as methyl group. This greatly reduces the number of atoms in the structure and provides results with acceptable accuracy. Examples: Morokuma's ONIOM method; QM/MM methods. [138]
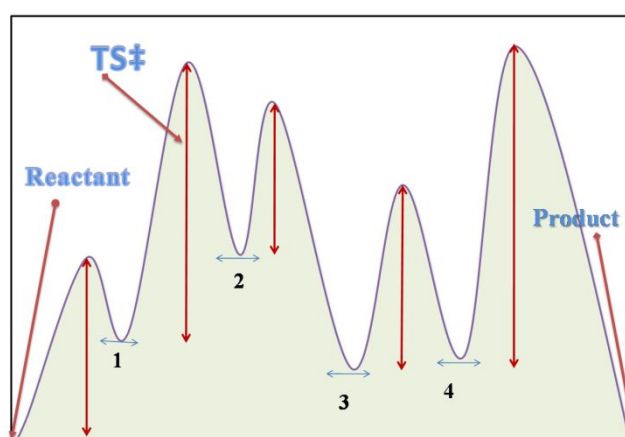
Fig. 1.5: Energy profile of a multistep catalytic pathway for reactant leading to product via TS‡

Solvent Effect: Considering a geometry optimization job, a molecule is assumed to be uninfluenced by presence of other molecules, that is, it is surrounded by empty space. We can assume that the molecule is in gas phase and calculations so performed are gas phase calculations. Practically it is quiet improbable as, molecule always keeps interacting with surrounding molecule such as solvent molecules. Practically solvents have major role in determining catalytic activity and product selectivity. Hence, the role played by solvent cannot be denied and a new concept of solvent effect comes into action. COSMO, CPCMC are important and most popular method employed to study the solvent effect. COSMO is abbreviation of COnduction like Screening Model. COSMO method is mainly used in the upcoming sections for calculation of solvent effect. COSMO model assumes that solvent molecule forms a cavity within the dielectric continuum of permittivity ϵ that represents the solvent. Dielectric medium is polarized by the charge of the solute molecule, in response to which solvent generates surface charges on cavity surfaces. [139]

1.8. Objective and Scope of the Present Work

As discussed in the previous sections there are several reports in the literature for molybdenum based heterogeneous and homogeneous catalysts and there catalytic applications in oxidation reaction. In oxidation reactions molybdenum peroxo species is known to be catalytically active species especially in the presence of peroxides as oxidants. To the best of our knowledge there are no reports in the literature on systematic study of different structural environment of molybdenum peroxo species on oxidation efficiency of molybdenum based catalyst. Here the objective of the thesis is to prepare molybdenum peroxo species in different homogeneous as well as heterogeneous environment and study its effect on oxidation efficiency with respect to conversion as well as selectivity. Therefore, to understand the importance of the effect of structural environment of molybdenum peroxo species, which is known to be catalytically active species for olefin oxidation, the following main objectives were set for the thesis:

- Synthesis of molybdenum peroxo species in different homogeneous as well as heterogeneous environment.

- Synthesis of supported molybdena catalysts using reverse micelle microemultion, hydrolysis condensation (HC) and impregnation followed by

hydrolysis condensation (IHC) for development of new catalyst to obtain better catalytic activity as well as selectivity for olefin oxidation reaction.

- Detailed physicochemical characterization of the synthesized supported molybdena catalyst using techniques such as FT-IR, IR of adsorbed pyridine, XRD, FT-Raman, UV-visible, SEM, TEM and EDAX.

- Screening of the synthesized catalysts for oxidation of olefin.

- Structure-activity, structure-selectivity co-relations with the help of advance spectroscopic characterization techniques for olefin oxidation.

- Mechanistic aspects using experimental evidences as well as theoretical calculation for using DFT calculations for development of more realistic model for the olefin oxidation mechanism using TURBOMOLE and GAUSSIAN 09 packages.

The **first chapter** presents with a detailed literature review on catalytic applications of various transition metals especially with reference of oxidation reactions. Detailed discussion on various homogeneous and heterogeneous catalysts with molybdenum centre as active site of the catalyst for oxidation reaction and structure activity co-relation. This chapter also deals with experimental as well as theoretical studies done in the past by various group of workers for investigating the mechanism for oxidation reaction with an emphasis on olefin epoxidation and *cis*-dihydroxylation. Significance of such studies will helps us to understand the role of ligand environment and oxidant in altering the mechanism of a catalytic reaction. Theoretical methodology used in elucidating the comparative study of olefin epoxidation as well as *cis*-dihydroxylation will be discussed in this chapter.

The ***second chapter*** deals with the synthesis of the ultrasmall molybdenum oxide (MoO_3) nanoparticles supported on various oxides nanosphers (SiO_2, TiO_2 or ZrO_2) synthesized in one pot using reverse micelles method. The prepared catalysts were extensively characterized by various physicochemical methods and tested for catalytic applications in olefin oxidation reaction.

The ***third chapter*** deals with synthesis of molybdenum oxide supported on silica microspheres synthesized by two different methods, i.e., hydrolysis-condensation (HC) and impregnation followed by hydrolysis-condensation (IHC).

The FT-IR and Raman spectroscopy confirmed the presence of isolated MoO_6 O_h, Mo_8O_{26} O_h and polyoxo-molybdate clusters species in the molybdena supported on silica microspheres prepared by IHC, whereas α-MoO_3 was present in material synthesized by HC method. These catalysts were used in olefin epoxidation.

In the ***chapter 4***, experimental as well as theoretical study of mechanism for olefin epoxidation as well as *cis*-dihydroxylation using CpMo(O-O)(O)-C≡CPh complex as catalyst, cyclohexene as substrate and H_2O_2 or TBHP as oxidants. Characterization of intermediates formed by treatment of catalyst with H_2O_2 or TBHP was done using FT-IR spectroscopy. Quantum mechanical study for comparative mechanism for olefin oxidation and *cis*-dihydroxylation was carried out using TURBOMOLE 6.4 and GAUSSIAN 9.0 packages. Experimental results were found in agreement with theoretical results.

The major outcome of all the chapters from present study is summarized in the section ***Summary and future outlook***.

1.9. References

[1] J. A. Moulijn, P. W. van Leeuwen, R. A. van Santen, *Catalysis: an integrated approach to homogeneous, heterogeneous and industrial catalysis, Vol. 79*, Elsevier Science, **1993**.

[2] A. Robertson, *Platinum Met. Rev.* **1975**, *19*, 64-69.

[3] J. N. Armor, *Catal. Today* **2011**, *163*, 3-9.

[4] W. Hermann, B. Cornils, *A Comprehensive Handbook in Two Volumes* **1999**, *2*.

[5] R. Noyori, *Angew. Chem. Int. Ed.* **2002**, *41*, 2008-2022.

[6] P. W. Atkins, J. De Paula, *Atkins' physical chemistry, Vol. 8*, Oxford University Press Oxford, 2006.

[7] J. Coenen, *Recl. Trav. Chim. Pays-Bas.* **1983**, *102*, 57-64.

[8] A. Frost, R. Pearson, *J. Phys. Chem.* **1961**, *65*, 384-384.

[9] R. A. Van Santen, M. Neurock, *Molecular heterogeneous catalysis: a conceptual and computational approach*, Wiley-VCH, **2009**.

[10] P. Jolly, *Angew. Chem. Int. Ed.* **1980**, *92*, 975-975.

[11] H.-U. Blaser, A. Indolese, A. Schnyder, *Current Science-Banglore* **2000**, *78*, 1336-1344.

[12] J. H. Clark, D. J. Macquarrie, *Org. Process Res. Dev.* **1997**, *1*, 149-162.

[13] J. M. Thomas, W. J. Thomas, J. Anderson, M. Boudart, *Principles and practice of heterogeneous catalysis, Vol. 638*, VCH Weinheim, **1997**.

[14] D. J. Cole-Hamilton, *Science* **2003**, *299*, 1702-1706.

[15] N. Creamer, I. Mikheenko, P. Yong, K. Deplanche, D. Sanyahumbi, J. Wood, K. Pollmann, M. Merroun, S. Selenska-Pobell, L. Macaskie, *Catal. Today* **2007**, *128*, 80-87.

[16] B. Cornils, W. A. Herrmann, *Aqueous-phase organometallic catalysis*, Wiley-VCH, **2004**.

[17] B. Cornils, W. A. Herrmann, *J. Catal.* **2003**, *216*, 23-31.

[18] J. D. Lee, *Concise inorganic chemistry*, Wiley. com, **2008**.

[19] F. A. Cotton, G. Wilkinson, C. A. Murillo, M. Bochmann, *Advanced inorganic chemistry, Vol. 5*, Wiley New York, **1988**.

[20] J. E. Huheey, E. A. Keiter, R. L. Keiter, O. K. Medhi, *Inorganic chemistry: principles of structure and reactivity*, Harper & Row New York, **1983**.

[21] D. Astruc, *Nanoparticles and catalysis*, Wiley Online Library, **2008**.

[22] I. J. Fairlamb, *Annual Reports Section" B"(Organic Chemistry)* **2003**, *99*, 104-137.

[23] P. W. Van Leeuwen, P. W. Leeuwen, *Homogeneous catalysis: understanding the art,* Springer, **2004**.

[24] C. Elschenbroich, A. Salzer, *Organometallics: a concise introduction, Vol. 13*, Vch Weinheim, **1989**.

[25] S. Albonetti, F. Cavani, F. Trifiro, *Catal. Rev.* **1996**, *38*, 413-438.

[26] T. Punniyamurthy, S. Velusamy, J. Iqbal, *Chem. Rev.* **2005**, *105*, 2329-2364.

[27] T. Mukaiyama, T. Yamada, *Bull. Chem. Soc. Jpn.* **1995**, *68*, 17-35.

[28] Y.-C. Kim, N.-C. Park, J.-S. Shin, S. R. Lee, Y. J. Lee, D. J. Moon, *Catal. Today* **2003**, *87*, 153-162.

[29] J. Bäckvall, B. Akermark, S. Ljunggren, *J. Am. Chem. Soc.* **1979**, *101*, 2411-2416.

[30] M. Beller, C. Bolm, *Transition Metals for Organic Synthesis: Building Blocks and Fine Chemicals, 2 Volume Set*, Wiley-VCH New York:, **2004**.

[31] R. Sheldon, *Metal-catalyzed oxidations of organic compounds: mechanistic principles and synthetic methodology including biochemical processes*, Academic press, **1981**.

[32] W. Partenheimer, *Catal. Today* **1995**, *23*, 69-158.

[33] Y. Ishii, S. Sakaguchi, T. Iwahama, *Adv. Synth. Catal.* **2001**, *343*, 393-427.

[34] M. S. Wainwright, T. W. Hoffman, *Chemical reaction engineering II. Advances in chemistry series* **1974**, 669.

[35] J. T. Groves, G. A. McClusky, R. E. White, M. J. Coon, *Biochem. Biophys. Res. Commun.* **1978**, *81*, 154-160.

[36] R. Sheldon, in *Organic Peroxygen Chemistry*, Springer, **1993**, pp. 21-43.

[37] G. Sienel, R. Rieth, K. T. Rowbottom, *Ullmann's Encyclopedia of Industrial Chemistry* **2000**.

[38] K. Bauer, D. Garbe, H. Surburg, *Common fragrance and flavor materials*, Wiley-VCH, **2008**.

[39] B. S. Lane, K. Burgess, *Chem. Rev.* **2003**, *103*, 2457-2474.

[40] D. Hoegaerts, B. F. Sels, D. E. De Vos, F. Verpoort, P. A. Jacobs, *Catal. Today* **2000**, *60*, 209-218.

[41] A. K. Yudin, *Aziridines and epoxides in organic synthesis*, Wiley-VCH, **2006**.

[42] M. H. Dickman, M. T. Pope, *Chem. Rev.* **1994**, *94*, 569-584.

[43] C. C. Romão, F. E. Kühn, W. A. Herrmann, *Chem. Rev.* **1997**, *97*, 3197.

[44] W. Adam, W. Malisch, K. J. Roschmann, C. R. Saha-Möller, W. A. Schenk, *J. Organomet. Chem.* **2002**, *661*, 3-16.

[45] R. Hutter, T. Mallat, A. Baiker, *J. Catal.* **1995**, *153*, 177-189.

[46] S. B. Kumar, S. Mirajkar, G. C. Pais, P. Kumar, R. Kumar, *J. Catal.* **1995**, *156*, 163-166.

[47] M. Clerici, G. Bellussi, U. Romano, *J. Catal.* **1991**, *129*, 159-167.

[48] J. Van der Waal, M. Rigutto, H. Van Bekkum, *Appl. Catal. A: Gen.* **1998**, *167*, 331-342.

[49] G. Grigoropoulou, J. Clark, J. Elings, *Green Chem.* **2003**, *5*, 1-7.

[50] W. Nam, R. Ho, J. S. Valentine, *J. Am. Chem. Soc.* **1991**, *113*, 7052-7054.

[51] A. Murphy, G. Dubois, T. Stack, *J. Am. Chem. Soc.* **2003**, *125*, 5250-5251.

[52] J. P. Collman, X. Zhang, V. J. Lee, E. S. Uffelman, J. I. Brauman, *Science* **1993**, *261*, 1404-1411.

[53] K. Kamata, K. Yonehara, Y. Sumida, K. Yamaguchi, S. Hikichi, N. Mizuno, *Science* **2003**, *300*, 964-966.

[54] D. V. Deubel, J. Sundermeyer, G. Frenking, *J. Am. Chem. Soc.* **2000**, *122*, 10101-10108.

[55] D. V. Deubel, J. Sundermeyer, G. Frenking, *Inorg. Chem.* **2000**, *39*, 2314-2320.

[56] P. Gisdakis, I. V. Yudanov, N. Rösch, *Inorg. Chem.* **2001**, *40*, 3755-3765.

[57] G. Wahl, D. Kleinhenz, A. Schorm, J. Sundermeyer, R. Stowasser, C. Rummey, G. Bringmann, C. Fickert, W. Kiefer, *Chem. Eur. J.* **1999**, *5*, 3237-3251.

[58] J.-E. Bäckvall, *Modern oxidation methods*, Wiley-VCH, **2011**.

[59] T. Katsuki, K. B. Sharpless, *J. Am. Chem. Soc.* **1980**, *102*, 5974-5976.

[60] T. Katsuki, *Asymmetric Oxidation Reactions: A Practical Approach in Chemistry*, Oxford University Press, Incorporated, **2001**.

[61] R. A. Sheldon, J. K. Kochi, J. Richardson, *Metal-catalyzed oxidations of organic compounds: mechanistic principles and synthetic methodology including biochemical processes*, Academic press New York, **1981**.

[62] T. Hudlicky, A. J. Thorpe, *Chem. Commun.* **1996**, 1993-2000.

[63] M. Schroeder, *Chem. Rev.* **1980**, *80*, 187-213.

[64] H. C. Kolb, M. S. Van Nieuwenhze, K. B. Sharpless, *Chem. Rev.* **1994**, *94*, 2483-2547.

[65] C. Bolm, J. Hildebrand, K. Muniz, I. Ojima, *Catalytic Asymmetric Synthesis*, Wiley-VCH, New York, **2000**.

[66] G. Cainelli, M. Contento, F. Manescalchi, L. Plessi, *Synthesis* **2002**, *1989*, 45-47.

[67] W. A. Herrmann, R. M. Kratzer, J. Blümel, H. B. Friedrich, R. W. Fischer, D. C. Apperley, J. Mink, O. Berkesi, *J. Mol. Catal.* **1997**, *120*, 197-205.

[68] S. Kobayashi, M. Endo, S. Nagayama, *J. Am. Chem. Soc.* **1999**, *121*, 11229-11230.

[69] C. Bolm, A. Maischak, *Synlett* **2001**, *2001*, 0093-0095.

[70] I. Motorina, C. M. Crudden, *Org. Lett.* **2001**, *3*, 2325-2328.

[71] B. M. Choudary, S. Madhi, N. S. Chowdari, M. L. Kantam, B. Sreedhar, *J. Am. Chem. Soc.* **2002**, *124*, 14127-14136.

[72] W.-J. Tang, N.-F. Yang, B. Yi, G.-J. Deng, Y.-Y. Huang, Q.-H. Fan, *Chem. Commun.* **2004**, 1378-1379.

[73] A. Severeyns, D. E. De Vos, L. Fiermans, F. Verpoort, P. J. Grobet, P. A. Jacobs, *Angew. Chem. Int. Ed.* **2001**, *40*, 586-589.

[74] X. Lu, Z. Xu, G. Yang, *Org. Process Res. Dev.* **2000**, *4*, 575-576.

[75] H. Becker, K. B. Sharpless, *Angew. Chem. Int. Ed.* **1996**, *35*, 448-451.

[76] K. Bergstad, S. Y. Jonsson, J. E. Backvall, *J. Am. Chem. Soc.* **1999**, *121*.

[77] S. Y. Jonsson, K. Färnegårdh, J.-E. Bäckvall, *J. Am. Chem. Soc.* **2001**, *123*, 1365-1371.

[78] C. Döbler, G. M. Mehltretter, U. Sundermeier, M. Beller, *J. Am. Chem. Soc.* **2000**, *122*, 10289-10297.

[79] A. H. Ell, A. Closson, H. Adolfsson, J. E. Baeckvall, *Adv. Synth. Catal.* **2003**, *345*, 1012-1016.

[80] J. W. de Boer, J. Brinksma, W. R. Browne, A. Meetsma, P. L. Alsters, R. Hage, B. L. Feringa, *J. Am. Chem. Soc.* **2005**, *127*, 7990-7991.

[81] T. W.-S. Chow, E. L.-M. Wong, Z. Guo, Y. Liu, J.-S. Huang, C.-M. Che, *J. Am. Chem. Soc.* **2010**, *132*, 13229-13239.

[82] P. C. Bruijnincx, I. L. Buurmans, S. Gosiewska, M. A. Moelands, M. Lutz, A. L. Spek, G. van Koten, R. J. Klein Gebbink, *Chem. Eur. J.* **2008**, *14*, 1228-1237.

[83] P. C. Bakala, E. Briot, L. Salles, J.-M. Brégeault, *Appl. Catal. A, Gen.* **2006**, *300*, 91-99.

[84] K. S. Oh, B. G. Lee, M. S. Han, Y. G. Shul, *React. Kinet. Catal. Lett.* **2002**, *77*, 51-58.

[85] M. K. Dongare, V. V. Bhagwat, C. Ramana, M. K. Gurjar, *Tetrahedron Lett.* **2004**, *45*, 4759-4762.

[86] Y.-K. Park, S. J. Kim, N. You, J. Cho, S. J. Lee, J. H. Lee, J.-K. Jeon, *J. Ind. Eng. Chem.* **2011**, *17*, 186-190.

[87] Z. Li, L. Gao, S. Zheng, *Appl. Catal. A: Gen.* **2002**, *236*, 163-171.

[88] H. Balcar, P. Topka, J. Pérez-Pariente, J. Čejka, *Stud. Surf. Sci. Catal.* **2005**, *156*, 795-802.

[89] S. B. Umbarkar, T. V. Kotbagi, A. V. Biradar, R. Pasricha, J. Chanale, M. K. Dongare, A.-S. Mamede, C. Lancelot, E. Payen, *J. Mol. Catal. A: Chem.* **2009**, *310*, 150-158.

[90] S. B. Umbarkar, A.V. Biradar, S. Mathew, S. Shelke, K. Malshe, P. Patil, S. Dagde, S. Niphadkar, M. K. Dongare, *Green Chem.* **2006**, *8*, 488-493.

[91] T. V. Kotbagi, A. V. Biradar, S. B. Umbarkar, M. K. Dongare, *ChemCatChem* **2013**, *5*, 1531-1537.

[92] A. Biradar, S. Umbarkar, M. Dongare, *Appl. Catal. A: Gen.* **2005**, *285*, 190-195.

[93] N. A. Dhas, A. Gedanken, *Chem. Maters.* **1997**, *9*, 3144-3154.

[94] N. A. Dhas, A. Gedanken, *J. Phys. Chem. B* **1997**, *101*, 9495-9503.

[95] M. De Boer, A. Van Dillen, D. Koningsberger, J. W. Geus, M. Vuurman, I. Wachs, *Catal. Lett.* **1991**, *11*, 227-239.

[96] a) M. Shokouhimehr, Y. Piao, J. Kim, Y. Jang and T. Hyeon, *Angew. Chem., Int. Ed.*, **2007**, 46, 7039–7043. b) J. Dou, H. C. Zeng, *J. Am. Chem. Soc.* **2012**, *134*, 16235-16246. c) C.-J. Jia, F. Schüth, *Phys. Chem. Chem. Phys.* **2011**, *13*, 2457-2487.

[97] C. Burda, X. Chen, R. Narayanan, M. A. El-Sayed, *Chem. Rev.* **2005**, *105*, 1025-1102.

[98] M. A. El-Sayed, *Acc. Chem. Res.* **2004**, *37*, 326-333.

[99] A. R. Tao, S. Habas, P. Yang, *Small* **2008**, *4*, 310-325.

[100] S. Eriksson, U. Nylén, S. Rojas, M. Boutonnet, *Appl. Catal. A: Gen.* **2004**, *265*, 207-219.

[101] W. R. Thiel, T. Priermeier, *Angew. Chem. Int. Ed.* **1995**, *34*, 1737-1738.

[102] V. Conte, B. Floris, *Dalton Trans.* **2011**, *40*, 1419-1436.

[103] J. P. Thielemann, T. Ressler, A. Walter, G. Tzolova-Müller, C. Hess, *Appl. Catal. A: Gen.* **2011**, *399*, 28-34.

[104] J. C. Alonso, P. Neves, M. J. Pires da Silva, S. Quintal, P. D. Vaz, C. Silva, A. A. Valente, P. Ferreira, M. J. Calhorda, V. Félix, *Organometallics* **2007**, *26*, 5548-5556.

[105] S. E. Jacobson, D. A. Muccigrosso, F. Mares, *J. Org. Chem.* **1979**, *44*, 921-924.

[106] A. D. Westland, F. Haque, J. M. Bouchard, *Inorg. Chem.* **1980**, *19*, 2255-2259.

[107] E. Vedejs, *J. Am. Chem. Soc.* **1974**, *96*, 5944-5946.

[108] S. Campestrini, V. Conte, F. Difuria, G. Modena, O. Bortolini, *J. Org. Chem.* **1988**, *53*, 5721-5724.

[109] G. Keilen, T. Benneche, K. Gaare, K. Undheim, , *Acta. Chem. Scand.* **1992**, *46*, 867-871.

[110] W. R. Thiel, J. Eppinger, *Chem. Eur. J.* **1997**, *3*, 696-705.

[111] K. A. Jørgensen, *Chem. Rev.* **1989**, *89*, 431-458.

[112] M. Cousins, M. Green, *J. Chem. Soc. (Resumed)* **1964**, 1567-1572.

[113] M. Cousins, M. Green, *J. Chem. Soc. A* **1969**, 16-19.

[114] C. Freund, M. Abrantes, F. E. Kühn, *J. Organomet. Chem.* **2006**, *691*, 3718-3729.

[115] A. M. Martins, C. C. Romão, M. Abrantes, M. C. Azevedo, J. Cui, A. R. Dias, M. T. Duarte, M. A. Lemos, T. Lourenço, R. Poli, *Organometallics* **2005**, *24*, 2582-2589.

[116] M. Abrantes, A. M. Santos, J. Mink, F. E. Kühn, C. C. Romão, *Organometallics* **2003**, *22*, 2112-2118.

[117] G. Grivani, S. Tangestaninejad, M. H. Habibi, V. Mirkhani, *Catal. Commun.* **2005**, *6*, 375-378.

[118] A. A. Valente, J. D. Seixas, I. S. Gonçalves, M. Abrantes, M. Pillinger, C. C. Romão, *Catal. Lett.* **2005**, *101*, 127-130.

[119] F. Javier de la Mata, P. Giner, P. Royo, *J. Organomet. Chem.* **1999**, *572*, 155-161.

[120] A. U. Barlan, A. Basak, H. Yamamoto, *Angew. Chem. Int. Ed.* **2006**, *118*, 5981-5984.

[121] C.-W. Shiu, C.-J. Su, C.-W. Pin, Y. Chi, P. Peng, G.-H. Lee, *J. Organomet. Chem.* **1997**, *545*, 151-156.

[122] F. Maseras, A. Lledós, *Computational modeling of homogeneous catalysis, Vol. 25*, Kluwer Academic Pub, **2002**.

[123] G. Schaftenaar, J. H. Noordik, *J. Comput. Aided Mol. Des.* **2000**, *14*, 123-134.

[124] N. Mills, *J. Am. Chem. Soc.* **2006**, *128*, 13649-13650.

[125] J. Parsons, J. B. Holmes, J. M. Rojas, J. Tsai, C. E. Strauss, *J. comput. Chem.* **2005**, *26*, 1063-1068.

[126] F. Maseras, A. Lledós, in *Computational Modeling of Homogeneous Catalysis*, Springer, **2002**, pp. 1-21.

[127] K. Morokuma, D. G. Musaev, *Computational modeling for homogeneous and enzymatic catalysis*, Wiley-VCH, **2008**.

[128] N. Allinger, U. Burkert, Washington, DC: American Chemical Society, **1982**.

[129] W. J. Hehre, *A guide to molecular mechanics and quantum chemical calculations*, Wavefunction Irvine, CA, **2003**.

[130] N. L. Allinger, *J. Am. Chem. Soc.* **1977**, *99*, 8127-8134.

[131] J. H. Lii, N. L. Allinger, *J. Am. Chem. Soc.* **1989**, *111*, 8576-8582.

[132] N. L. Allinger, Y. H. Yuh, J. H. Lii, *J. Am. Chem. Soc.* **1989**, *111*, 8551-8566.

[133] W. D. Cornell, P. Cieplak, C. I. Bayly, I. R. Gould, K. M. Merz, D. M. Ferguson, D. C. Spellmeyer, T. Fox, J. W. Caldwell, P. A. Kollman, *J. Am. Chem. Soc.* **1996**, *118*, 2309-2309.

[134] B. R. Brooks, R. E. Bruccoleri, B. D. Olafson, S. Swaminathan, M. Karplus, *J. Comput. Chem.* **1983**, *4*, 187-217.

[135] P. W. Atkins, R. S. Friedman, *Molecular quantum mechanics, Vol. 3*, Oxford university press Oxford, **1997**.

[136] P. Hohenberg, W. Kohn, *Phys. Rev.* **1964**, *136*, B864.

[137] S. Kozuch, S. Shaik, *Acc. Chem. Res.* **2010**, *44*, 101-110.

[138] A. Warshel, M. Levitt, *J. Mol. Biol.* **1976**, *103*, 227-249.

[139] R. Ahlrichs, COSMOlogic GmbH & Co. KG Leverkusen, Germany, **2004**.

2

One Pot Synthesis of Ultrasmall MoO$_3$ Nanoparticles Supported on SiO$_2$, TiO$_2$, and ZrO$_2$ Nanospheres: An Efficient Epoxidation Catalyst

---

Ultrasmall molybdenum oxide (MoO$_3$) nanoparticles supported on various (SiO$_2$, TiO$_2$ or ZrO$_2$) nanosphers were synthesized in one pot using reverse micelles method. The prepared catalysts were extensively characterized by various physico-chemical methods. TEM images showed uniform dispersion of MoO$_3$ nanoparticles (0.5-3 nm) onto silica (~275 nm). Separate MoO$_3$ particles were not observed on titania (~10.5 nm) and zirconia (~6.5 nm) nanosphers due to the reaction of titanium and zirconium hydroxide with ammonium heptamolybdate (AHM) during synthesis. Acidity measurements by TPD analysis revealed weak acidity for all the catalysts. Among all prepared catalysts MoO$_3$/SiO$_2$ showed excellent catalytic activity for cyclooctene oxidation with up to 90% cyclooctene conversion and 100% epoxide selectivity within 2-6 h reaction time. The catalyst was successfully recycled up to five cycles without losing much activity and selectivity.
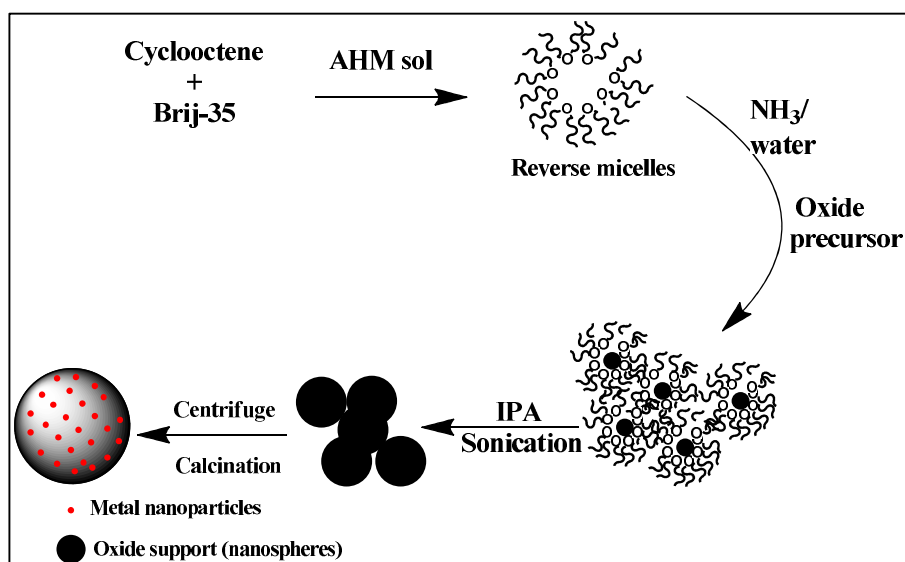
2.1. Introduction

In the recent past "Nanoscience and Nanotechnology" has made tremendous advancement in fundamental studies as well as in the development of numerous technologies. Particularly, it directly relates the method of synthesis, structures, devices with their particle size (1 to 100 nm) at the atomic, molecular, or macromolecular levels.[1] Nanomaterials so formed find applications in electronics, medicine, engineering and catalysis.[2] Recent advancement in novel nanotechnologies have proven to be expedient in synthesis of complex solid materials with chiseled size and shape which can be useful to satisfy specific requirements in catalysis in terms of selectivity. The study of mutual effect of both surface chemistry and catalysis has done admirable job in revolutionizing chemical manufacturing. The main synthetic methodologies employed for synthesis of such nanomaterials are atomic layer deposition (ALD), dendrimer encapsulation[3], sol-gel synthesis[4], core-shell, york-shell[5], immobilization procedures, colloidal and reverse micelle etc.[6] Out of these frequently employed methods for catalyst synthesis, reverse micelle or "resin burn" method is quiet popular amongst the researchers worldwide.

Metal nanoparticles, synthesized by reverse micelle showed narrow and uniform size[7] distribution.[8] Reverse micelle microemultions are thermodynamically stable and employs surfactant or co-surfactants, water and organic solvent. Surfactants include cetyltrimethylammonium bromide (CTAB), bis(2-ethylhexyl) sulfosuccinate (AOT), sodium dodecyl sulphate (SDS), Brij, Triton-X, large block copolymers or fatty acid molecules and organic solvents include n-alkanes and cycloalkanes. Reverse micelle solubilises water and provide optimum conditions for synthesis of small nanoparticles as water droplets in nanometre range.[9-10] In the literature there are number of examples illustrated e.g. Pileni *et al.* [11] synthesized Cu nanoparticles by AOT oil in water system. Shape of the nanoparticles was varied by changing the oil: water ratio and salt concentration. Murphy and co-workers[12] reported the synthesis of tiny gold nanoparticles (2-10 nm) using CTAB as surfactant, and tetradodecylammonium bromide as cosurfactant. In another example Au@TiO$_2$ core@shell nanocomposites were prepared using reverse micelle technique and used as an efficient catalyst for 4-nitrophenol reduction. [7] Zang *et al.* [13] synthesized palladium core@shell materials and used for photocatalytic activity. Yang *et al.* [14]

incorporated CdSe/ZnS quantum dots (QD) into SiO_2 beads and obtained high photoluminescence brightness and non-blinking nature due to the collective and averaging effects. More recently Wang *et al.* [15] have employed reverse micelle microemultion method for synthesis of molybdea on silica nanosphers as efficient solid acid catalyst for acetalization of ethylene glycol with benzeldehyde. All these examples demonstrated the expediency of this method.

It is well known that MoO_3 supported on silica is an excellent solid acid catalyst for various organic transformations [16-18] however their oxygen transfer properties at nanoscale size have not been fully explored for epoxidation reaction. As olefin epoxidation reaction is an industrially important reaction and the formed epoxides can be used for the production of a variety of commodity chemicals such as drug intermediates, agrochemicals and food additives.[19-20] Various homogeneous transition metal complexes are known for epoxidation reaction.[21] Among known oxidation catalysts high-valent molybdenum complexes have shown promising activity.[21-22] Furthermore, to make more practical these complexes were anchored or supported onto various hybrid mesoporous materials.[23-24] Particularly, Newmann *et al.* have used of MoO_3/SiO_2 for epoxidation of olefins using TBHP as an oxidant.[25] Also Arnold *et al.* [26] used acid catalyzed sol-gel synthesis of MoO_3/SiO_2 taking Mo (V)-isopropoxide as molybdenum precursor for olefin epoxidation. However, both the catalysts show leaching of the active species after three recycles. Hyoen *et al.* have carried out olefin epoxidation using magnetically separable mesoporous molybdena silica microspheres. Some of the drawbacks of the methods mentioned include lengthy synthetic procedures and the possibility of leaching of the active metal from supports.[27]

Herein we report the easy synthesis of ultrasmall MoO_3 nanoparticles supported on different oxide nanosphers like SiO_2, TiO_2 and ZrO_2 by reverse micelle microemultion, i.e, "resin burn" method and its application for olefin epoxidation.

2.2. Catalyst Synthesis and Characterization

All the reagents viz., ammonium heptamolybdate (Thomas Baker), cyclohexene, 5.5M TBHP in decane, *tetra*-ethyl orthosilicate (TEOS), tianium(IV) butoxide (Aldrich), zirconium(IV) butoxide (Aldrich), isopropyl alcohol, polyoxyethylene (23) lauryl ether (Brij-35) (Thomas Baker) and 1,2-dichloroethane (S.D. fine chemicals) were used as received.

2.2.1. Synthesis of MoO₃/SiO₂. In a typical synthesis procedure, 250 mL two necked round-bottom flask was charged with 2.42 g Brij-35 (3 mmol) and 60 mL cyclohexene. The mixture was stirred at 323 K for 30 min or until complete dissolution of Brij-35. Then 2 mL ammonium heptamolybdate (AHM) solution (0.1M) was added and reaction mixture was stirred for 1 h. 4.8 mL 27% ammonium hydroxide solution was added after complete dissolution of Brij-35 in cyclohexane. To this solution, 4 g TEOS was added slowly and allowed to stir for additional 2 h. The reaction was quenched by addition of 40 mL *iso*-propanol followed by ultrasonication for 5 min. The final AHM on SiO₂ nanosphers were collected by centrifugation (5000 rpm for 10 min). The precipitate was washed with 40 mL each IPA and methanol and dried at room temperature and then calcined at 773 K for 5 h under air to get MoO₃/SiO₂.

2.2.2. Synthesis of MoO₃/TiO₂. In a typical synthesis, 250 mL two necked round-bottom flask was charged with 2.42 g Brij-35 (3 mmol) suspended in 60 mL cyclohexane and the flask was stirred at 323 K for 30 min until Brij-35 was completely dissolved. Then 2 mL ammonium heptamolybdate solution (0.1M) was added and reaction mixture was stirred for 1h. After this 2 mL distilled water was added slowly and again stirred for 15 min and 5.2 g titanium (IV) butoxide was slowly added and allowed to stir for another 2 h. The reaction was quenched by addition of 40 mL *iso*-propanol and ultrasonication for 5 min. The final AHM on titania nanoparticles were collected by centrifugation (5000 rpm for 5 min). The precipitate was washed with 40 mL each of IPA and methanol and dried at room temperature and then calcined at 773 K for 5 h under air which gave MoO₃/TiO₂.

2.2.3. Synthesis of MoO₃/ZrO₂. In a typical synthesis, 250 mL two necked round-bottom flask was charged with 2.42 g Brij-35 (3 mmol) suspended in 60 mL cyclohexane and the flask was stirred at 323 K for 30 min to until Brij-35 completely dissolved. Then 2 mL ammonium heptamolybdate solution (0.1M) was added and reaction mixture was stirred for 1h. After this 2.0 mL distilled water was added slowly and again stirred for 15 min and 4 g zirconia(IV) butoxide slowly added and allowed to stir for another 2 h. The reaction was quenched by addition of 40 mL *iso*-propanol and ultrasonication for 5 min. The final AHM on zirconia nanosphers were collected by centrifugation (5000 rpm for 5 min). The precipitate was washed with 40 mL each of IPA and methanol and dried at room temperature and then calcined at 773 K for 5 h under air which gave MoO₃/ZrO₂.

2.2.4. Catalyst Characterization

A. Powder X-ray Analysis. X-ray diffractograms were recorded using a Rigaku X-ray diffractometer (Model DMAX IIIVC) using CuKa (1.5406 Å) radiation from 2θ=10 to 80º by 4º steps with an integration time of 4 s.

B. Raman Analysis. Raman spectra were recorded under ambient conditions on a LabRAM infinity spectrometer (Horiba–Jobin–Yvon) equipped with a liquid nitrogen detector and a frequency doubled Nd-YAG laser supplying the excitation line at 532 nm with 1–10 mW power. The spectrometer is calibrated using the Si line at 521 cm^{-1} with a spectral resolution of 3 cm^{-1}.

C. Electron Microscopy. Scanning electron microscopy (SEM) measurements were performed on a FEI quanta 200 3D dual beam (ESEM) having thermionic emission tungsten filament in the 3 nm range at 30 kV and HRTEM was done on a Tecnai G2-30 FEI instrument operating at an accelerating voltage of 300 kV. Before analysis, the powders were ultrasonically dispersed in *iso*-propanol, and two drops of *iso*-propanol containing the solid were deposited on a carbon coated copper grid for TEM analysis.

D. FT-IR Spectroscopy. The types of acidity present on the sample was determined by adsorption of pyridine on the sample and surface adsorption was monitored by Shimadzu 8000 series FTIR spectrometer in the diffuse reflectance infrared Fourier transform (DRIFT) mode. For pretreatment, the sample was placed in the DRIFT cell and heated to 673 K under the flow of inert gas (N_2) for 2 h. After cooling to 373 K, pyridine was introduced in an N_2 flow. The physisorbed pyridine was first removed by flushing the cell with N_2 for 45 min, and then spectrum was recorded. Then, pyridine was desorbed at 373, 423, 473 and 573 K for 45 min and spectra were recorded at each temperature. The spectrum of the neat catalyst (before pyridine adsorption) at 373 K was subtracted from the obtained spectrum at each temperature.

 E. Acidity Measurements. The NH_3-TPD experiments were performed using a Micromeritics Autochem 2910 instrument. A weighed amount of the sample (~100 mg) was placed in a quartz reactor, pretreated in a flow of He gas at 773 K for 1h (ramp rate of 10 K/min) and cooled to 373 K. The catalyst was then exposed to a gas mixture of NH_3 (5% NH_3–95% He, 50 mL/ min) at 373 K, followed by evacuation at 373 K for 3h. Then, the measurement was carried out from 373 K to 973 K with a heating rate of 5 K/min in He as a carrier gas at a flow rate of 60 mL/min until ammonia was desorbed completely.

F. BET Surface Area Measurement. N_2 adsorption–desorption isotherms were

recorded at 77 K by using an automated quantasorb instrument from quantachrome. Before each run, a known mass of sample (around 0.2 g) was heated at 423 K under vacuum for 2.5 h. Specific surface areas were calculated from the linear part of the Brunauer–Emmett–Teller line. Pore-size distributions were obtained by applying the Barrett–Joyner–Halenda (BJH) equation to the desorption branch of the isotherm. The total pore volume was estimated from the N_2 uptake at a P/P_0 value of 0.991.

G. X-ray Photoelectron Spectroscopy Study. X-ray photoelectron spectroscopy (XPS) was used for the characterization of surface of fresh catalysts. XPS experiments were performed using ESCA 3000 spectrometer equipped with magnesium source for excitation in the analysis chamber under ultra high vacuum (10^{-10} Torr). Binding energy (B.E.) values were referenced to the binding energy of the Al 2p core level (74.6 eV).

H. Typical Reaction Procedure. The liquid phase catalytic oxidation was carried out in a 25 mL two necked round bottom flask equipped with a magnetic stirrer and immersed in a thermostat oil bath. The flask was charged with olefin (2.5 mmol), oxidant, (2.5 mmol) TBHP in decane, 0.02 g catalyst and 1, 2-dichloroethane (6 g) as a solvent. The samples were withdrawn periodically and analysed on Agilent 6890 Gas chromatograph equipped with a HP-5 dimethyl polysilaxane column (60 m length, 0.25 mm diameter and 0.25 µm film thicknesses) with flame ionization detector. Products were confirmed by GC-MS 6890N.

2.3. Results and Discussion

Ultrasmall molybdenum oxide nanoparticles supported on various SiO_2, TiO_2 and ZrO_2 nanosphers were synthesized in one pot by following previously reported method with slight modifications (scheme-2.1).[15] Briefly, Brij-35 was dispersed in cyclohexane by stirring at 323 K. After the formation of homogeneous solution, ammonium heptamolybdate (AHM) solution was added into it, this results into the formation of oil in water (o/w) micro emulsion. In this process Brij molecules act as an amphiphilic molecule and water droplet formed act as nanoreactor for synthesis of MoO_3 nanoparticles in the bulk oil phase. [28] To the same reaction mixture ammonium hydroxide solution was added followed by tetraethyl orthosilicate (TEOS) to form silica nanosphers. After calcination final sample was named as MoO_3/SiO_2. Similarly, titanium(IV) butoxide and zirconium(IV) butoxide were used as TiO_2 and ZrO_2 precursor for synthesis of MoO_3 nanoparticles supported on TiO_2 and ZrO_2

nanospheres and named as MoO_3/TiO_2 and MoO_3/ZrO_2 respectively.
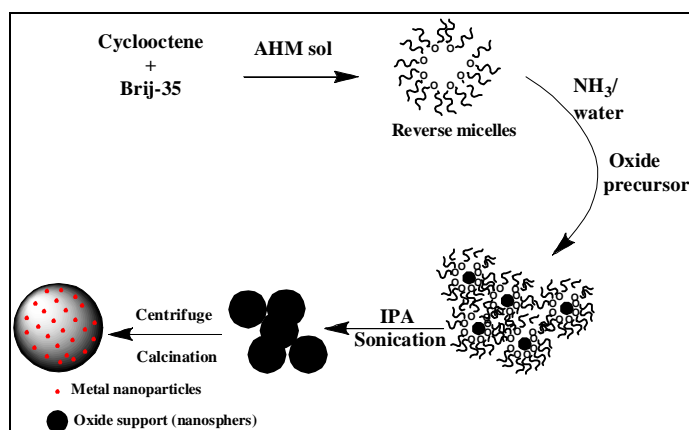
Scheme 2.1: Schematic representation of the stepwise synthesis of MoO_3/MO_2 (M= Si, Ti or Zr) nanospheres by reverse micelle method.

The prepared catalysts were fully characterized for their physiochemical properties. The formation of nanospheres and dispersion of MoO_3 nanoparticles on to the oxide support was characterized by transmission electron microscopy (TEM) (Fig. 2.1). In case of MoO_3/SiO_2, it was found that SiO_2 nanospheres formed were very well mono-dispersed nanospheres and in the range of 275 nm size. The nanospheres size is far bigger than the reported method. [15] Wang *et al.* used Brij-58 and obtained 23 nm size silica spheres and in the present work using Brij-35, much bigger silica spheres were obtained, which can accommodate not only large number of MoO_3 nanoparticles but also easy to separate from reaction mixture. After careful analysis by HRTEM, the MoO_3 nanoparticles were found to be of 2.5 nm size having d-spacing of 0.35 nm for (021) plane of α-MoO_3.[15b] Also MoO_3 nanoparticles were monodispersed onto the surface of silica nanospheres. SEM metal mapping of the same samples supported the fact of uniform dispersion of MoO_3 nanoparticles on silica surface (See Fig. 2.2 A). Yellow spots in the Fig. 2.2 B represent molybdenum nanoparticles on silica surface. Furthermore, the EDAX analysis showed MoO_3 loading to be 12.48 wt%, on the silica nanospheres.

HRTEM analysis of MoO_3/TiO_2 and MoO_3/ZrO_2 samples (See Fig. 2.3 and 2.5) showed the formation of uniform titania and zirconia nanospheres. The size of spheres was about 10.5 nm and 6.5 nm respectively with d-spacing for 0.357 nm for (101) plane of titania and 0.318 nm for (101) plane for tetragonal zirconia.[15c-15d] No separate MoO_3 particles were identified from TEM in MoO_3/TiO_2 and MoO_3/ZrO_2. This may be due to reaction of AHM with titanium and zirconium hydroxides forming

solid solution hence no separate molybdena particles were observed. The nanosphers formed are far smaller than the silica. In the case of TEOS, the alkoxide is more stable, resulting into slower rate of hydrolysis and slower nucleation and crystal growth, hence formation of bigger particles in the range of 250 to 300 nm. Whereas in case of zirconia and titana the alkoxide precursor, zirconium(IV) butoxide and titanium(IV) butoxide are less stable, resulting in fast hydrolysis and nucleation, hence formation of smaller nanoparticles in the range of 5 to 20 nm. EDAX analysis revealed that MoO_3 content was 9.85% and 9.57% on zirconia and titania nanosphers respectively.
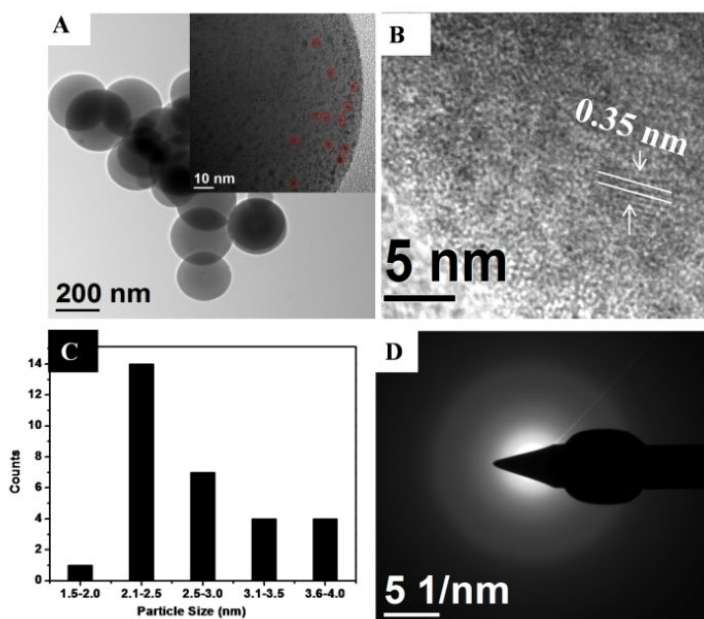
Fig. 2.1: HRTEM image of MoO_3/SiO_2 at (A) 200 nm scale; inset image shows magnified image at 10 nm scale; (B) d-spacing of (021) plane of α-MoO_3 nanoparticles on MoO_3/SiO_2 surface. (C) Particle size distributions and (D) SAED pattern of MoO_3/SiO_2.

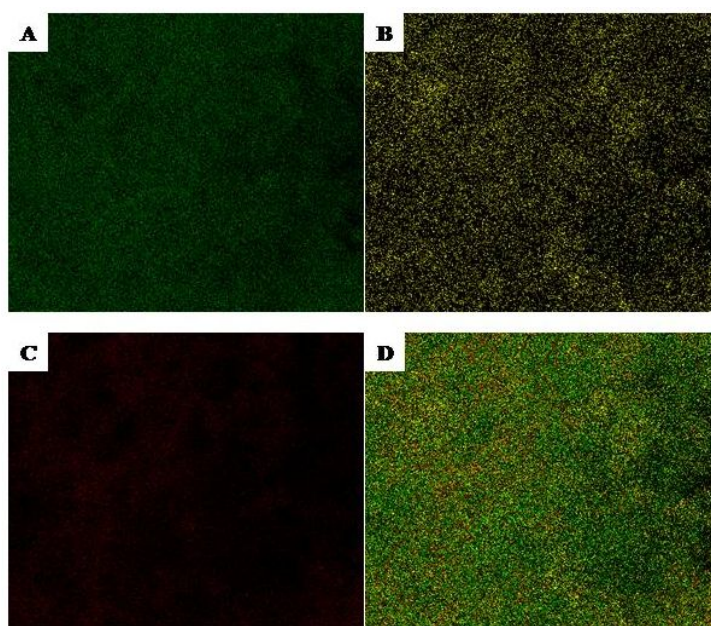**Fig. 2.2:** Showing elemental mapping of the MoO_3/SiO_2 surface by SEM; (A) green colour showing Si content; (B) yellow colour shows molybdenum atoms; (C) red colour represents oxygen atoms present on surface and (D) MoO_3/SiO_2 on the surface.

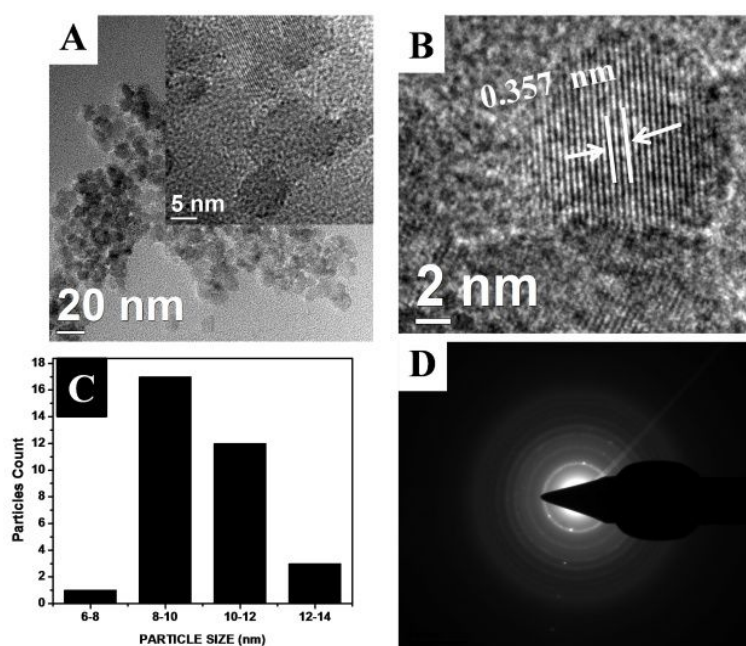**Fig. 2.3:** HRTEM image of MoO_3/TiO_2 at (A) 20 nm scale; inset image shows magnified image at 5 nm scale; (B) d-spacing for MoO_3/TiO_2 nanoparticles at (101) plane of titania; (C) Particle size distributions and; (D) SAED pattern of MoO_3/TiO_2.
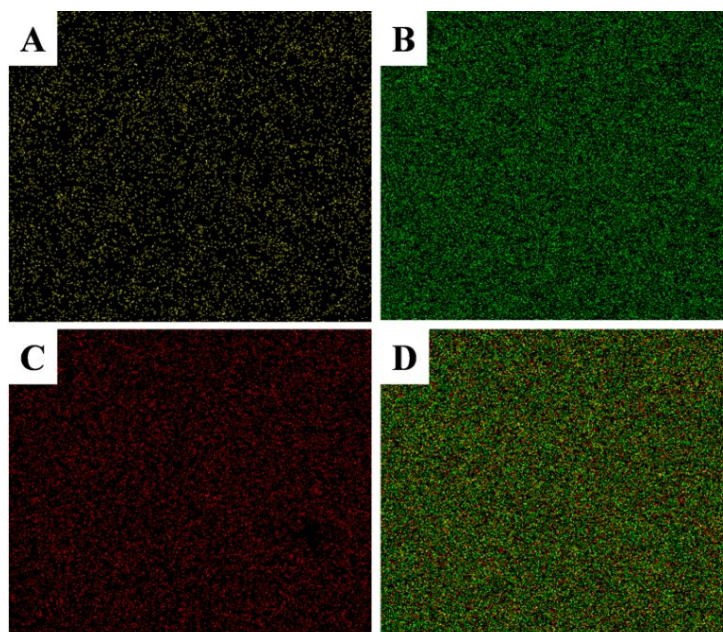
Fig. 2.4: Showing elemental mapping of the MoO_3/TiO_2 nanosphers; (A) yellow colour shows molybdenum atom; (B) green colour shows titania atoms; (C) red colour shows oxygen atoms present on surface and (D) MoO_3/TiO_2 on the surface.

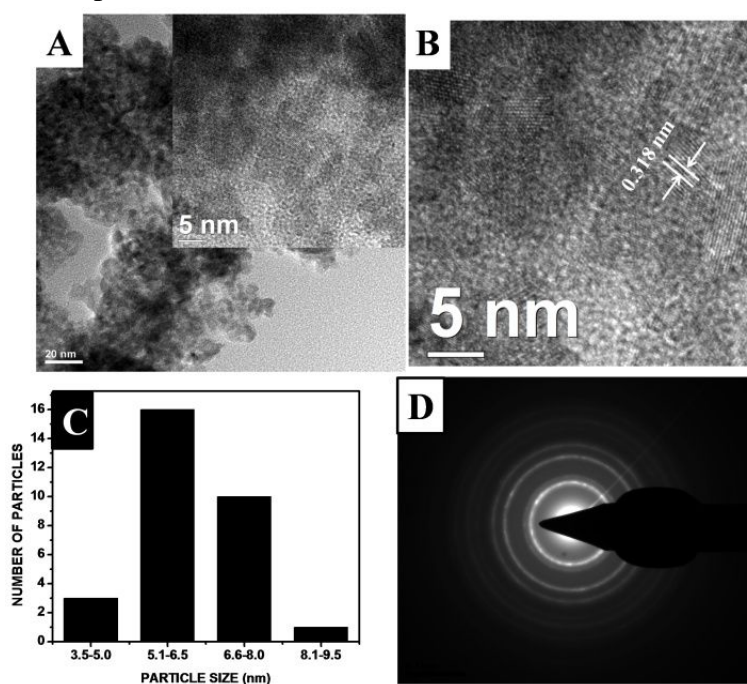**Fig 2.5:** HRTEM image of MoO_3/ZrO_2 at (A) 20 nm scale; inset image shows magnified image at 5 nm scale; (B) d-spacing for (101) plane of tetragonal ZrO_2; (C) Particle size distributions and (D) SAED pattern of MoO_3/ZrO_2.
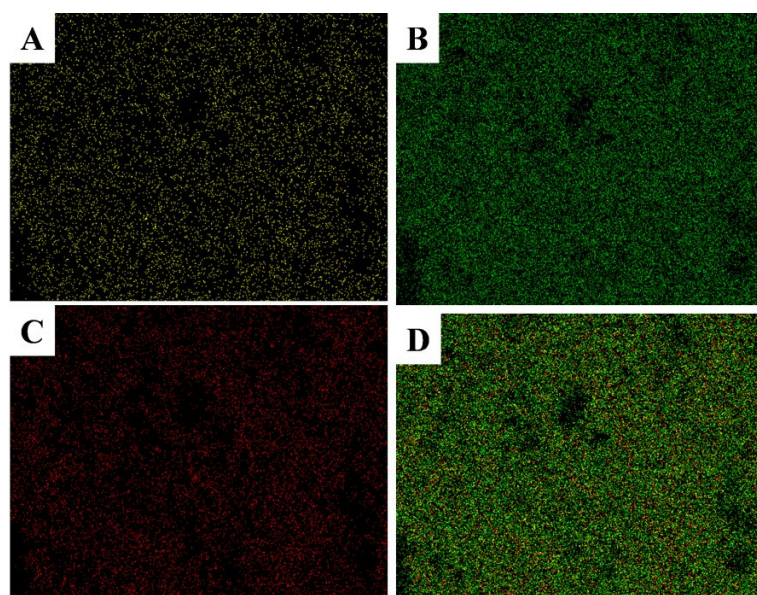
Fig 2.6: Showing elemental mapping of the MoO_3/ZrO_2 synthesized nanosphers; (A) yellow colour shows molybdenum content; (B) green colour shows zirconia atoms; (C) red colour shows oxygen atoms present on surface and (D) MoO_3/ZrO_2 on the surface.

The crystinility and phase purity was examined by powder X-ray diffraction (Fig 2.7). The MoO_3 nanoparticles dispersed on the silica nanosphers (Fig 2.7 A) showed the sharp Bragg reflection peaks at 2θ = 12.7 (020), 23.4 (110), 25.7 (040) and 27.4° (021) characteristic of α-MoO_3 orthorhombic phase with crystalline nature (JCPDS No. 05-0508).[15],[17],[29] The bulk structure of pure ZrO_2 and supported MoO_3/ZrO_2 was determined by X-ray diffraction (Fig 2.7 B). Broad XRD peaks observed are due the small size of the zirconia nanoparticles. Four diffraction peaks in the 2θ range of 20-40° were detected at 24.2°, 28.3°, 31.3°, and 34.3° with a shoulder at 35.4°. These are attributed to monoclinic ZrO_2 structures (JCPDS card no. 37- 1484). (Fig 2.7 C) However in case of MoO_3/ZrO_2, the XRD pattern showed broad peaks at 2θ = 30.3°, 35.3°, 50.4° and 60° indicating the formation of exclusively tetragonal zirconia phase.[30] Appearance of peaks at 30.3°, 35.3° and 50.4° indicated the formation of $Zr(MoO_4)_2$ species and confirms strong interaction between molybdena and zirconia.[31-33] Hence no separate MoO_3 phase was observed in XRD.
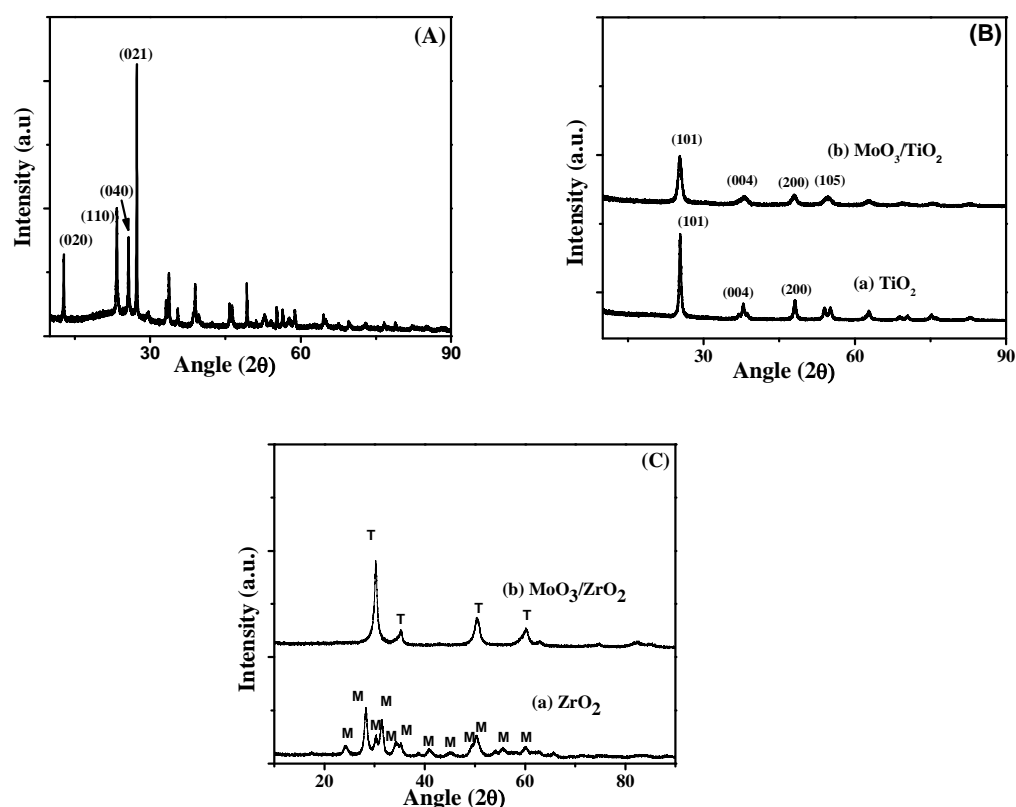
Fig 2.7: Powder XRD pattern of (A) MoO_3/SiO_2; (B) (a) TiO_2 and MoO_3/TiO_2; (C) (a) ZrO_2 and MoO_3/ZrO_2 nanosphers.

In case of MoO_3/SiO_2, the MoO_3 nanoparticles formed during the interactions with Brij get dispersed on silica nanospheres and forms bulk MoO_3 which is seen in XRD (Fig. 2.7 A). MoO_3/TiO_2 showed characteristic peaks for anatase TiO_2 phase (JCPDS No. 21-1272).[34] In case of MoO_3/TiO_2 and MoO_3/ZrO_2 system MoO_3 nanoparticles initially formed with Brij treatment react with titanium and zirconium hydroxides forming solid solutions with TiO_2 and ZrO_2, henceforth uniformly dispersed as amorphous MoO_3 and are not seen as bulk crystalline MoO_3 in XRD.

Furthermore, the structure of molybdenum supported on various oxide supports was examined using Raman spectroscopy (Fig. 2.8). The Raman spectrum of MoO_3/SiO_2 (Fig. 2.8 A) showed bands around 998 cm^{-1} due to terminal M=O stretching mode. The band at 819 cm^{-1} was due to bulk MoO_3 species. A small and broad peak in the range 660 cm^{-1} and 270-280 cm^{-1} was due to Mo-O-Mo asymmetric stretching and deformation respectively.[17],[29] Remaining bands were in agreement with α-MoO_3 species present on the SiO_2 surface.[35]
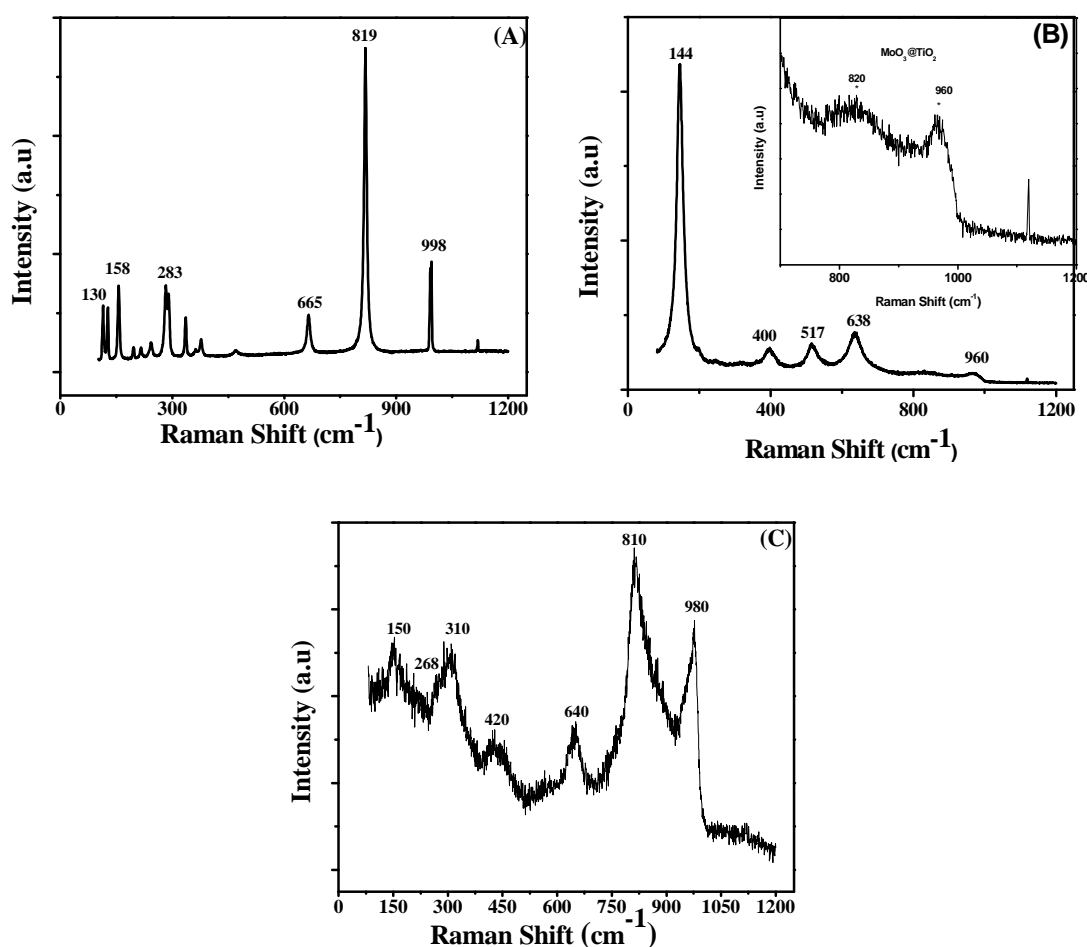
Fig 2.8: Raman spectra of (A) MoO_3/SiO_2; (B) MoO_3/TiO_2; inset graph shows expanded view in range the 700 - 1200 cm^{-1} and (C) MoO_3/ZrO_2.

Raman spectrum of MoO_3/TiO_2 (Fig. 2.8 B) clearly showed the formation of anatase phase, due to the appearance of peaks in the region 144, 400, 517 and 638 cm^{-1}. A broad band around 960 cm^{-1} clearly represents the formation of well dispersed polymolybdate species on the titania surface. Raman spectrum of MoO_3/ZrO_2 (Fig. 2.8 C) showed tetragonal ZrO_2 at 150, 268, 310, 420, 600 (shoulder), and 640 cm^{-1}. The bands around 810 cm^{-1} and 980 cm^{-1} of MoO_3/ZrO_2 were due to Mo-O-Mo vibrations and Mo=O stretching frequency respectively.[36-37], [33] To determine the quantitative analysis of Mo=O to Mo-O-Mo content present in molybdenum supported on oxide was determined using following formula.[38]

$$fm = \sqrt{0.19 - \frac{0.13}{Xm - 1.01}} - 0.56 \quad (1)$$

Here X_m = I $_{Mo=O}$ /{I $_{Mo=O}$ + I $_{Mo-O-Mo}$ }, m is Mo=O or Mo-O-Mo and fm represents

the Mo=O or Mo-O-Mo content present in catalyst. The Mo-O-Mo/Mo content for MoO_3/SiO_2 was 6.5, MoO_3/ZrO_2 was 1.31 and MoO_3/TiO_2 was 1.14.

The presence of Lewis and Brönsted acidic sites was determined by FTIR of studied of adsorbed pyridine. MoO_3/SiO_2 did not show any peak at 1445 or 1540 cm^{-1} for Lewis and Brönsted acidity after adsorption of pyridine indicating very weak acidity. However MoO_3/TiO_2 and MoO_3/ZrO_2 showed peak at 1447 cm^{-1} and 1540 cm^{-1} indicating presence of Lewis as well as Brönsted acidity. MoO_3/TiO_2 showed stronger peak for Brönsted acidity (1540 cm^{-1}) where as MoO_3/ZrO_2 showed stronger peak for Lewis acidity (1447 cm^{-1}) as shown in Fig. 2.9. [39]

To determine total acidity and the acid strength of the molybdenum nanoparticles dispersed on various oxide nanosphers, NH_3-temperature programmed desorption (TPD) was carried out. MoO_3/SiO_2, MoO_3/TiO_2 and MoO_3/ZrO_2 (Fig 2.10 (A), (B) and (C)) showed one signal below 673 K. Total acidity of the all the supported molybdenum catalysts was in the order MoO_3/TiO_2 (0.45 mmol/g) $\approx$ MoO_3/ZrO_2 (0.45 mmol/g) > MoO_3/SiO_2 (0.196 mmol/g).
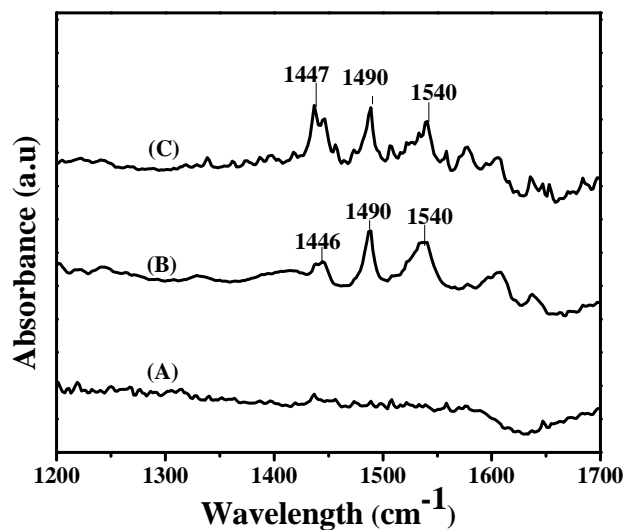
Fig 2.9: Pyridine adsorption spectra of (A) MoO_3/SiO_2; (B) MoO_3/TiO_2 and (C) MoO_3/ZrO_2 at 100 °C.
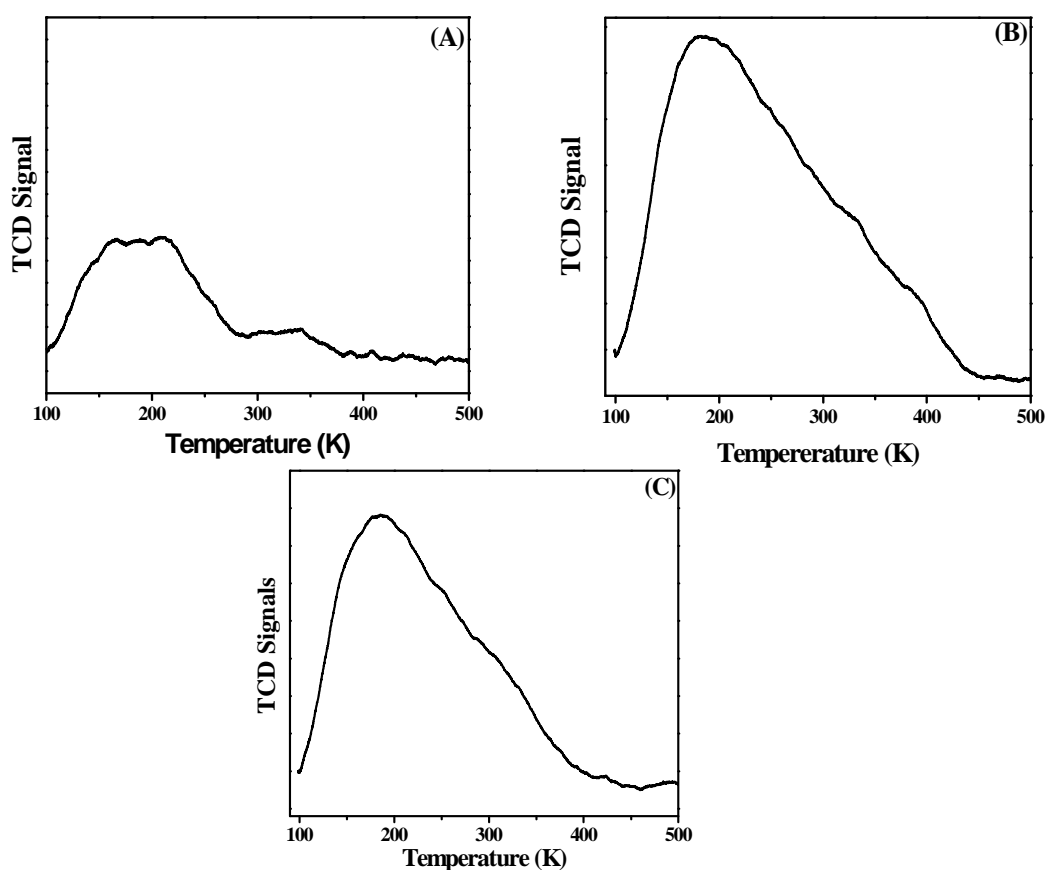
Fig 2.10: NH$_3$-TPD profile for (A) MoO$_3$/SiO$_2$; (B) MoO$_3$/TiO$_2$ and (C) MoO$_3$/ZrO$_2$

XPS spectroscopy was used to obtain the elemental composition, chemical and electronic state of molybdenum on oxide support. All the binding energies were calibrated using the C 1s peak at 284.6 eV. XPS analysis of MoO$_3$/SiO$_2$ shows peak at 232.7 eV and 235.9 eV due to Mo 3d$_{5/2}$ and Mo 3d$_{3/2}$ of Mo(VI) in MoO$_3$, respectively. The single peak of Si 2p with binding energy of 102.8 eV corresponds to Si(IV) in SiO$_2$ (See Fig. 2.11).

XPS spectra of MoO$_3$/TiO$_2$ showed peaks at 3d$_{5/2}$ and 3d$_{3/2}$ at 232.9 eV and 235.9 eV due to presence of Mo(VI) species. Peaks around 458.9 eV and 464.5 eV were due Ti (IV) of 2p $_{3/2}$ and Ti 2p $_{1/2}$ respectively. (Fig. 2.12) XPS spectra of MoO$_3$/ZrO$_2$ showed peak at 232.9 eV and 235.9 eV corresponding to Mo(VI) of Mo3d $_{5/2}$ and Mo 3d $_{3/2}$ present in MoO$_3$. Zr 3d $_{5/2}$ and Zr 3d $_{3/2}$ showed peaks at 182.6 eV and 184.9 eV (Fig. 2.13).
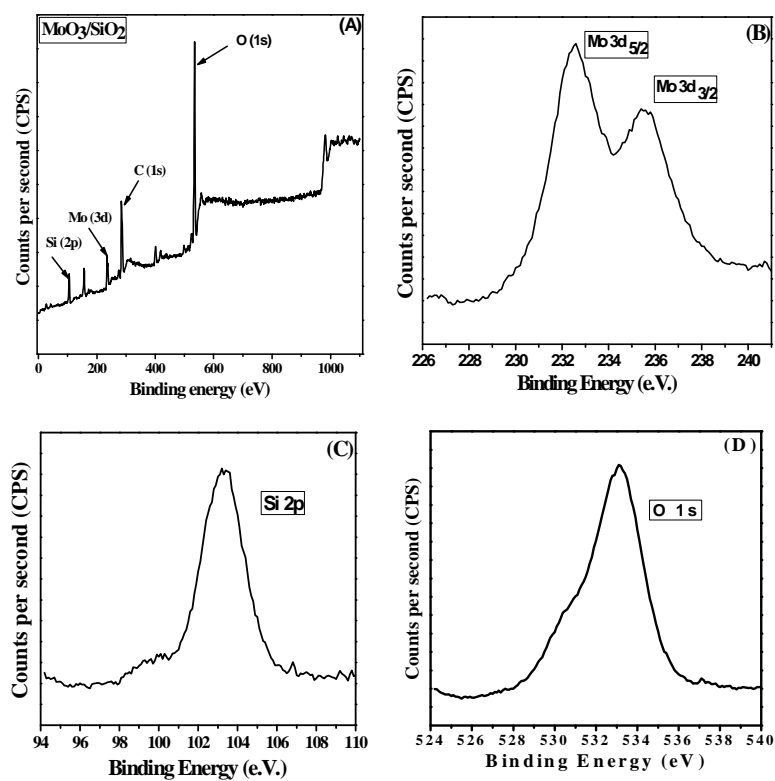
Fig 2.11: XPS spectra of (A) survey mode of MoO$_3$/SiO$_2$; (B) Mo present in MoO$_3$/SiO$_2$; (C) Si 2p; (D) O1s.
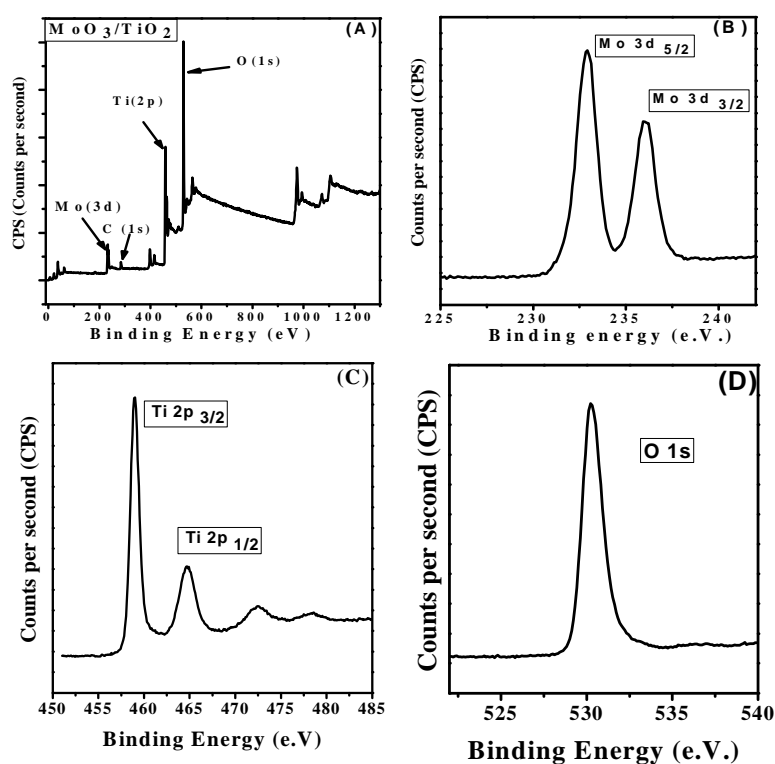

Fig 2.12: XPS spectra of (A) survey mode of MoO$_3$/TiO$_2$; (B) Mo present in MoO$_3$/TiO$_2$; (C) Ti 2p and (D) O 1s
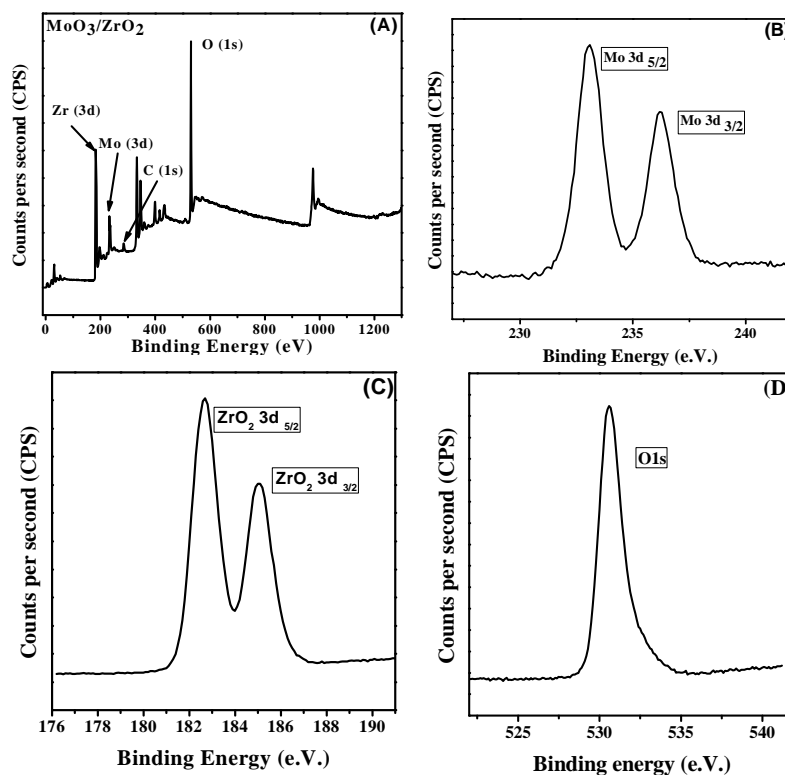
Fig 2.13: XPS spectra of (A) survey mode of MoO_3/ZrO_2; (B) Mo present in MoO_3/ZrO_2; (C) Zr $3d_{5/2}$ and; (D) Zr $3d_{3/2}$

The Brunauer–Emmett–Teller (BET) surface area and pore diameters of the molybdena on different oxide supports was determined by N_2 adsorption measurements (See Fig. 2.14). All the samples showed a type-IV isotherm and the presence of mesoporosity on the catalyst surface having pore diameter in the range 20 to 500 Å. Surface area of MoO_3/SiO_2 was found to be 22.8 m^2/g.

The total pore volume and average pore diameter were found to be 0.009982 cc/g and 33.4950 Å. Whereas surface area of MoO_3/TiO_2 was found to be 89.1 m^2/g. The total pore volume was 0.09281 cc/g and average pore diameter was about 20.8203 Å. MoO_3/ZrO_2 had surface area of 139.6 m²/g with total pore volume and average pore diameter were found to be 0.2494 cc/g and 34.7939 Å. The surface area of the materials decreased in the order $MoO_3/ZrO_2 > MoO_3/TiO_2 > MoO_3/SiO_2$.
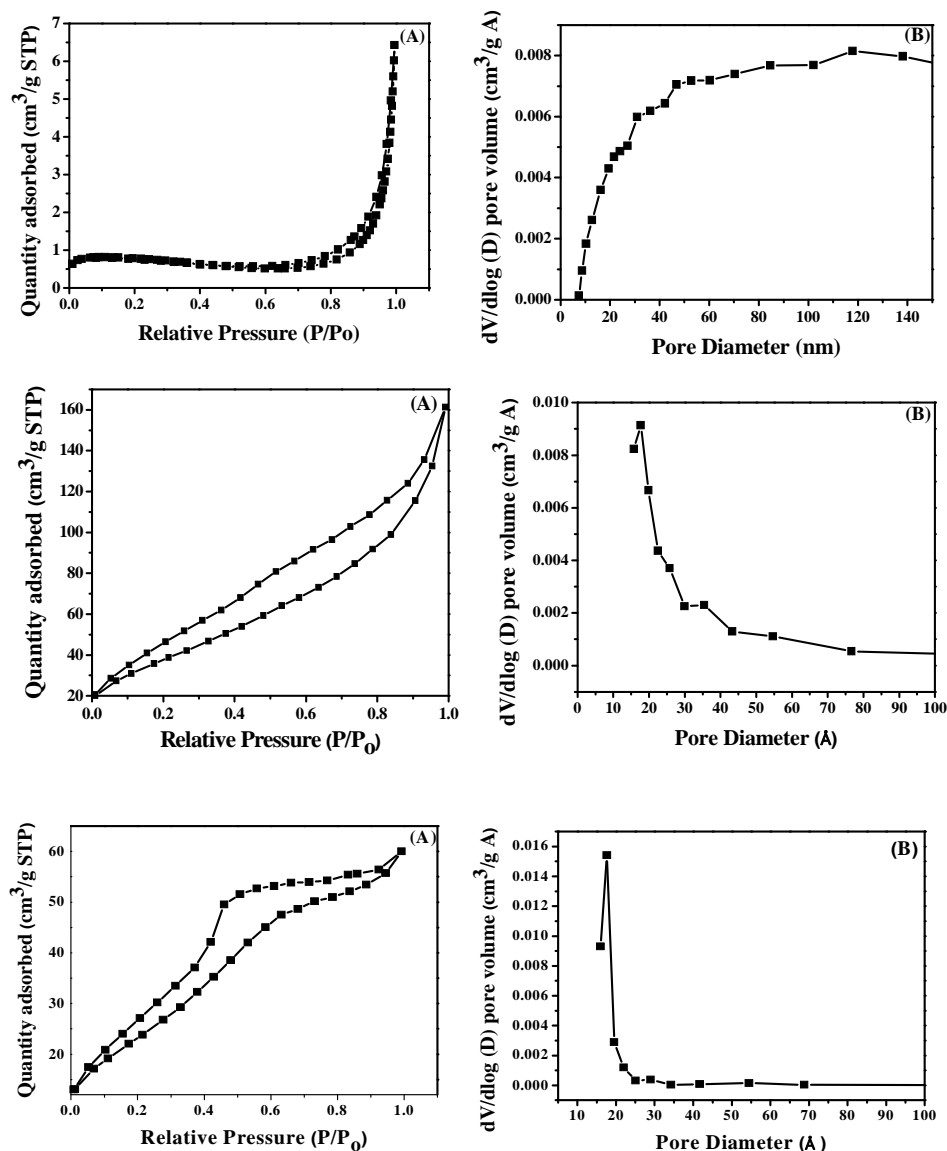
Fig 2.14: (A) BET surface area isotherms and (B) pore size distribution curve for MoO$_3$/SiO$_2$; MoO$_3$/TiO$_2$; and MoO$_3$/ZrO$_2$ respectively

2.4. Catalytic Reactions

       The catalytic activity of the prepared MoO$_3$ nanoparticles supported on different nanospheres was tested by selecting cyclooctene as a probe reactant and TBHP as an oxidant (scheme-2.2). First, the reaction was carried out without catalyst to check the oxidation capabilities of the oxidant (TBHP) itself; and only 12% cyclo-octene conversion was obtained after stirring the reaction mixture at 353 K for 2 h, with cyclooctene epoxide as the sole product (Table 2.2 entry 1).
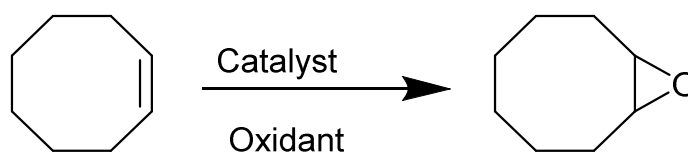
Scheme 2.2: Represents the oxidation of cyclooctene.

       Furthermore, when MoO_3/SiO_2 was used as catalyst and 1:1 substrate to oxidant ratio, it gave 90% cyclooctene conversion and 100% selectivity to cyclooctene epoxide within 2 h reaction time with TOF 72.3 h^{-1}. Furthermore, MoO_3 nanoparticles supported on both zirconia and titania nanosphers were used as catalyst under same reaction condition. In the case of MoO_3/TiO_2 as a catalyst it gave 37% conversion of cyclocetene with 100% selectivity for epoxide. MoO_3/ZrO_2 catalyst gave only 39.6% conversion of cyclooctene in 2 h and 100% epoxide selectivity. These results clearly indicated that MoO_3/SiO_2 nanosphers gave the best results considering catalytic activities of all the catalysts. The higher activity may be attributive to the presence of large number of MoO_3 oxide nanoparticles on the surface of silica nanosphers and are not available in the case of ZrO_2 and TiO_2 nanosphers.
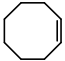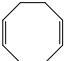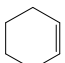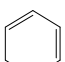
Table 2.2: Results of epoxidation of cyclooctene using MoO_3 nanoparticles dispersed onto the different nanosphers as a catalysts

Entry	Catalyst	% Conv.	% Epoxide Sel.	TOF $h^{-1\#}$
1.	Blank[b]	12	100	-
2.	MoO_3/SiO_2	90	100	122.7
3.	MoO_3/TiO_2	37	100	51.7
4.	MoO_3/ZrO_2	39.6	100	38.3

[a]**Reaction condition:** Cyclooctene: 0.282 g (2.5 mmol); Oxidant: 5.5 molar TBHP in decane (2.5 mmol); Catalyst: 0.028 g; Temperature: 353 K; Solvent: 1, 2-dichloroethane (6 g); Time-2 h; [b]: Without catalyst. [#] TOF calculated after 1 h.

Furthermore, we studied the substrate scope by selecting other olefins using MoO_3/SiO_2 nanosphers. When cyclooctene was used as substrate it gave very high conversion and selectivity for epoxides (Table 2.3 entry 1). When cyclooctadiene was oxidized it gave 74% conversion with mono and di-epoxide as product (Table 2.3 entry 2). However cyclohexene gave poor conversion in 2 h (Table 2.3 entry 3). Further extending the reaction time it gave 90% conversion in 6 h with 90% selectivity to epoxide. When cyclohexadiene was used as substrates it gave 70% conversion and 58% and 42% selectivity to mono and di-epoxide respectively.

Table 2.3: Results of epoxidation of other olefins using MoO_3/SiO_2 nanosphers as catalyst

Entry	Substrates	% Conv.	% Epoxide Sel.	TOF $h^{-1\#}$
1.		90	100	72.3
2.		74	85.3, 14.6[*]	61.7
3.		44 90[@]	100 90	49.5
4.		70	58.3, 41.7[$]	78.7

Reaction conditions: Substrates: 2.5 mmol; Oxidant: 5.5 molar TBHP in decane (2.5 mmol); Catalyst: 10 wt% of substrates; Temperature: 353 K; Solvent: 1,2-dichloroethane (6 g); Time-2 h; [#] TOF calculated after 2 h..[@] 6h reaction time * 5,10-dioxatricyclo[7.1.0.04,6]decane; $ 3,8dioxatricyclo[5.1.0.02,4]octane

These results are in line with the reported methods, for instance Arnold *et al.* [26] used acid catalysed sol-gel synthesis of MoO_3/SiO_2 taking Mo (V)-isopropoxide as molybdenum precursor for olefin epoxidation. Bakala and co-workers [40] have

reported the olefin epoxidation using molybdenum supported on mesoporous silica (MCM-41, SBA-15). TBHP was taken as oxidant in a molar ratio three times as compared to the cyclooctene. They obtained 97% conversion and 95% epoxide selectivity using decane as solvent at 40 ^{o}C in 3 h. However, both the catalysts showed leaching of the active species after three recycles, and the problem of catalyst leaching was persistent as in the previous cases.

Furthermore, the best catalyst i.e. MoO_3/SiO_2 nanosphers was used to check the reusability for epoxidation reaction. After each reaction cycle the catalyst was separated by centrifugation and washed with solvent and used for next run. There was no considerable decrease in conversion and epoxide selectivity was found even after five cycles (See Fig. 2.15). TEM investigations also showed no change in shape and size of MoO_3 and silica nanosphers. Particle size after fifth cycle was found to be around 2.5 nm which was similar to the fresh catalyst (Fig. 2.16).
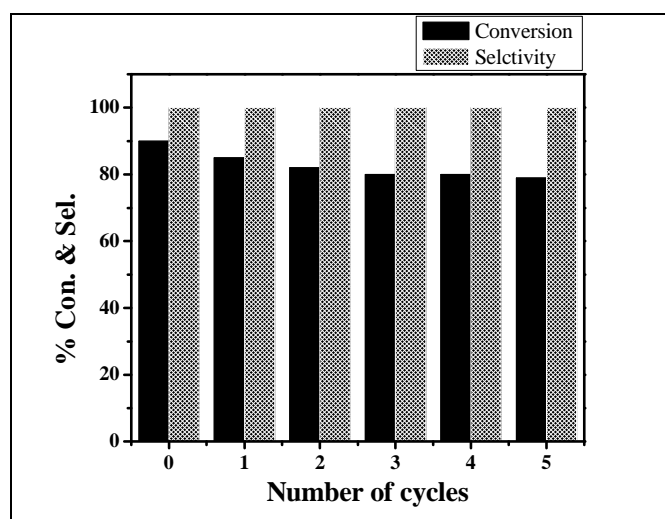
Fig 2.15: Represents the catalytic recycle study for cyclooctene epoxidation using MoO_3/SiO_2 nanosphers as a catalyst.
Reaction condition: Cyclooctene: 0.285 g (2.5 mmol); Oxidant: (2.5 mmol) 5.5 molar TBHP in decane; Temperature: 353 K; Solvent: 1, 2-dichloroethane (6 g); Catalyst: 0.028 g; Time-2 h

Leaching test was carried out using hot filtration experiment and results are shown in Fig. 2.17. After 1 h. reaction time, the reaction was stopped and catalyst was removed from reaction media by centrifugation and supernatant was allowed to react further without catalyst. It gave only additional 12% conversion in 1 h. which may be due to thermal reaction catalysed by TBHP, as shown in blank reaction (table 2.2

entry 1). This indicated that the reaction is truly catalyzed by MoO_3 nanoparticles supported onto the surface of silica nanosphers.
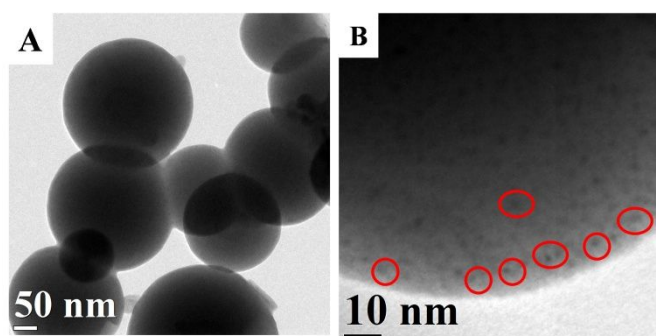
Fig 2.16: (A and B) represents the HRTEM image of spent catalyst MoO_3/SiO_2 at 50 nm and 10 nm scale.
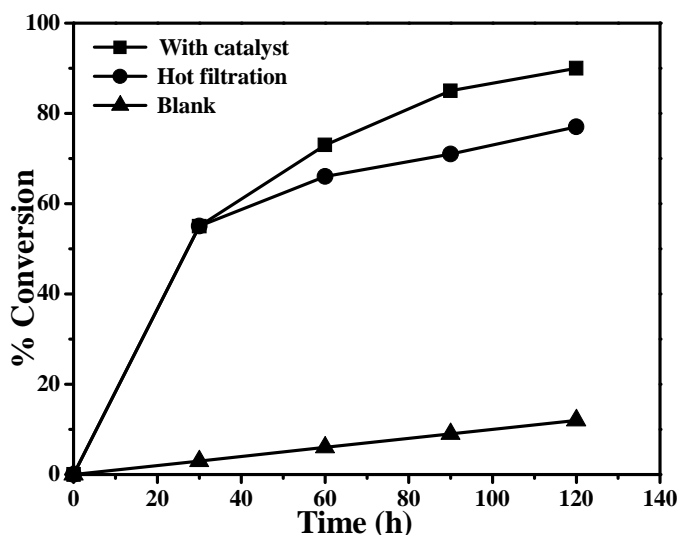
Fig 2.17: % cyclooctene conversion vs. time curve; in the catalytic, hot filtration and blank reactions.
Reaction condition: Cyclooctene: 0.282 g (2.5 mmol); Oxidant: (2.5 mmol) 5.5 molar TBHP in decane; Temperature: 353 K; Solvent: 1, 2-dichloroethane (6 g); Catalyst: 0.02 g; Time-2 h; no catalyst for blank reaction; catalyst removed via centrifugation after 1h and reactants were allowed to react further.

2.5. Conclusions

Reverse micelle micro-emulsion proved to be efficient method for the synthesis of ultrasmall molybdenum oxide nanoparticles with definite structure and uniform distribution over the SiO_2, TiO_2 and ZrO_2 nanosphers. These MoO_3 nanoparticles were found to be excellent olefin epoxidation catalysts and gave epoxide as an exclusive product. The particles size of MoO_3 does not seem to be very

important for conversion and selectivity. Catalyst was recyclable up to five cycles without any loss of catalytic activity or leaching of metal oxide nanoparticles from catalyst surface.

2.6. References

[1] R. Schlögl, S. B. Abd Hamid, *Angew. Chem. Int. Ed.* **2004**, *43*, 1628-1637.

[2] H. H. Kung, M. C. Kung, *Catal. Today* **2004**, *97*, 219-224.

[3] A. V. Biradar, A. A. Biradar, T. Asefa, *Langmuir* **2011**, *27*, 14408-14418.

[4] R. D. Gonzalez, T. Lopez, R. Gomez, *Catal. Today* **1997**, *35*, 293-317.

[5] Y. Wang, A. V. Biradar, C. T. Duncan, T. Asefa, *J. Mater. Chem.* **2010**, *20*, 7834-7841.

[6] F. Zaera, *Chem. Soc. Rev.* **2013**, 42, 2746-2762.

[7] L. Han, C. Zhu, P. Hu, S. Dong, *RSC Adv.* **2013**, 3, 12568-12570.

[8] A. Roucoux, J. Schulz, H. Patin, *Chem. Rev.* **2002**, *102*, 3757-3778..

[9] A. R. Tao, S. Habas, P. Yang, *Small* **2008**, *4*, 310-325.

[10] C. Burda, X. Chen, R. Narayanan, M. A. El-Sayed, *Chem. Rev.* **2005**, *105*, 1025-1102.

[11] M.-P. Pileni, *Nat. Mater.* **2003**, *2*, 145-150.

[12] N. R. Jana, L. Gearheart, C. J. Murphy, *J. Phys. Chem. B* **2001**, *105*, 4065-4067.

[13] N. Zhang, S. Liu, X. Fu, Y.-J. Xu, *J. Phys. Chem. C.* **2011**, *115*, 22901-22909

[14] P. Yang, N. Murase, M. Suzuki, C. Hosokawa, K. Kawasaki, T. Kato, T. Taguchi, *Chem. Comm.* **2010**, *46*, 4595-4597.

[15] J. Wang, X. Li, S. Zhang, R. Lu, *Nanoscale.* **2013**, *5*, 4823-4828; (b) A. Klinbumrung, T. Thongtem, S. Thongtem, *J. Nano Mat.* **2012**, *2012*, 10. (c) Z. Zhang, X. Zhong, S. Liu, D. Li, M. Han, *Angew. Chem. Int. Ed.* **2005**, *117*, 3532-3536. (d) C.-C. Chen, W.-Y. Cheng, S.-Y. Lu, Y.-F. Lin, Y.-J. Hsu, K.-S. Chang, C.-H. Kang, K.-L. Tung, *CrystEngComm* **2010**, *12*, 3664-3669

[16] C. Louis, J.-M. Tatibouët, M. Che, *J. Catal.* **1988**, *109*, 354-366.

[17] S. B. Umbarkar, T. V. Kotbagi, A. V. Biradar, R. Pasricha, J. Chanale, M. K. Dongare, A.-S. Mamede, C. Lancelot, E. Payen, *J. Mol. Catal. A: Chem.* **2009**, *310*, 150-158.

[18] S. B. Umbarkar, A.V. Biradar, S. M. Mathew, S. B. Shelke, K. M. Malshe, P. T. Patil, S. P. Dagde, S. P. Niphadkar, M. K. Dongare, *Green Chem.* **2006**, *8*, 488-493.

[19] B. S. Lane, K. Burgess, *Chem. Rev.* **2003**, *103*, 2457-2474.

[20] A. K. Yudin, *Aziridines and epoxides in organic synthesis*, Wiley-VCH, **2006**.

[21] K. A. Jørgensen, *Chem. Rev.* **1989**, *89*, 431-458.

[22] W. R. Thiel, T. Priermeier, *Angew. Chem. Int. Ed.* **1995**, *34*, 1737-1738.

[23] M. Jia, A. Seifert, M. Berger, H. Giegengack, S. Schulze, W. R. Thiel, *Chem. Mater.* **2004**, *16*, 877-882.

[24] M. Jia, A. Seifert, W. R. Thiel, *J. Catal.* **2004**, *221*, 319-324.

[25] D. Juwiler, R. Neumann, J. Blum, *Chem. Commun.* **1998**, 1123-1124.

[26] U. Arnold, R. Serpa da Cruz, D. Mandelli, U. Schuchardt, *J. Mol. Catal. A: Chem.* **2001**, *165*, 149-158.

[27] M. Shokouhimehr, Y. Piao, J. Kim, Y. Jang, T. Hyeon, *Angew. Chem. Int. Ed.* **2007**, *119*, 7169-7173.

[28] S. Santra, R. Tapec, N. Theodoropoulou, J. Dobson, A. Hebard, W. Tan, *Langmuir* **2001**, *17*, 2900-2906.

[29] T. V. Kotbagi, A. V. Biradar, S. B. Umbarkar, M. K. Dongare, *ChemCatChem* **2013**, *5*, 1531-1537.

[30] Z. Liu, Y. Chen, *J. Catal.* **1998**, *177*, 314-324.

[31] E. El-Sharkawy, A. Khder, A. Ahmed, *Micropo. Mesopo. Mater.* **2007**, *102*, 128-137.

[32] K. Chen, S. Xie, E. Iglesia, A. T. Bell, *J. Catal.* **2000**, *189*, 421-430.

[33] B. Samaranch, P. Ramírez de la Piscina, G. Clet, M. Houalla, N. Homs, *Chem. Mater.* **2006**, *18*, 1581-1586.

[34] T. V. Kotbagi, D. L. Nguyen, C. Lancelot, C. Lamonier, K. A. Thavornprasert, Z. Wenli, M. Capron, L. Jalowiecki-Duhamel, S. B. Umbarkar, M. K. Dongare, *ChemSusChem* **2012**, *5*, 1467-1473.

[35] M. Cornac, A. Janin, J. Lavalley, *Polyhedron* **1986**, *5*, 183-186.

[36] E. Djurado, P. Bouvier, G. Lucazeau, *J. Solid State Chem.* **2000**, *149*, 399-407.

[37] M. M. Mohamed, *Appl. Catal. A: Gen.* **2004**, *267*, 135-142.

[38] Z. Liu, L. Dong, W. Ji, Y. Chen, *J. Chem. Soc., Faraday Trans.* **1998**, *94*, 1137-1142.

[39] S. Xie, K. Chen, A. T. Bell, E. Iglesia, *J. Phys. Chem. B.* **2000**, *104*, 10059-10068.

[40] P. C. Bakala, E. Briot, L. Salles, J.-M. Brégeault, *Appl. Catal. A:Gen.* **2006**, *300*,91-99.

3

Synthesis and Catalytic Activity of Molybdenum oxide Supported on Silica Microspheres

---

Molybdenum oxide supported on silica microspheres were synthesized by two different methods, i.e., hydrolysis and condensation (HC) and impregnation followed by hydrolysis and condensation (IHC). The synthesized materials were characterized by various physiochemical methods such as UV-Visible, FT-IR, Raman, XRD and SEM. The UV-visible, FT-IR and Raman spectroscopy confirmed the presence of isolated MoO_6 O_h, Mo_8O_{26} O_h and polyoxo-molybdate clusters species in the molybdenum supported on silica microspheres prepared by IHC, whereas α-MoO_3 species was present in material synthesized by HC method. SEM images showed the formation of molybdenum supported on silica microspheres at low molybdenum weight loadings, whereas at high weight loading aggregation of the microspheres was observed in catalyst synthesized by HC and IHC method. These catalysts were used in olefin epoxidation then molybdenum on silica synthesized by hydrolysis condensation method has shown maximum efficiency catalyst with 91% cyclohexene conversion and 98% epoxide selectivity using 5.5 M TBHP in decane as oxidant. Furthermore the catalyst was recycled without losing much activity and selectivity.
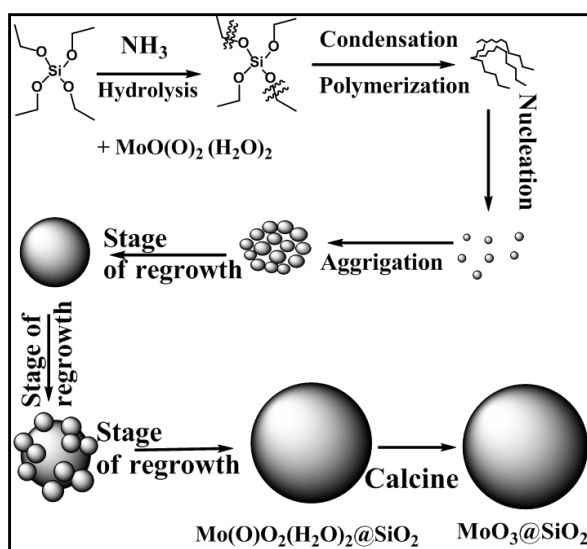
3.1. Introduction

The insertion of oxygen across carbon-carbon double bond is well known as epoxidation reaction. Olefin epoxidation is an important industrial reaction for the production of a wide variety of chemicals.[1-4] Oxirane group being highly reactive, can be used in synthesis of many organic intermediates such as drugs intermediates, agrochemicals, food additives.[5-7] Particularly, cyclohexane epoxide is very important intermediate and occurs in class of naturally occurring epoxides, which can be found in large spectrum of applications in biological activity. Therefore it has attracted considerable interest of biologist, pharmacologist and synthetic chemist.[8] The usefulness of the epoxidation reaction has been demonstrated by its effectiveness in enabling the synthesis of many interesting drug intermediates, and drug molecules such as anticapsin, paniculide, croteperoxide and basesnoxide (Fig. 3.1 A) Another very good example of naturally occurring epoxide is sex pheromone (+)-disparlure (2-methyl-7*R*,8*S*-epoxy-octadecane) found in pheromone gland of gypsy moth. The alkene precursor, 2-methyl-*Z* 7-octadecene, is most likely made in oenocyte cells associated with abdominal epidermal cells. (Fig. 3.1 B) The alkene is then transported to the pheromone gland through the hemolymph, most probably by lipophorin. At the pheromone gland, the alkene is unloaded and transformed into the epoxide disparlure for release into the environment.[9]
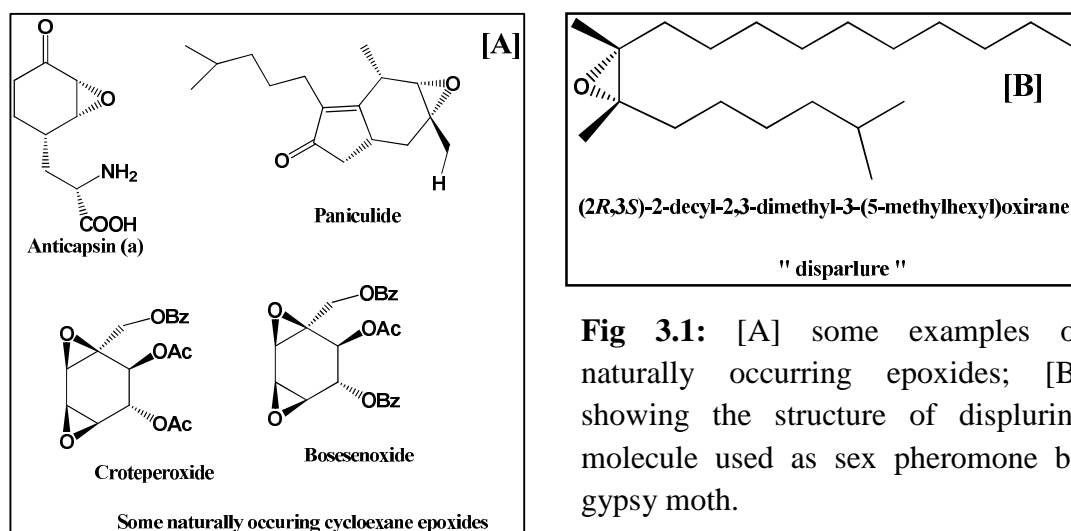
Fig 3.1: [A] some examples of naturally occurring epoxides; [B] showing the structure of displurine molecule used as sex pheromone by gypsy moth.

There are a large number of reports available in literature for catalytic and non-catalytic processes for olefin epoxidation. The most important non-catalytic processes are chlorohydrins process, application of trifloro alcohols[10] as solvent as well as catalysts for olefin oxidation with H_2O_2 as an oxidant and silica supported peracids.[11] Three membered ring compounds containing two heteroatoms such as dioxiranes, oxaziridines, and oxaziridinium[12-14] have been effectively used for olefin epoxidation. The major disadvantage from the economic point of view with these processes is that they are expensive and show poor recyclability. Schuchardt *et al.* [15] have shown that metal free sol-gel $\gamma-Al_2O_3$ to be an effective catalyst with more than 99% epoxide selectivity. But the major shortcoming of the catalyst is deactivation caused by non-radical decomposition of H_2O_2.

First metal mediated epoxidation reaction of olefin was the HALCON-ARCO process, which uses the peroxides of group 4-7 metals. [16-18] The reaction proceeds via peroxo-metal pathway and the metal centre is present in higher oxidation states.[19] Metals with low oxidation potential and high Lewis acidity in their highest oxidation states are superior catalyst with reactivity in the order Mo>W>V>Ti. Metals which readily decompose peroxides by one electron transfer such as Cu, Co, Mn and Fe are not considered as catalysts. [20-21] Furthermore to use these metals efficiently, they were supported on various supports. For example titanium containing silicates, including amorphous titania–silica materials and Ti-substituted molecular sieves are the most efficient catalysts for epoxidation reactions. [22-24] Main drawback of this catalyst is small pore diameter which makes it accessible to small reactants only and gets fast deactivated. To overcome this difficulty mesoporous and microporous materials have been developed such as titanium containing beta-zeolite which has three dimensional pore structures. [25-26] However, presence of alumina imparts Brösted acidity which leads to acid catalyzed side reactions. Somma *et al.* [27] used WoO_3/SiO_2 synthesized by sol-gel method under basic conditions for epoxidation of higher olefins such as *cis*-cycloctene, n-octene, geraniol using H_2O_2 as oxidant. Oxidation of geraniol gave 100% conversion with 94% epoxide selectivity. Rigutto *et al.* [28] used V-SAPO-5 for olefin epoxidation using organic peroxides as oxidants. Other catalyst such molybdenum trioxide supported on mesoporous silica (MCM-41, SBA-15 and SiO_2) has been effectively utilized for olefin epoxidation. Maio and co-workers[29] performed liquid phase oxidation of propylene using cumene hydroperoxide (CHP) as

an oxidant using MoO_3/SiO_2 catalyst. They found that catalytic activity varied with the catalyst synthesis procedure and solvent used during the catalytic reaction. Depending on synthesis procedure highly dispersed polymolybdates, α-MoO_3, β-MoO_3, monomeric molybdenum species and small amount of silicomolybdic acid (SMA) were also formed. It was found that β-MoO_3 species assisted the catalytic performance. Very recently highly dispersed MoO_3/SiO_2 synthesized by sol-gel method was reported for propylene oxidation using CHP as oxidant. Studies revealed that catalytic activity of MoO_3/SiO_2 for olefin epoxidation varied with pH of the precipitant. MoO_3/SiO_2 synthesized at pH 9 gave best results with highest yield for propylene oxide. [30]

Out of various heterogeneous catalysts MoO_3/SiO_2 has been studied widely and the structure of support has decisive role to play in its catalytic performance. There are several synthesis procedures reported in the literature for MoO_3/SiO_2, but the most common method employed are impregnation[31] and sol-gel[32] with ammonium heptamolybdate as Mo precursor. MoO_3/SiO_2 synthesized by wet impregnation of ammonium heptamolybdate over silica at low weight loading have shown presence of hexaco-ordinated mono-oxo or tetra co-ordinated dioxo species on the surface.[33-34] Alternative synthesis procedures reported in the literature using $MoCl_5$, $Mo_2(OAc)_4$, $Mo(\eta^3$-$C_3H_5)_4$ which resulted in better interaction of MoO_3 with surface Si-OH species. Collart *et al.* employed $MoO_2(acac)_2$ for synthesis of uniformly dispersed molybdenum species on silica surface. Such type of dispersion methods on silica surface are classified as molecular design dispersion (MDD). [35a] Another significant approach used to enhance the interaction between MoO_3 and SiO_2 was utilizing less acidic Mo^{3+} species. De Boer *et al.* [35b] impregnated Mo^{3+} ions resulting into better interaction of molybdenum with silica surface. Further oxidation of this Mo^{3+} species resulted in the formation of Mo^{6+} species forming mono-oxo Mo(VI) octaheadra.

However there are numerous reports available on conventional methods for synthesis of supported molybdenum catalyst, but very few examples are available in the literature for synthesis of these catalysts for regular size and shape with special emphasis on using modern nanoscience and nanotechnology approach. Hyeon *et al.*[36] have synthesized efficiently recyclable and magnetically separable MoO_x/SiO_2 nanosphers as an efficient olefin epoxidation catalyst. Zeng *et al.* [37] synthesised MoO_3/SiO_2 mesoporous core@shell and hollow core@shell using *inside-out*

preinstallation infusion-hydration method for Fridel-Craft alkylation. Wang *et al.* [38] have synthesized MoO_3/SiO_2 nanoparticles by reverse micelle or "rasin burn" method for glycerol acetalization with ethylene glycol. The major drawbacks of these methods are either very lengthy synthesis procedure or it utilizes expensive surfactant molecules such as CTAB, Brij, Pluronic-123, etc.

Present chapter of the thesis describes the template free synthesis of molybdenum supported on silica microspheres and efficiently used for olefin epoxidation using TBHP in decane as an oxidant.

3.2. Catalyst Synthesis and Characterization

3.2.1. Chemicals and Methods

All the reagents viz., MoO_3 (Loba chemie India), cyclohexene, *cis*-cyclooctene, allyl-benzene, n-heptene, 5.5M TBHP in decane, *tetra*-ethylorthosilicate (TEOS) (Aldrich India), ethyl alcohol, acetonitrile (Thomas Baker) and 1,2-dichloroethane (S.D. fine chemicals India) were purchased and used without further purification.

3.2.2. Catalyst Synthesis

Molybdenum supported on silica microspheres was synthesized by two approaches i) hydrolysis and condensation (HC) and ii) impregnation-hydrolysis-condensation (IHC).

i) Synthesis of Molybdenum Supported on Silica Microspheres via Hydrolysis and Condensation (HC)

A series of catalysts with Mo loading from 8 to 24 wt % supported on silica microspheres were prepared by HC method. The MoO_3 was dissolved in 25 mL 50% H_2O_2 at 333 K until yellow coloured transparent solution of soluble molybdenum-peroxo species[39] was formed. Then this solution was heated for 1 h at 333 K under stirring, which results in pale yellow coloured molybdenum peroxo powder. Then in a plastic 500 mL bottle, above obtained yellow coloured powder was dispersed in solution of 200 mL ethanol, 20 mL ammonium hydroxide (27%) solution and 6.8 mL distilled deionised water and stirred vigorously for 10 min. Then 11.6 g TEOS was added and reaction mixture was stirred for another 12 h, resulting yellowish solution was centrifuged at 5000 rpm for 5 min. The residue was washed three times with ethanol: water 50:50 v/v and obtained Mo-silica microspheres were kept for drying at room temperature. The resulting yellowish solid was calcined at 773 K for 5 h

resulting in formation of blue coloured solid. The final sample was named as 8, 12, 16, 20, 24% HC-MoO$_3$/SiO$_2$.

ii) Synthesis of Molybdenum Supported on Silica Microspheres via Impregnation-Hydrolysis-Condensation (IHC). Synthesis of molybdenum supported on silica microspheres by impregnation-hydrolysis-condensation involves multi-step processes described below:

Synthesis of Silica Spheres. A 500 mL plastic bottle was charged with 400 mL ethanol, 14.4 mL distilled water and 40 mL ammonium hydroxide solution and stirred vigorously for 2 minutes. Then 23.39 g TEOS was added slowly into the reaction mixture and stirred at moderate stirring rate (600 rpm) for 3 h. The white solid was collected by centrifugation and washed with ethanol water mixture (50%) and final product was dried at ambient temperature.

Synthesis of Etched Silica Sphere. Silica spheres as obtained above (4g) were dispersed in 25 mL deionised water by sonication. Then 1500 mL (0.02 N) KOH was added into it and the reaction mixture was stirred at slow speed (at 250 rpm) for 4 h, and finally etched silica was collect by centrifugation, washed with copious amount of water and dried at room temperature.

Synthesis of Molybdenum Supported on Silica Microspheres by Impregnation-Hydrolysis-Condensation (IHC). The etched silica (1.75g) obtained above was further dispersed in 15 mL distilled water. 8, 12, 16, 20, 24 wt.% molybdenum peroxo air dried yellow solid was dissolved in 30 mL distilled deionised water added to a slurry of etched silica followed by heating and stirring the resulting solution at 333-343 K until completely dry yellow coloured powder was obtained. This powder was further dispersed in 100 mL ethanol and vigorously stirred for 1 h. After dispersion, followed by addition 3.5 mL distilled deionised water, 10 mL ammonium hydroxide solution and 5.8 g TEOS and kept for continuous stirring for 12h. Resulting solution was centrifuged at 5000 rpm for 5 min and residue was washed twice with 30 mL of 50:50 ethanol: water mixture. Pale yellow air dry powder so obtained was calcined at 773 K for 5 h at heating rate of 5 K/min.

3.2.3. Catalyst Characterization

All the catalyst synthesized by hydrolysis-condensation (HC) and impregnation-hydrolysis-condensation (IHC) were characterized with the help of various physicochemical techniques such as UV-visible, FT-IR, Raman, XRD, SEM

and EDAX to determine the chemical composition as well as morphology of the surface of catalytic material.

A. Powder X-ray Analysis. X-ray diffractograms were recorded using a Rigaku X-ray diffractometer (Model DMAX IIIVC) using CuKa (1.5406 Å) radiation from $2\theta=10$ to 80° by 4° steps with an integration time of 4 s.

B. Raman Analysis. Raman spectra were recorded under ambient conditions on a LabRAM infinity spectrometer (Horiba–Jobin–Yvon) equipped with a liquid nitrogen detector and a frequency doubled Nd-YAG laser supplying the excitation line at 532 nm with 1–10 mW power. The spectrometer is calibrated using the Si line at 521 cm^{-1} with a spectral resolution of 3 cm^{-1}.

C. Electron Microscopy. Scanning electron microscopy (SEM) measurements were performed on a FEI quanta 200 3D dual beam (ESEM) having thermionic emission tungsten filament in the 3 nm range at 30 kV and HRTEM was done on a Tecnai G2-30 FEI instrument operating at an accelerating voltage of 300 kV. Before analysis, the powders were ultrasonically dispersed in *iso*-propanol, and two drops of *iso*-propanol containing the solid were deposited on a carbon coated copper grid for TEM analysis.

D. FT-IR Spectroscopy. The type of acidity present on the sample was determined by adsorption of pyridine on the sample and surface adsorption was monitored by Shimadzu 8000 series FTIR spectrometer.

E. Catalytic Activity. The catalytic epoxidation was carried out selecting cyclohexene as a probe reactant and TBHP as oxidant (Scheme 3.4). Typically reaction was carried out in a 25 mL two necked round bottom flask equipped with a magnetic stirrer and immersed in a thermostat oil bath fitted with condenser. The reaction was carried out at 353 K using 1, 2-dichloroethane as solvent and 5.5 TBHP in decane as oxidant, olefin (2.5 mmol), oxidant 5.5 M TBHP in decane (7.5 mmol) and heated at 353 K. The samples were withdrawn periodically and analyzed on Agilent 6890 Gas chromatograph equipped with a HP-5 dimethylpolysiloxane column (60 m length, 0.25 mm diameter and 0.25 µm film thicknesses and flame ionization detector. Products were confirmed by GC-MS 6890N.

3.3. Result and Discussion

The molybdenum supported on silica microspheres were synthesized by template free route by either, hydrolysis and condensation (HC) or impregnation followed by hydrolysis and condensation (IHC) (Scheme 3.1-3.2). Synthesis

procedure for HC method was quiet similar to that of method used for Stöber silica synthesis.[40-41] In this method ammonia catalysed reaction of TEOS with water in low-molecular weight alcohol produces monodispersed silica spheres in the range of 5-2000 nm. In general the hydrolysis reaction producing singly hydrolysed monomer which eventually condenses to form silica.
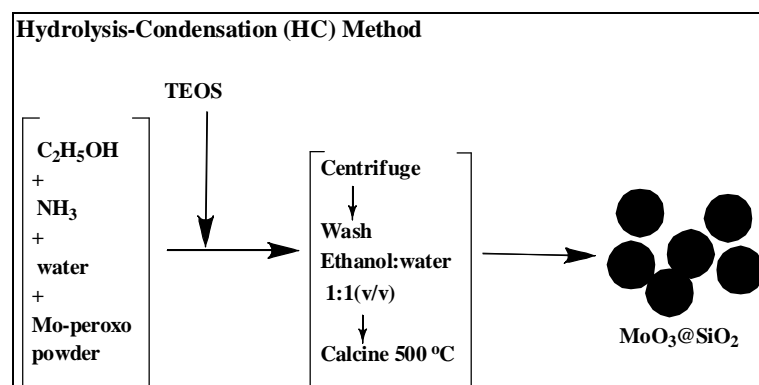
Scheme 3.1: MoO_3/SiO_2 microspheres synthesized by hydrolysis-condensation (HC) method
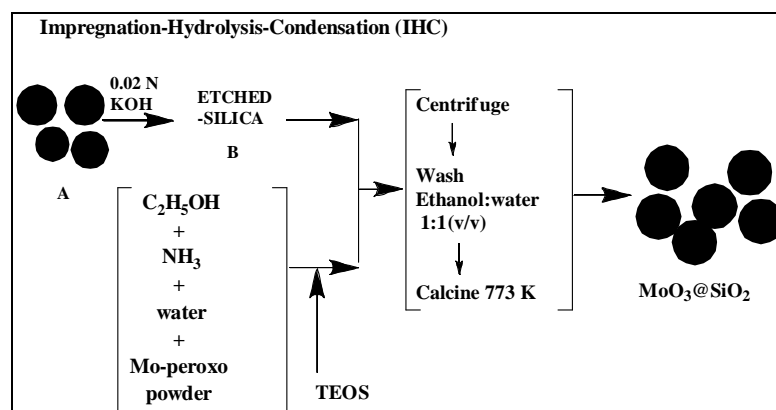
Scheme 3.2: MoO_3/SiO_2 synthesized by impregnation-hydrolysis-condensation IHC method; (A) represents Stöber SiO_2 and (B) represents 4h etched SiO_2.

Mechanism to elucidate the monodispersed silica particles can be explained by two models, that is monomer addition (nucleation) and controlled aggregation (growth). First model follows the LaMer-Like mechanism [42] where after initial burst of nucleation, growth occurs via addition of monomers to the particle surface. In contrast the second model supports that nucleation, occurs continuously throughout the reaction. These primary particles aggregate with one another to form particles

with narrow size distribution. Lee *et al.* and several other group have supported the controlled aggregation mechanism, where only one isomer $(OR)_3Si$-OH was detected by ^{29}Si-NMR spectroscopy.[43-44] Harris and Blaaderen are of the opinion that both the mechanism are responsible for the formation of monodispersed silica microspheres. [45-47] Emelchenko and co-workers have proposed model using modified Stöber–Fink–Bohn (SFB) method. According to this model, first TEOS molecules are hydrolyzed to $Si(OH)_4$ which undergo polymerization followed by nucleation. These nuclei aggregate to form primary particles of 5 nm diameter. These particles further aggregate via multiples stages of regrowth to form monodispersed silica spheres. These silica spheres have a dense core covered by shell containing numerous secondary particles. Present chapter focuses on effect on structure, morphology, catalytic activity of MoO_3/SiO_2 obtained by addition of various loadings of molybdenum peroxo to TEOS: NH_3: Water mixture.

All the samples were analyzed by UV-Visible spectroscopy (See Fig. 3.2). The UV- visible spectrum of both the samples synthesized by HC and IHC method showed the broad absorption band around 200–350 nm. The band at 250 nm is ascribed to expected ligand-metal charge transfer (LMCT) bands originating from the promotion of electrons from the filled Mo=O (p) levels to the d orbital's. These metal-ligand transitions are dependent on local symmetry of metal ions. For oxygen ligand around metal centre tetrahedral transition are expected to be more symmetric than octahedral ones. The Mo (T_d) and Mo (O_h) LMCT bands normally appear at the 220-270 nm range and 270-340 nm, respectively. Distortion of the symmetry of the [Mo (T_d)/ Mo (O_h)] structure would cause the LMCT band to shift to a shorter wavelength.[48-49] Broad absorption around 747 nm is more prominent in case of molybdenum silica synthesized by HC method could be due to d–d transitions involving Mo(V) and inter valence charge transfer transition (IVCT) between Mo(V) and Mo(VI) via an oxo bridge, which diminished in case of molybdenum silica synthesized by IHC method. This may be the reason for blue color in molybdenum silica synthesized by HC method.[50]
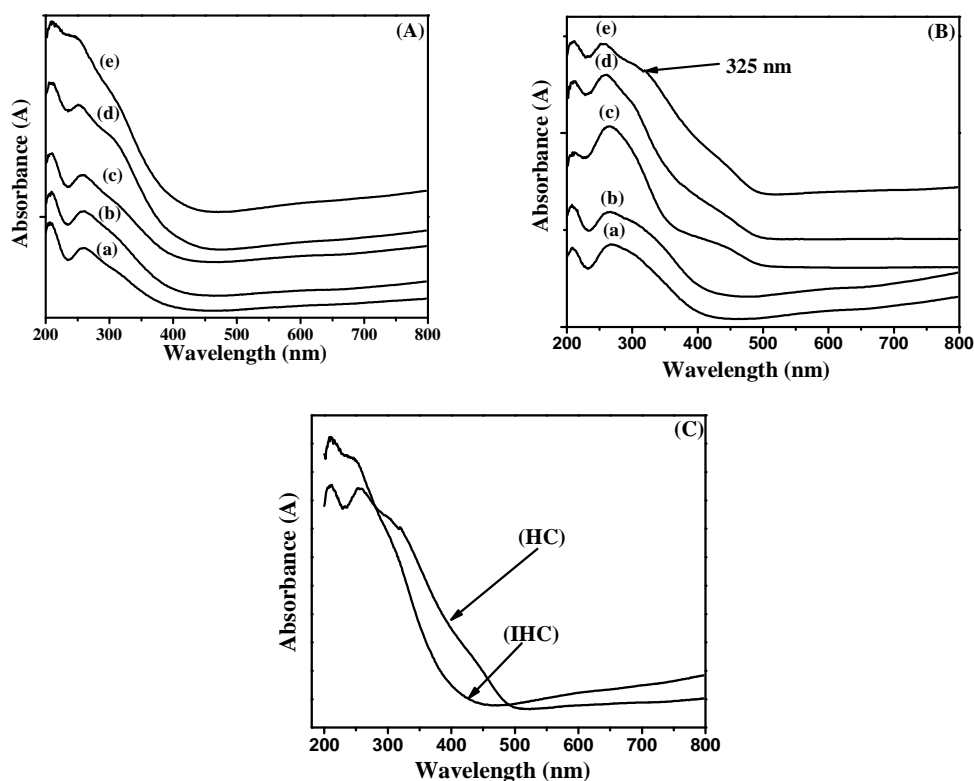
Fig. 3.2: UV visible spectra of MoO_3/SiO_2 microspheres synthesized by HC (A) and IHC (B) method for various molybdenum loadings (a) 8%, (b) 12%, (c) 16%, (d) 20% and (e) 24%; (C) represents the overlapping spectra of 24% MoO_3/SiO_2 loading synthesized by HC and IHC method.

The crystaillinty and phase purity of the samples was characterized by powder X-ray method and XRD patterns are shown in Fig. 3.3. The XRD pattern of molybdenum silica synthesized by HC method (Fig. 3.3 A) showed crystalline nature of the powders for weight loading of 8% to 24% with sharp peaks due to the α-MoO_3 dispersed on the silica nanosphers with Bragg reflections at 2θ = 12.7 (020), 23.4 (110), 25.7 (040), 27.4 (021) characteristics of orthorhombic phase (JCPDS No. 05-0508).[51-52] Molybdenum silica synthesized by IHC (Fig. 3.3 B) method showed absences of orthorhombic molybdenum oxide and XRD spectra predominantly contained peaks of amorphous nature due to the presence of silica.

XRD spectra also showed formation of the Mo_8O_{26} (O_h) clusters in the MoO_3/SiO_2 synthesised by (IHC) method. XRD spectra of the samples was quite similar to the XRD spectra of $Na_4Mo_8O_{26}$ reported previously in the literature (JCPDS No. 35-1465). Whereas at higher weight loadings, that is, 24% MoO_3/SiO_2 showed

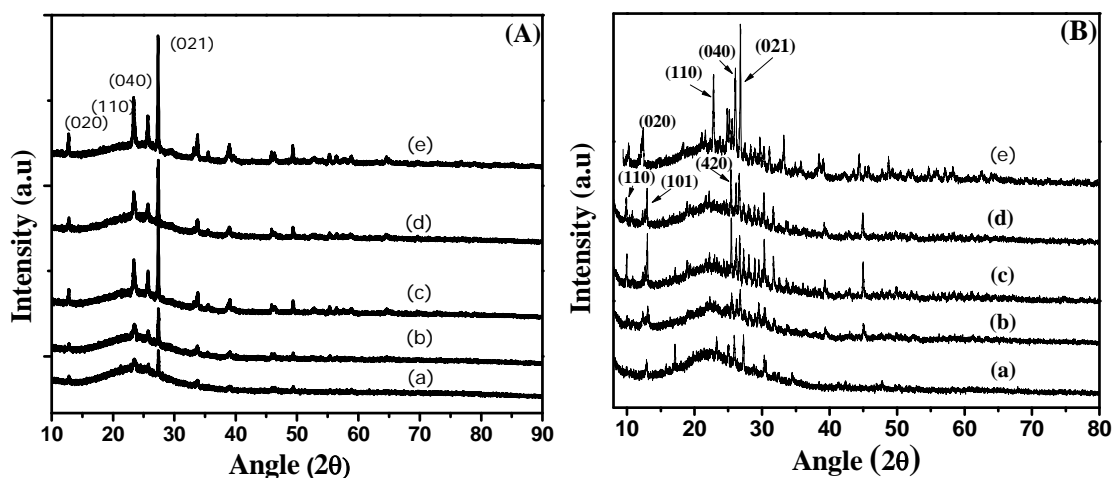formation of α-MoO$_3$ species clearly indicting transformation of Mo$_8$O$_{26}$ (O$_h$) clusters to α-MoO$_3$ species.

Fig. 3.3: XRD spectra of (a) 8%, b) 12%, (c) 16%, (d) 20%, (e) 24% MoO$_3$/SiO$_2$ microspheres synthesized by HC (A) method and IHC (B) method respectively.

All the samples were analyzed by FT-IR spectroscopy and results are plotted in the Fig. 3.4. In the case of MoO$_3$/SiO$_2$ synthesized by HC (Fig. 3.4) method Mo=O stretching frequency was observed at 950 cm^{-1}, diffused peak at 910 cm^{-1} and 870 cm^{-1} is due to Mo-O-Si and Mo-O-Mo bonds respectively. Whereas 16% to 24% molybdenum silica synthesized by IHC method showed the band around 950 cm^{-1}, 940 cm^{-1} were due to Mo=O. 917 cm^{-1}, 900 cm^{-1} 890 cm^{-1}, 865 cm^{-1}, 754 cm^{-1}, 700 cm^{-1} and 625 cm^{-1} were due to distorted MoO$_6$ O$_h$ units (isolated as well as clustered) clearly confirming the presence of isolated MoO$_6$ O$_h$, Mo$_8$O$_{26}$ O$_h$ and polyoxomolybdate clusters. Whereas such bands were absent in the molybdenum silica microspheres synthesized by HC method. Band around 1000-1200 cm^{-1} and 800-820 cm^{-1} are common in both the cases is due to the Si-O-Si bond of Silica. [53-54]
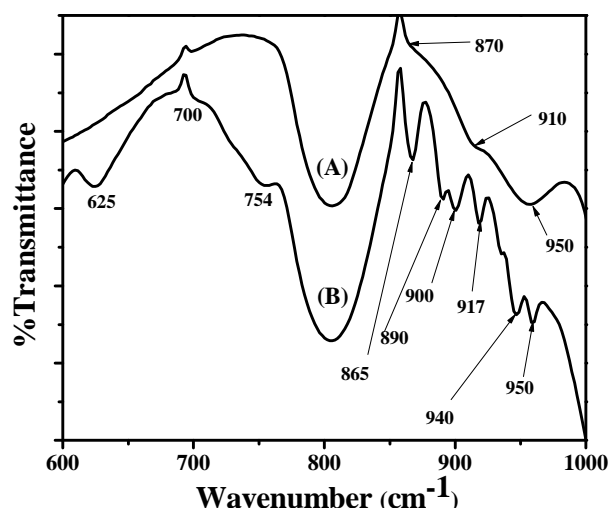
Fig. 3.4: FT-IR spectra of 24% MoO_3/SiO_2 synthesized by HC (A) and IHC (B) respectively.

Raman spectra in the case of molybdenum silica microspheres synthesized by HC method shows vibrational band around 995 cm^{-1} due to terminal M=O stretching mode. Band at 825 cm^{-1} was due to bulk MoO_3 species. A small and broad band at 672 cm^{-1} and 270 and 280 cm^{-1} were due to Mo-O-Mo stretching and deformation respectively.[50],[51-52],[55] Rest of the bands were in agreement with α-MoO_3 species present on the SiO_2 surface.[56-57] Additional bands were observed due to O–Mo–O scissoring modes at 378 and 364 cm^{-1}, O–Mo–O bending modes at 337 cm^{-1}, O=Mo=O wagging modes at 292 cm^{-1}, O=Mo=O twisting modes at 244 cm^{-1} and 217 cm^{-1}, O=Mo=O twisting modes at 197 cm^{-1} and 158 cm^{-1}. MoO_3/SiO_2 synthesized by IHC method showed presence of isolated MoO_6 (O_h) as well as MoO_8O_{26} (O_h) octahedral species due to symmetric stretch at 965 cm^{-1} from the distorted MoO_6 unit and several weaker bands at 800-940 cm^{-1} from the related asymmetric stretches. The weak Raman bands at 500-750 cm^{-1} and 157 cm^{-1} originate from the symmetric and asymmetric stretches of the bridging Mo-O-Mo bonds. The asymmetric and symmetric bending modes of the MoO_6 unit occur at 340 and 400 cm^{-1}. Whereas at high weight loading, which is 24% MoO_3 shows appearance of bulk MoO_3 species as compared to polymolybdate species clearly indicating transformation of polymolybdate species to α-MoO_3 at higher weight loadings.
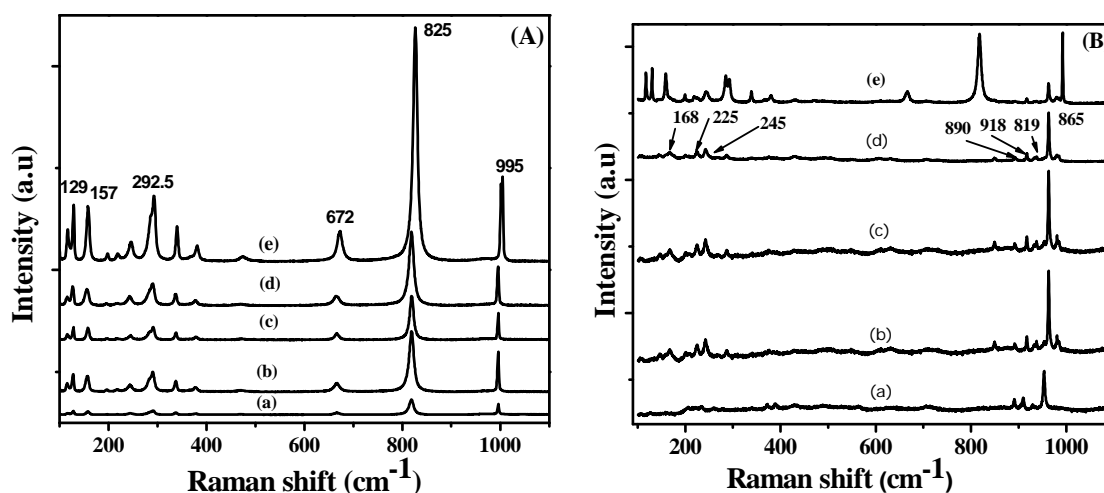
Fig. 3.5: Raman spectra of MoO₃/SiO₂ microspheres synthesized by (A) HC; and (B) IHC for molybdenum loadings form (a) 8%, (b) 12%, (c) 16%, (d) 20% and (e) 24%.

All the samples were analyzed by scanning electron microscopy (SEM) and images are shown in the Fig. 3.6 (A-G) to 3.7 (A-H) The molybdenum supported on silica synthesized by HC and IHC methods showed the formation of spherical molybdenum silica formed by both HC and IHC method. At lower weight loadings the spheres obtained were of uniform size and shape, but at higher weight loading there was agglomeration of the microspheres because addition of homogeneously dispersed $MoO(O_2)_2$ particles affect rate of crystallization and crystal growth in both the case HC and IHC methods. Another probable reason can be that NH_3 added for hydrolysis of TEOS was consumed by molybdenum peroxo particles resulting into improper hydrolysis of TEOS at higher molybdenum loading. EDAX analysis showed deviation of actual weight% of the sample to the weight% loaded during the synthesis in both the case of HC and IHC methods clearly indicated that molybdenum was not completely consumed during the synthesis and was left behind in the solution. In the case of hydrolysis condensation method loss of molybdenum peroxo in the solution was more as compared to that of impregnation hydrolysis condensation at lower molybdenum weight loading. SEM metal mapping of the same samples supported the fact of uniform dispersion of MoO_3 nanoparticles on silica surface See Fig. 3.8 (A) and (B). Yellow spots in the Fig. 3.8 A and 3.9 A represent molybdenum nanoparticles on silica surface. EDAX analysis shows deviation of actual weight% of the sample to the weight % loaded during the synthesis in both the case of HC and IHC methods, clearly indicating that molybdenum was not completely consumed

during the synthesis and was left behind in the solution during hydrolysis and condensation of TEOS. At lower weight loadings amount of molybdenum peroxo consumed was less as compared to higher weight loadings because at lower weight loading the solution was dilute hence the molybdenum peroxo particles were less readily consumed as compared to a concentrated solution at higher weight loadings.

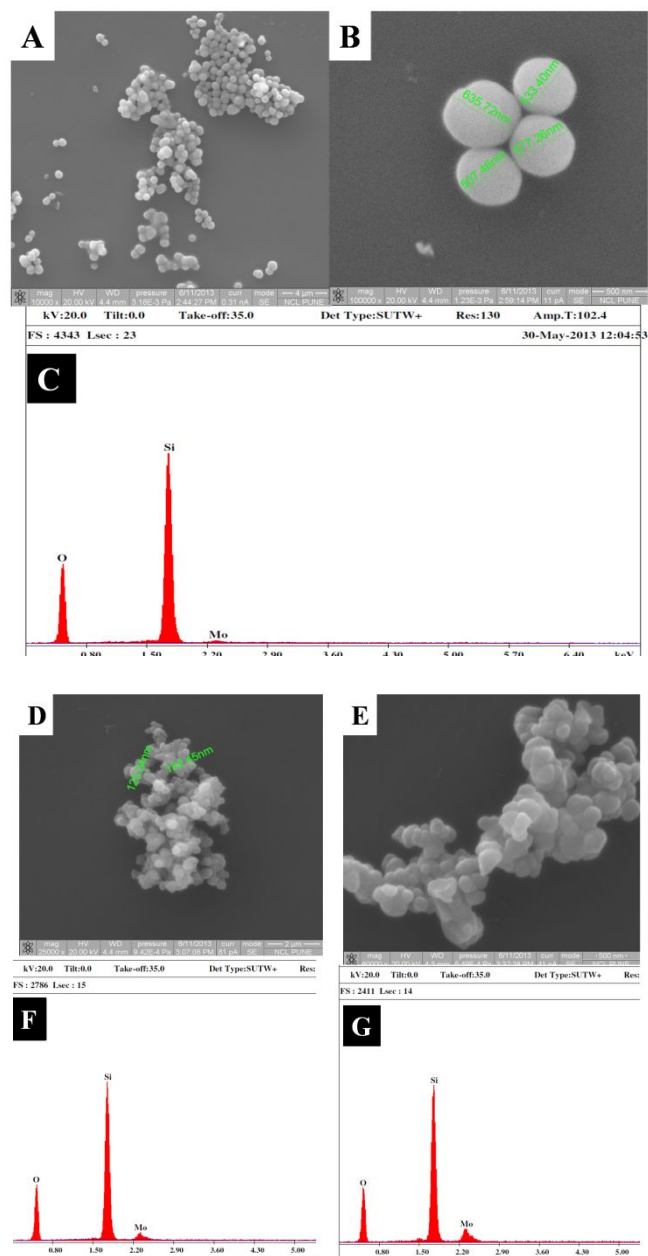**Fig. 3.6:** (A) SEM image of 8% HC-MoO$_3$/SiO$_2$; (B) magnified image of (A); (C) SEM-EDAX of 8% HC-MoO$_3$/SiO$_2$; (D) 16% HC-MoO$_3$/SiO$_2$; (E) 24% HC-MoO$_3$/SiO$_2$; (F) SEM-EDAX of 16% HC-MoO$_3$/SiO$_2$; (G) SEM-EDAX of 24% HC-MoO$_3$/SiO$_2$
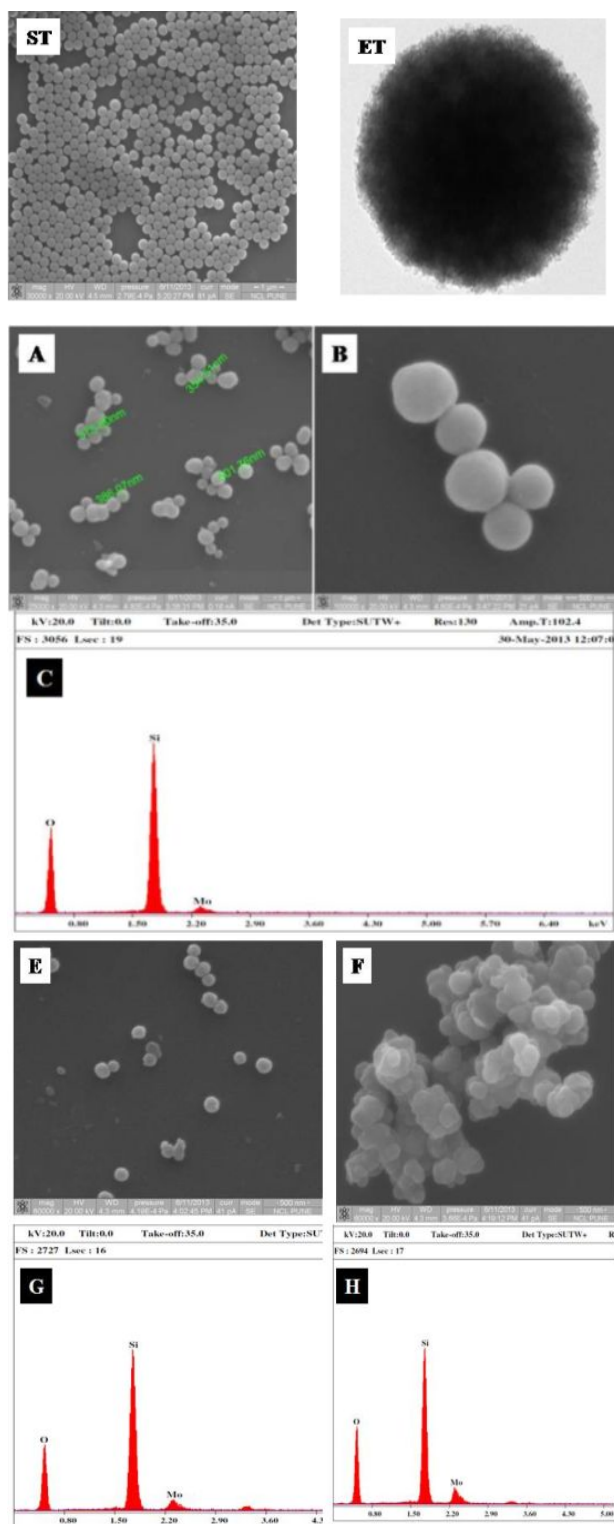
Fig. 3.7: (ST) SEM image of Stöber Silica; (ET) TEM image of 4 h etched silica; SEM image of (A) 8% IHC-MoO$_3$/SiO$_2$; (B) magnified image of (A); (C) SEM-EDAX of IHC-MoO$_3$/SiO$_2$; (E) 16% IHC-MoO$_3$/SiO$_2$ (F) 24% IHC-MoO$_3$/SiO$_2$; (G) SEM-EDAX of 16% IHC-MoO$_3$/SiO$_2$; (H) SEM-EDAX of 24% MoO$_3$/SiO$_2$

Fig. 3.8: Elemental mapping images of 24% MoO_3/SiO_2 synthesized by HC; (A) yellow color shows molybdenum atoms; (B) green color showing Si content; (C) red colors represents oxygen atoms present on surface and (D) MoO_3/SiO_2 on the surface.
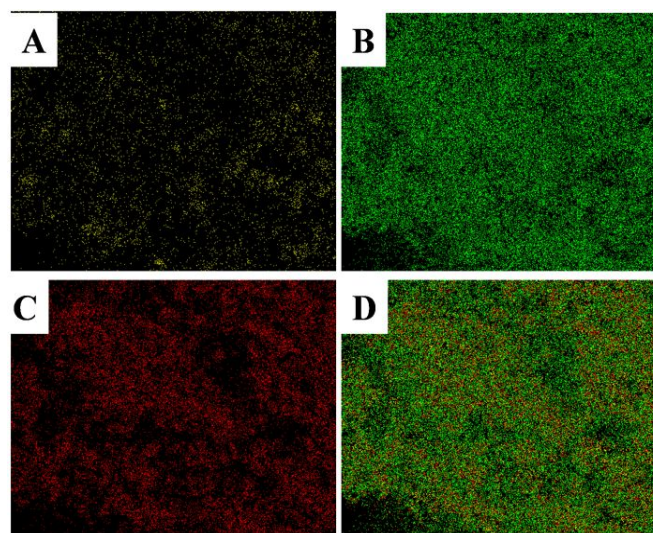

Fig. 3.9: Elemental mapping images of 24% MoO_3/SiO_2 synthesized by IHC; (A) yellow color shows molybdenum atoms; (B) green color showing Si content; (C) red colors represents oxygen atoms present on surface and (D) MoO_3/SiO_2 on the surface.
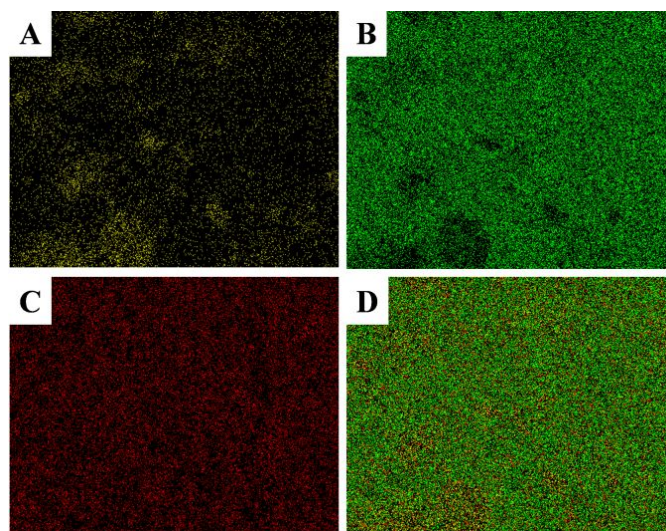
Table 3.1: SEM-EDAX analysis of MoO$_3$/SiO$_2$ synthesized by hydrolysis-condensation (HC) method

Entry	Weight% added during synthesis	Actual wt.% by MoO$_3$ EDAX
1.	8	3.1
2.	16	12.4
3.	24	18.5

Table 3.2: SEM-EDAX analysis of MoO$_3$/SiO$_2$ synthesized by impregnation-hydrolysis-condensation (IHC) method

Entry	Weight% added during synthesis	Actual wt.% by MoO$_3$ EDAX
1.	8	2.5
2.	16	15.0
3.	24	19.2

3.4. Catalytic Activity

Cyclohexene was taken as a model substrate to test the catalytic activity of the MoO$_3$/SiO$_2$ catalyst using organic TBHP as oxidant and 1, 2-dichloroethane at 353 K. Generalized cyclohexene oxidation scheme is given below (scheme 3.4).
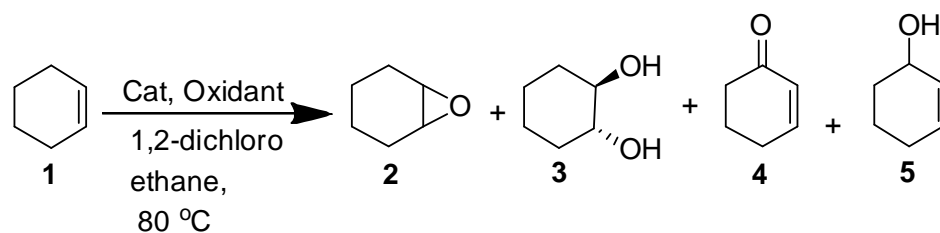
Scheme 3.4: Represents the oxidation of cyclohexene and its possible oxidations products.

　　　　Cyclohexene oxidation was carried out using 8% to 24 % loading of MoO_3/SiO_2 prepared by HC method using anhydrous TBHP as oxidant and 1, 2-dichloroethane as solvent (table 3.3). 8% MoO_3/SiO_2 gave 22% cyclohexene conversion into epoxide as major product with 57% selectivity in 4 h. With increase in molybdenum loading to 12% there was an increase in epoxide selectivity to 90% under identical condition. The most probable reason for increase in epoxide selectivity may be due to the formation of the bulk MoO_3 increasing the number of surface Mo=O species responsible for enhanced epoxide selectivity. With further increase in molybdenum loadings cyclohexene conversion was enhanced with very good epoxide selectivity in 4h. 16% MoO_3/SiO_2 gave 69% cyclohexene conversion with 85% epoxide selectivity. 20% MoO_3/SiO_2 gave 85% cyclohexene conversion with 95% epoxide selectivity. Although it was found that there was increase in cyclohexene conversion and epoxide selectivity, but it was also observed that there was decrease in turn over frequency (TOF)/h from 32.2 to 21.6 from 8% to 16% molybdenum loadings, due to decrease in surface molybdenum atoms and increase in bulk molybdenum atoms not involved in the catalytic transformation. At higher molybdenum loadings greater than 16% showed irregular trend in TOF due to formation of non-uniform silica spheres with aggregation of these spheres. Catalytic activity of 24% MoO_3/SiO_2 was studied by varying the loadings of TBHP as oxidant. It was found that there was increase in % cyclohexene conversion with increase in oxidant loadings from 1, 2 and 3 equivalent with respect to cyclohexene (0.025 M), with corresponding cyclohexene conversions of 36%, 80% and 91% with epoxide selectivity 92%, 96% and 98% respectively. With increase in oxidant loading, it was found that both cyclohexene conversions as well as epoxide selectivity increased from 92%, 96% and 98% clearly indicating that increase in oxidant has positive effect on epoxide selectivity. Turn over frequency (TOF)/h

also doubled from 10 to 21.5 with increase in oxidant loading from 1 equivalent to 3 equivalents.

Table 3.3: Catalytic activity of cyclohexene using MoO_3/SiO_2 prepared by HC method

S. No.	Mo wt% in catalyst	% Conversion 1	%Selectivity		TOF/h
			2	4	
1.	8	22	57	43	32.2
2.	12	45	80	20	26
3.	16	69	85	15	21.8
4.	20	85	95	5	24.3
5.	24	36	92	8	10.1
6.	24	80[@]	96	4	16
7.	24	91[#]	98	2	21.5

Reaction conditions: Cyclohexene: 2.5 mmol, 5.5M TBHP in decane: 1.2 mL (7.5 mmol);[@] oxidant: 5.5M TBHP in decane 0.4 mL; [#]oxidant: 5.5M TBHP in decane: 0.8 mL; Catalyst: 10 wt% of cyclohexene; Solvent; 6 gm 1, 2-dichloroethane; Time: 4h; Temperature: 353 K [b]

Furthermore the catalytic activity of MoO_3/SiO_2 synthesized by IHC method was also studied for cyclohexene oxidation (table 3.4). With 8% MoO_3/SiO_2 IHC was used as catalyst, it gave 31% cyclohexene conversion with 54% epoxide selectivity in 12 h. With 12% MoO_3/SiO_2 43% cyclohexene conversion and 52% epoxide selectivity in 12 h was obtained. With 16% MoO_3/SiO_2 there was 53% conversion and 50% epoxide selectivity. 20% and 24% MoO_3 (as shown in table 3.4 and entry 3 and 4) on silica again shows improvement in catalytic activity as increase in aggregation was countered by each time increase in molybdenum content by 4%. Cyclohexene oxidation with 24% MoO_3/SiO_2 synthesized by impregnation-hydrolysis-condensation (IHC) within 12 h gave 90% conversion with 95% epoxide selectivity. Turn over frequency (TOF) for MoO_3/SiO_2 was found to be maximum at 8% MoO_3/SiO_2

reaching to a value of 12.1 and then decreases up to 16% molybdenum loadings and then increase to 5 at 24% molybdenum loading, probably due to non-uniform coating by silica and aggregation of MoO_3/SiO_2 microspheres. TOF values were lower than MoO_3/SiO_2 synthesized by HC method probably during the coating of the molybdenum silica particles by silica, resulted in the reduction of molybdenum oxide particles present on catalyst surface. Briot and co-workers[39],[58] have done olefin epoxidation using molybdenum supported on mesoporus silica (MCM-41, SBA-15) for cycloctene oxidation. TBHP was taken as oxidant in a molar ratio three times as compared to the cycloctene. They obtained 97% conversion and 95% epoxide selectivity using decane as solvent at 313 K in 3 h with Mo-MCM-41 catalyst, whereas Mo-SBA-15 gave > 99% conversion and 93% selectivity.[39] However, both the catalyst showed leaching of the active species after three recycles, and the problem of catalyst leaching was persistent as in the previous cases. Hyoen *et al.* have done olefin epoxidation using magnetically separable mesoporous molybdenum silica microspheres for cyclohexene oxidation and carbon tetrachloride as solvent and reported 87% epoxide yield in 5 h at reflux temperature.[36]

Table 3.4: Catalytic activity of molybdenum silica prepared by IHC method

Entry	Mo wt% in catalyst	% Conversion	% Selectivity			TOF/h^{-1}
		1	2	3	4	
1.	8	31	54	-	46	12.1
2.	12	43	52	-	48	6.7
3.	16	53	50	10	40	1.7
4.	20	58	68	7	25	5
5.	24	90	95	-	5	5

Reaction conditions: Cyclohexene: 2.5 mmol, 5.5 M TBHP in decane: 7.5 mmoles; Solvent: 6 gm 1, 2-dichloroethane; Temperature: 353 K; Time: 12 h.

Leaching test was carried out using hot filtration experiment with 24% MoO_3/SiO_2 synthesized by HC method and results are shown in Fig. 3.10. After 40% cyclohexene conversion, the reaction was stopped and catalyst was removed from reaction media by centrifugation and supernatant was allowed to react further without catalyst. It gave only additional 4% conversion in 3 h with increase in selectivity for cyclohex-2-enone, which may be due to thermal reaction catalysed by TBHP, as shown in blank reaction.[35],[59] This indicated that the reaction was truly catalysed by MoO_3 nanoparticles dispersed onto the surface of silica microspheres. Recycle studies were also carried out using 24% HC and 24% IHC MoO_3/SiO_2 using 5.5 M TBHP in decane as oxidant under identical condition and showed that catalytic activity was retained for almost three cycle recycles without losing much activity and selectivity for both the cases, i.e., HC and IHC method.

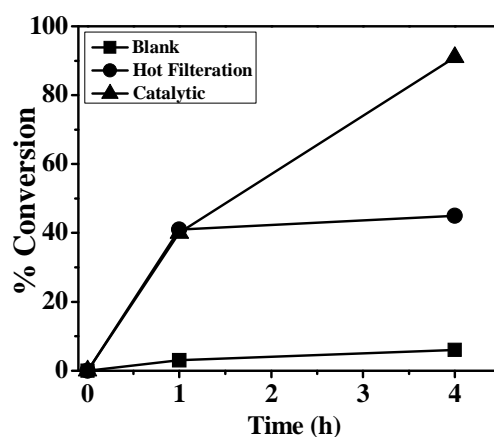
Fig. 3.10: Represents % cyclohexene conversion vs. time curve using 24% MoO_3/SiO_2 synthesized by HC method
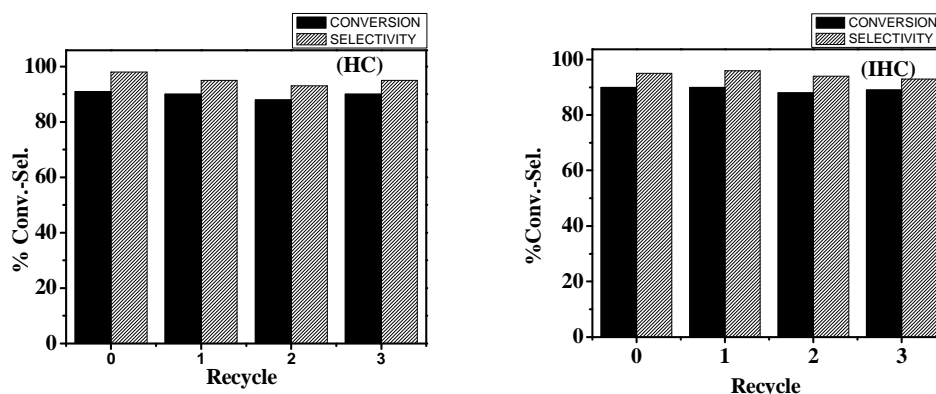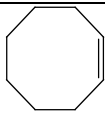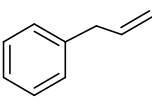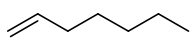

Fig. 3.11: Represents the graph for catalytic recycle study for cyclohexene oxidation by (HC) and (IHC) methods respectively

Reaction conditions: Cyclohexene: 0.2 g (2.5 mmol); 5.5 TBHP in decane as oxidant 1.5 mL (7.5 mmol); 1, 2-dichloroethane as solvent; catalyst = 0.02 g (HC-24% MoO$_3$/SiO$_2$); catalyst = 0.02 g (IHC-24% MoO$_3$/SiO$_2$)

Oxidation of Other Olefins. The catalytic activity of 24% HC and 24% IHC MoO$_3$/SiO$_2$ catalyst was extended for the wider applicability to other olefins such as cycloctene, allyl benzene and n-heptene under identical conditions and results are shown in table 3.5. When cyclooctene was used as substrate, 24% HC catalyst gave 91% conversion and 100% epoxide selectivity in 12h. 24% IHC gave 80% conversion and 100% epoxide selectivity under identical reaction conditions. Allyl-benzene oxidation when carried out with 24% HC gave 36% conversion and 60% selectivity for epoxide. However, when same reaction carried out using IHC method gave 46% conversion and 57% epoxide selectivity. Furthermore for n-heptene epoxidation reaction 24% HC catalyst gave 50% conversion and 100% epoxide selectivity, while with 24% IHC gave 45% conversion and 60.6% epoxide selectivity after 20 h.

Table 3.5: Epoxidation of other olefins using 5.5 M TBHP in decane as oxidant and 1.2-dichloroethane as solvent

S. No.	Substrate	Catalyst	% Conv./ (Time, h)	% Selectivity		TOF /h
				epoxide	others	
1.		A	91/(4)	100	-	70
		B	80/(4)	100	-	68.6
2.		A	36/(20)	60	40	4.7
		B	46/(20)	57	43	10.8
3.		A	50/(20)	100	-	11.8
		B	45/(20)	60.6	39.4	10.6

Reaction conditions: Substrate: 2.5 mmol; Oxidant = 5.5M TBHP in decane: 7.5 mmol; Solvent: 1, 2-dichloroethane; Temperature: 353 K; Catalyst A represents 24% MoO$_3$/SiO$_2$ HC and B represents 24% MoO$_3$/SiO$_2$ IHC.

3.5. Conclusion

Molybdenum supported on silica microspheres were synthesized by two methods without using any template, i.e., HC and IHC methods. SEM images showed the silica microspheres were of uniform shapes and size and EDAX analysis showed the Mo content was lower as compared to added metal. The structure of molybdenum species formed by using different synthesis procedures and different molybdenum loadings was studied and were supported by Raman, FT-IR, and UV-Visible spectroscopy. The prepared catalysts showed excellent activity for olefin epoxidation, using 5.5 M TBHP as oxidant and 1, 2-dichloroethane as solvent at 353 K. Molybdenum silica synthesized by hydrolysis-condensation (HC) method was more effective as compared to molybdenum silica synthesized by impregnation-hydrolysis-condensation (IHC) method for cyclohexene oxidation in terms of catalytic activity as well as selectivity for the desired product, i.e., epoxide. In the case of other olefins other than cyclohexene gave mixed response. MoO_3/SiO_2 synthesis by (IHC) was more catalytically active as for cyclooctene and allylbenzene, while MoO_3/SiO_2 synthesized by HC method was more active in catalyzing n-heptene oxidation. To conclude we can say that just by varying the synthesis procedure we can obtain material with same chemical composition having different catalytic activity and selectivity.

3.6. References

[1]   N. Mizuno, K. Yamaguchi, K. Kamata, *Coord.Chem. Rev.* **2005**, *249*, 1944-1956.

[2]   W. R. Thiel, M. Angstl, N. Hansen, *J. Mol. Catal. A: Chem.* **1995**, *103*, 5-10.

[3]   R. A. Sheldon, J. K. Kochi, J. Richardson, *Metal-catalyzed oxidations of organic compounds: mechanistic principles and synthetic methodology including biochemical processes*, Academic press New York, **1981**.

[4]   D. V. Deubel, G. Frenking, P. Gisdakis, W. A. Herrmann, N. Rösch, J. Sundermeyer, *Acc. Chem. Res.* **2004**, *37*, 645-652.

[5]   B. S. Lane, K. Burgess, *Chem. Rev.* **2003**, *103*, 2457-2474.

[6]   D. Hoegaerts, B. F. Sels, D. E. De Vos, F. Verpoort, P. A. Jacobs, *Catal. Today* **2000**, *60*, 209-218.

[7]   A. K. Yudin, *Aziridines and epoxides in organic synthesis*, Wiley-VCH, **2006**.

[8]   J. Marco-Contelles, M. T. Molina, S. Anjum, *Chem. Rev.* **2004**, *104*, 2857-2900.

[9]   R. A. Jurenka, M. Subchev, J.-L. Abad, M.-Y. Choi, G. Fabriàs, *PNAAS* **2003**, *100*, 809-814.

[10]   K. Neimann, R. Neumann, *Org. Lett.* **2000**, *2*, 2861-2863.

[11]   R. Mello, A. Alcalde-Aragonés, A. Olmos, M. a. E. González-Núñez, G. Asensio, *J. Org. Chem.* **2012**, *77*, 4706-4710.

[12]   O. A. Wong, Y. Shi, *ChemInform* **2008**, *39*, i.

[13]   R. Del Rio, B. Wang, S. Achab, L. Bohe, *Org. Lett.* **2007**, *9*, 2265-2268.

[14]   W. Adam, C. Saha-Moller, P. A. Ganeshpure, *Chem. Rev. Columbus* **2001**, *101*, 3499-3548.

[15]   R. Rinaldi, J. Sepulveda, U. Schuchardt, *Adv. Synth. Catal.* **2004**, *346*, 281-285.

[16]   M. H. Dickman, M. T. Pope, *Chem. Rev.* **1994**, *94*, 569-584.

[17]   C. C. Romão, F. E. Kühn, W. A. Herrmann, *Chem. Rev.* **1997**, *97*, 3197.

[18]   W. Adam, W. Malisch, K. J. Roschmann, C. R. Saha-Möller, W. A. Schenk, *J. Org. Chem.* **2002**, *661*, 3-16.

[19]   R. Sheldon, J. Van Doorn, *J. Catal.* **1973**, *31*, 427-437.

[20]   A. Corma, H. García, *Chem. Rev.* **2002**, *102*, 3837-3892.

[21]   R. Sheldon, *J. Mol. Catal. A: Chem.* **1980**, *7*, 107-126.

[22]   R. Hutter, T. Mallat, A. Baiker, *J. Catal.* **1995**, *153*, 177-189.

[23]   S. B. Kumar, S. Mirajkar, G. C. Pais, P. Kumar, R. Kumar, *J. Catal.* **1995**, *156*, 163-166.

[24]   M. Clerici, G. Bellussi, U. Romano, *J. Catal.* **1991**, *129*, 159-167.

[25]   J. Van der Waal, M. Rigutto, H. Van Bekkum, *Appl. Catal. A: Gen.* **1998**, *167*, 331-342.

[26]   G. Grigoropoulou, J. Clark, J. Elings, *Green Chem.* **2003**, *5*, 1-7.

[27]   F. Somma, G. Strukul, *J. Catal.* **2004**, *227*, 344-351.

[28]   M. Rigutto, H. Van Bekkum, *J. Mol. Catal. A: Chem.* **1993**, *81*, 77-98.

[29]   Y. Miao, G. Lu, X. Liu, Y. Guo, Y. Wang, Y. Guo, *J. Mol Catal A: Chem.* **2009**, *306*, 17-22.

[30]   K. Shen, X. Liu, G. Lu, Y. Miao, Y. Guo, Y. Wang, Y. Guo, *J. Mol Catal A: Chem.* **2013,** 373, 78-84.

[31]   P. Célestin Bakala, E. Briot, J.-Y. Piquemal, J.-M. Brégeault, P. Beaunier, *Catal. Commn.* **2007**, *8*, 1447-1451.

[32]   T. V. Kotbagi, A. V. Biradar, S. B. Umbarkar, M. K. Dongare, *ChemCatChem* **2013**, *5*, 1531-1537.

[33]   M. A. Banares, H. Hu, I. E. Wachs, *J. Catal.* **1994**, *150*, 407-420.

[34]   M. A. Banares, H. Hu, I. E. Wachs, *J. Catal.* **1995**, *155*, 249-255.

[35]   (a) P. Van Der Voort, R. Ramachandra Rao, B. M Weckhuysen, *Phy.Chem. Chem. Phy.* **1999**, *1*, 4099-4104; (b) M. De Boer, A. Van Dillen, D. Koningsberger, J. W. Geus, M. Vuurman, I. Wachs, *Catal. Lett.* **1991**, *11*, 227-239.

[36]   M. Shokouhimehr, Y. Piao, J. Kim, Y. Jang, T. Hyeon, *Angew. Chem. Int. Ed.* **2007**, *119*, 7169-7173.

[37]   J. Dou, H. C. Zeng, *J. Am. Chem. Soc.* **2012**, *134*, 16235-16246.

[38]   J. Wang, X. Li, S. Zhang, R. Lu, *Nanoscale* **2013**, *5*, 4823-4828.

[39]   P. C. Bakala, E. Briot, L. Salles, J.-M. Brégeault, *Appl. Catal. A: Gen.* **2006**, *300*, 91-99.

[40]   V. Masalov, N. Sukhinina, E. Kudrenko, G. Emelchenko, *Nanotech.* **2011**, *22*, 275718.

[41]   D. Green, J. Lin, Y.-F. Lam, M.-C. Hu, D. W. Schaefer, M. Harris, *J. Col. Inter. Sci.* **2003**, *266*, 346-358.

[42]   V. K. L. Mer, *Ind. Eng. Chem.* **1952**, *44*, 1270-1277.

[43]   K. Lee, J.-L. Look, M. T. Harris, A. V. McCormick, *J. Col. Inter. Sci.* **1997**, *194*, 78-88.

[44]   S. Sadasivan, A. K. Dubey, Y. Li, D. H. Rasmussen, *J. Sol-Gel Sci. Tech.* **1998**, *12*, 5-14.

[45]   M. T. Harris, R. R. Brunson, C. H. Byers, *J. Non-Cryst. Solids.* **1990**, *121*, 397-403.

[46]   M. T. Harris, *Ultrafine ceramic precursor powders by homogeneous precipitation and electrodispersion,* University of Tennessee, Knoxville **1992**.

[47]   A. Van Blaaderen, J. Van Geest, A. Vrij, *J. Col. Inter. Sci.* **1992**, *154*, 481-501.

[48]   C. C. Williams, J. G. Ekerdt, J. M. Jehng, F. D. Hardcastle, A. M. Turek, I. E. Wachs, *J. Phy. Chem.* **1991**, *95*, 8781-8791.

[49] N. A. Dhas, A. Gedanken, *J. Phys. Chem. B* **1997**, *101*, 9495-9503.

[50] A. V. Biradar, B. R. Sathe, S. B. Umbarkar, M. K. Dongare, *J. Mol Catal A: Chem.* **2008**, *285*, 111-119.

[51] T. V. Kotbagi, A. V. Biradar, S. B. Umbarkar, M. K. Dongare, *ChemCatChem* **2013**, *5*, 1531-1537.

[52] S. B. Umbarkar, T. V. Kotbagi, A. V. Biradar, R. Pasricha, J. Chanale, M. K. Dongare, A.-S. Mamede, C. Lancelot, E. Payen,J. Mol. Catal. A: *J. Mol. Catal. A: Chem.* **2009**, *310*, 150-158.

[53] (a) T. Siciliano, A. Tepore, E. Filippo, G. Micocci, M. Tepore, *Mater. Chem. Phy.* **2009**, *114*, 687-691; (b) H. Tian, C. A. Roberts, I. E. Wachs, *J. Phys. Chem. C.* **2010**, *114*, 14110-14120.(c) S. Ikegami, A. Yagasaki, *Materials* **2009**, *2*, 869-875.

[54] A. Klinbumrung, T. Thongtem, S. Thongtem, *J. Nanomaterials* **2012**, *2012*, 10.

[55] J. P. Thielemann, T. Ressler, A. Walter, G. Tzolova-Müller, C. Hess, *Appl. Catal. A : Gen.* **2011**, *399*, 28-34.

[56] M. Cornac, A. Janin, J. Lavalley, *Polyhedron* **1986**, *5*, 183-186.

[57] E. L. LeeÃ, I. E. Wachs, *D. Heter. Catal.* **2009**, 1.

[58] J. Melero, J. Iglesias, J. Arsuaga, J. Sainz-Pardo, P. de Frutos, S. Blázquez, *Appl. Catal. A: Gen.* **2007**, *331*, 84-94.

[59] J. Zhang, A. V. Biradar, S. Pramanik, T. J. Emge, T. Asefa, J. Li, *Chem. Commun.* **2012**, *48*, 6541-6543.

4

Mechanistic Studies Investigating the Role of the Oxidant and Hydrogen Bonding in Determining the Selectivity in Alkene Oxidation by Molybdenum Catalysts

Abstract: *When the molybdenum oxo-(peroxo) acetylide complex [CpMo(O-O)(O)C≡CPh] was used as a catalyst for the oxidation of olefins, completely different product selectivity was obtained depending on the oxidant employed. When tert-butyl hydroperoxide (TBHP, 5.5 M) in decane was used as the oxidant for the oxidation of cyclohexene, cyclohexene oxide was formed with high selectivity. However, when H_2O_2 was used as the oxidant, the corresponding cis-1, 2-diol was formed as the major product. Calculations performed by using density functional theory revealed the nature of the different competing mechanisms operating during the catalysis process and also provided an insight into the influence of the oxidant and hydrogen bonding on the catalysis process. The mechanistic investigations can therefore serve as a guide in the design of molybdenum-based catalysts for the oxidation of olefins.*

4.1. Introduction

The conversion of olefins to epoxides, is an extremely important reaction because it allows conversion of available crude oil fractions to epoxides, which are important organic intermediates for the production of a wide variety of chemicals [1-4] such as drugs, agrochemicals and food additives. They also play an important role in biological activity. [2],[5-7] While the epoxidation can take place without the need of a catalyst, much attention has been focused in recent years [8] on the metal-catalyzed epoxidation process due, in part, to the increased possibility of getting higher activity and selectivity through this route. Among the oxidants employed for the epoxidation process, the one most investigated is H_2O_2, [9] because of its low cost and ready availability. The transition metal based complexes that have been studied as epoxidation catalysts include complexes of iron [10-11] manganese [12-13] tungsten [14] and molybdenum. [15-16] Of these, the compounds most studied are the high oxidation state complexes of molybdenum.[16]

What is of interest in the epoxidation catalysis process is the mechanism of the reaction, which has been the subject of much debate. Assuming the presence of an peroxido ligand at the metal centre, Mimoun *et al.*[17] suggested a [2+3] cycloaddition route for this process, involving the reaction between olefin and the metal peroxo species (See Fig. 4.1a). Sharpless [18] has suggested the possibility of exogenous attack of the olefin at the electrophilic peroxo oxygen atom (See Fig. 4.1b). Both these proposed mechanistic routes assumed that the peroxido ligand attached to the molybdenum centre is the source of the oxygen atom for the epoxidation process. There have been several computational studies on the epoxidation reaction *via* the Sharpless and Mimoun pathways.[19-29] Of the two mechanisms, the Mimoun pathway was found to have a high barrier in comparison to the Sharpless mechanism.[23] Further experimental studies appeared to confirm this view.[30] However, recent work by Galindo *et al.*[15] has shown that a molybdenum diperoxo species is a stable intermediate during the epoxidation of *cis*-cyclooctene, with H_2O_2 as the oxidant, thus indicating that the Sharpless mechanism cannot be entirely ruled out. However, it appeared that a mechanism where the epoxide oxygen comes from H_2O_2 or TBHP, rather than from the oxido group on molybdenum, would be at least competitive, if not operative, during the catalysis. Such a mechanism, shown in Fig. 4.1c, was proposed by Thiels' *et al.* [31-32] This pathway involves the coordination of the oxidant

to the molybdenum centre followed by the transfer of the oxygen from the oxidant ligand to the olefin (See Fig. 4.1c). Finally, a mechanism that involves the insertion of the olefin between the metal-oxygen bond was proposed by Calhorda *et al.* [33]

We have recently reported experimental results [34] on the oxidation of cyclohexene using the peroxo species CpMo(O)(O-O)(-C≡CPh) as catalyst and, H_2O_2 as the oxidant. This was the first reported case of *cis*-1, 2-diol formation using molybdenum based catalyst. Since *cis*-1, 2-diols are important organic reagents in the pharmaceutical industry [35-38], the selectivity of the CpMo(O)(O-O)(-C≡CPh) catalyst in forming the *cis*-1, 2-diols was an important result. However, as will be discussed in the results and discussion section below, when, as alternatives to H_2O_2, organic TBHP in decane was used as the oxidant, the following interesting results are obtained: cyclohexene oxidation leads to the formation of the *cis*-1, 2-diol, rather than the epoxide, when H_2O_2 was used as the oxidant, while epoxide, rather than the *cis*-1, 2-diol, was formed as the major product when organic TBHP in decane was used as the oxidant. It is clear that the selectivity of the catalyst is significantly dependant on the nature of the oxidant employed. Moreover, it is possible that the presence of water can also have an effect on the barrier heights, as has been shown in calculations by Poli *et al.*[39], when investigating the epoxidation of cyclooctene by the H_2O_2 oxidant.

The observed differences in selectivity when using different oxidants suggested that there are competing mechanisms present during the catalysis process, leading to the formation of the *cis*-1, 2-diol or the epoxide as the major product. It is necessary to understand the nature of these competing mechanisms because such an understanding can help in the design of systems for specifically obtaining the epoxide or the *cis*-1, 2-diol as the major product. That is the objective of the current work. Full quantum mechanical computational studies, using density functional theory (DFT), have been conducted on the catalytic system: CpMoO(O)$_2$C≡CPh, with cyclohexene considered as the substrate and H_2O_2 or organic TBHP in decane considered as the oxidants. Three of the four mechanistic possibilities, shown in Fig. 4.1, have been considered: the Mimoun mechanism has not been considered because it has been computationally shown to be a high barrier process.[23] Furthermore, a new mechanism has been proposed to explain the formation of the *cis*-1, 2-diol product. It has been shown that the presence of water has a significant influence on the selectivity of the catalyst. It has been shown that changing the oxidant from H_2O_2 to TBHP leads to the change in preference of one mechanism over the other, and thus, to

the eventual choice of the product (epoxide in the case of organic TBHP and *cis*-1, 2 diol in the case of H_2O_2 as the oxidant).(See Fig. 4.2) The results therefore shed light on the mechanistic possibilities for the important epoxide and *cis*-1, 2-diol forming processes, and also provide insight into how one could tune the molybdenum based catalytic systems through the choice of oxidant, in order to obtain, as desired, the epoxide or the *cis*-1, 2-diol as the major product.
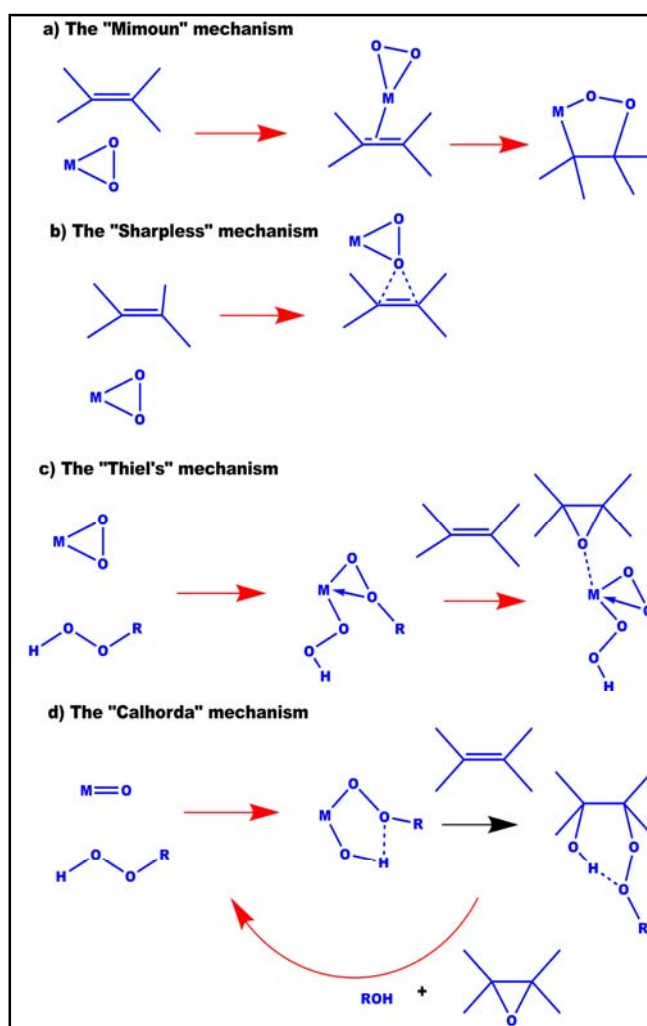

Fig. 4.1: The different mechanisms proposed in the literature for the olefin epoxidation reaction

The first sub-section of the Results and Discussion Section discusses the experimental evidence for the formation of the peroxo species upon addition of H_2O_2 or TBHP under reaction conditions, as well as the aforementioned observed selectivity for the epoxide when using the TBHP oxidant and the *cis*-1, 2-diol when H_2O_2 was used as an oxidant. The sub-sections following that discuss the

computational studies investigating the different mechanisms that are possible for the different systems, leading to results that corroborate the experimental findings.
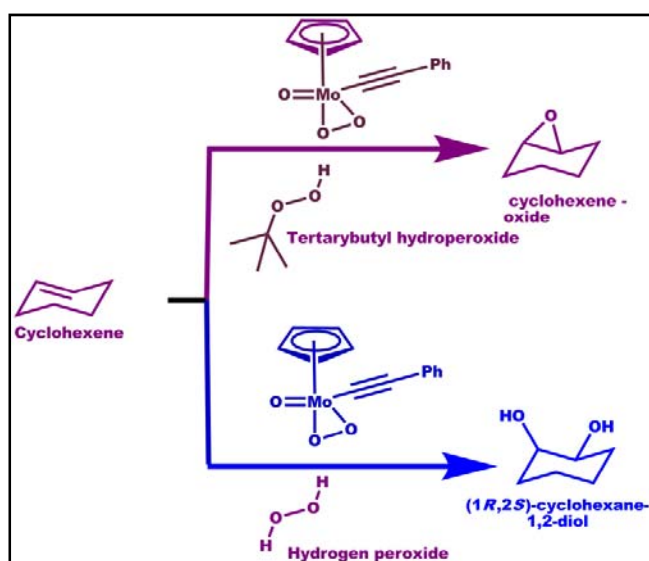

Fig. 4.2: The experimentally observed change in the selectivity towards epoxide and *cis*-1, 2-diol for the reaction of cyclohexene and hydrogen peroxide with a molybdenum catalyst.

4.2. Results and Discussion

4.2.1. Experimental Evidence for the Formation of the Peroxo Species for Acetylide Ligated Molybdenum Complexes. Experimental evidence of the formation of the peroxo molybdenum species: $CpMo(O)_2OC{\equiv}C$-Ph, during the catalytic oxidation of cyclohexene. $CpMo(O)_2OC{\equiv}C$-Ph was obtained from $CpMo(CO)_3C{\equiv}C$-Ph, which was prepared using the procedure as reported previously in the literature.[40-42] The FTIR spectrum of catalyst after addition of H_2O_2 confirmed the formation of molybdenum oxo–peroxo species. The peak at 930-960 cm^{-1} confirmed the presence of Mo=O terminal bond. The band at 840-860 cm^{-1} corresponds to the O-O stretching vibration of peroxo species. The weak bands at 669 and 575 cm^{-1} can be assigned to the $Mo-O_2$ (peroxo) asymmetric and symmetric stretching vibrations respectively. The IR positions for Mo oxo and peroxo were in good agreement with the literature reports [34], [41] for various Mo oxo–peroxo complexes. The bands due to C-H stretching vibrations of phenyl ring were observed in the range 2854–2955 cm^{-1} and the C=C stretching vibrations of the ring were observed at 1464 and 1377 cm^{-1} even after addition of hydrogen peroxide. Bands due

to carbonyl stretching (1940, 2031 cm^{-1}) disappeared after addition of H$_2$O$_2$. This clearly indicated the removal of all the CO ligands after addition of hydrogen peroxide and formation higher oxidation state Mo (VI) complex with retention of acetylide, -C≡C-Ph group attached to Mo center.[See Fig. 4.3 (a)] At higher concentration i.e., under reaction conditions of TBHP there is formation of the oxo-peroxo species, which is clearly indicated by the peaks at 940-950 cm^{-1} (due to Mo=O bond) and broad peak around 840 -860 cm^{-1} (due to O-O bond) .[See Fig. 4.3 (b)]

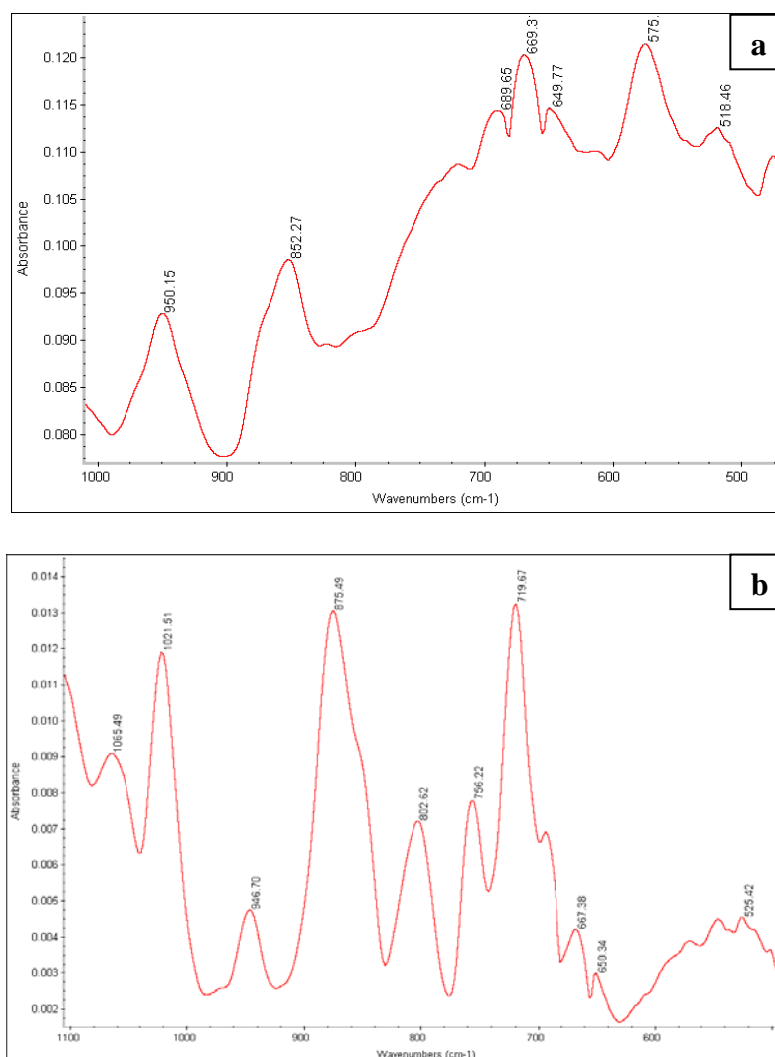**Fig. 4.3:** (a) The IR spectra indicating evidence for the formation of the oxo-peroxo species formed after treatment of the complex CpMo(CO)$_3$C≡CPh with H$_2$O$_2$. (b) The IR spectra indicating evidence for the formation of the dioxo-molybdenum species at higher concentration (that is, under reaction conditions) of TBHP in decane concentration CpMo(CO)$_3$C≡CPh complex.

Table 4.1: Cyclohexene oxidation using CpMo(CO)$_3$(C≡CPh) as a catalyst

Oxidant	Solvents	Time h.	Conversion %	Seletivity %		
				Epoxide	Diol	Others
TBHP	C$_2$H$_4$Cl$_2$	12	53	79.2	14.4[#]	6.4
50% H$_2$O$_2$	Tert-butanol	9	95	-	91[$]	9

Reaction condition: Cyclohexene (0.02 mol), Catalyst (0.01 mmol), oxidant 0.04 mol), temperature 80 ˚C; [#] *trans*-diol; [$] *cis*-diol .

Cyclohexene oxidation experiments conducted with CpMo(CO)$_3$C≡C-Ph using TBHP as the oxidant and 1, 2-dichloroethane as the solvent led to the formation of epoxide with selectivity as high as 79.2% within 12 hrs. 1, 2-dichloroethane was selected as the solvent to remove hydrogen bonding effects because of the use of protic solvents such as *tert*-butanol. It has been shown previously [34] that the -C≡CPh substituted molybdenum peroxo catalyst gives *cis*-1,2-diol with 91% conversion with 95% selectivity towards *cis*-dihydroxylation when *tert*-butanol was employed as the solvent. [34] The subsequent sections will focus attention on computational studies investigating the effect of the change of oxidant on the selectivity of the catalysis process.

4.2.2. Importance of Hydrogen Bonding on the Oxidation Reactions

Sharpless Mechanism. As stated in the Introduction, the fact that the use of CpMo(CO)$_3$C≡C-Ph as the catalyst produces the epoxide as the major product with TBHP as the oxidant while the use of CpMo(CO)$_3$C≡CPh produces the *cis*-1, 2-diol as the major product for cyclohexene oxidation [34] using 50% H$_2$O$_2$, indicates that there are competing mechanisms at work in the homogeneous catalysis systems. The possible mechanisms for the oxidation are illustrated in the Figs. 4.4, 4.5, 4.6 and 4.7 below. The possibility indicated in Fig. 4.4, also discussed in the Introduction, is that of the catalyst being approached directly by the cyclohexene: the "Sharpless" mechanism (See Fig. 4.1b). It is well established that CpMo(CO)$_3$C≡CPh would act as the precursor for CpMo(O-O)(O)(CCPh) (**b-1**).[18] As Fig. 4.4 indicates, **b-1** can be converted to the corresponding dioxo intermediate **b-2** and in the process yield the epoxide, denoted as **a-2**. The barriers obtained are 26.2 kcal/mol and 28.5 kcal/mol

for the reaction to occur in *tert*-butanol and 1, 2-dichloroethane respectively (ΔG values). For the case of aqueous H_2O_2 as the oxidant (with *tert*-butanol as the solvent), there is the possibility that the water molecules present in solution during the reaction, as well as the H_2O_2 oxidant itself, can hydrogen bond to the CpMo(O-O)(O)(-C≡CPh) catalyst molecule, and thereby affect the barrier height for this epoxidation reaction. These possibilities have been considered, with the epoxidation reaction considered with one, as well as two water molecules coordinated *via* hydrogen bonds with the CpMo(O-O)(O)(-C≡CPh) catalyst. The presence of one water molecule is found to lower the energy barrier to 22.3 kcal/mol (See Fig. 4.7a), while the presence of two water molecules, as shown in Fig. 4.4 (t-2), is found to lead to a barrier of 24.7 kcal/mol for this epoxidation reaction. These results therefore indicate that the presence of water molecules does have an effect on the kinetics of the epoxidation process. Similar calculations done to show the involvement of hydrogen bonded H_2O_2 in the "Sharpless mechanism" lowers the barrier to 24.7 kcal/mol. Hence, the results indicated that the interaction, *via* hydrogen bonding, of one H_2O_2 or two H_2O molecules shows the same lowering of the energy barrier for the "Sharpless mechanism". Henceforth, when considering aqueous H_2O_2 as the oxidant, the model that will be employed to take the effect of hydrogen bonding into account will be the presence of two water molecules hydrogen-bonded to the molybdenum catalyst. It is also to be noted that the solvent employed – *tert*-butanol – when aqueous H_2O_2 is used as the oxidant, can also hydrogen bond with the molybdenum catalyst, and thus could also influence the energetics of the oxidation process. However, it is likely that water would displace *tert*-butanol from the molybdenum catalyst, because of its superior ability to hydrogen bond with the catalyst. Calculations done indicated that given a choice to hydrogen bond with *tert*-butanol or with water, the peroxo group of the catalyst shows a preference, by 3.6 kcal/mol, for bonding *via* a hydrogen bond, to the water molecule.

For the TBHP oxidant case: when organic TBHP was employed, then there are no water molecules present that can contribute to hydrogen bonding with the catalyst. Moreover, the solvent used when organic TBHP is the oxidant: 1, 2-dichloroethane, also cannot form hydrogen bonds or participate in other weak interactions with the catalyst molecules: calculations that we have done attempting to non-covalently bind the chlorine atoms of 1, 2-dichloroethane to the oxygen atoms of the catalyst indicated that the two moieties drifted apart in the optimized structures. However TBHP itself,

in addition to acting as an oxidant, can interact with the catalyst through hydrogen bonding. Such an interaction also reduces the barrier for the epoxidation process, from 28.5 kcal/mol (See Fig. 4.9 (a) to 25.8 kcal/mol (See Fig. 4.4 **(t-3/1T)** and to 23.7 kcal/mol with two TBHP (See Fig. **(t-3/2T))** molecules hydrogen bonding to the catalyst. These results therefore underline the importance of hydrogen bonding of the oxidant and/or the water molecule in the oxidation processes occurring in the molybdenum systems.

Thiels'Mechanism. The first step of the Thiels' Mechanism involves the conversion of the CpMoC≡CPh(O)(OO) catalyst complex to CpMoC≡CPh(O)(OOH)(OOR), R = H (H_2O_2) and *t*-butyl (TBHP). In the absence of any hydrogen bonding interactions, the barriers are 28.6 kcal/mol for the H_2O_2 oxidant, and 30.5 kcal/mol for the TBHP oxidant [See Fig. 4.7 (ts-2) and 4.6 (t-4-H) respectively]. These barriers are reduced when two hydrogen bonding water molecules are considered for the H_2O_2 oxidant, and two TBHP molecules are considered for the TBHP oxidant case. For the H_2O_2 case, the barriers are reduced from 28.6 kcal/mol to 24.7 kcal/mol when one water molecule is hydrogen bonded to the peroxo group of the catalyst and to 22.7 kcal/mol when two water molecules are considered. For the TBHP case, the corresponding barriers are 30.5 kcal/mol when no extra TBHP molecules are employed, 29.4 kcal/mol with the addition of one extra TBHP molecule and 26.5 kcal/mol when two extra TBHP molecules are considered (See Fig. 4.5 (b-4/2T) below). The reason for the sharp decrease in the barrier, from 28.6 kcal/mol to 22.7 kcal/mol, for the H_2O_2 case is due to the fact that one of the two water molecules that have been considered performs the task of a "hydrogen atom relay" in the transition state (**t-6**): the water molecule accepts a hydrogen atom from the coordinating H_2O_2 oxidant species and donates one of its own hydrogen atoms to the peroxo group of the molybdenum catalyst (See Fig. 4.5 (t-6)). This leads to the conversion of the four-membered transition state for the hydrogen transfer in the absence of the water molecule to a sterically more favored six-membered transition state when the water molecule is considered. A similar hydrogen atom relay mechanism also occurs in the case of TBHP. However, the effect with TBHP is less pronounced, with the energy barrier decreasing by 6.1 kcal/mol, as compared with a decrease of 4.0 kcal/mol in the case of water.

The upshot of the calculations for the important first step of the competing Sharpless and Thiels's mechanisms is this: for the aqueous H_2O_2 case, the first step of

molecule accepts a hydrogen atom from the coordinating H_2O_2 oxidant species, and donates one of its own hydrogen atoms to the peroxo group of the molybdenum catalyst (See Fig. 4.5 (t-6) below). This leads to the conversion of the four membered transition state for the hydrogen transfer in the absence of the water molecule to a sterically more favoured six membered transition state when the water molecule is considered. Such a similar hydrogen atom relay mechanism also occurs in the TBHP case. However, the effect for the TBHP is less pronounced, with the barrier decreasing by only 1.0 kcal/mol as compared to a 4.0 kcal/mol decrease for the water case the Thiels' mechanism is more favoured than the first step of the Sharpless mechanism, whereas for the TBHP case, it is the other way around (See the Figs. 4.4 and 4.5). This indicates that when TBHP was employed as the oxidant, the Sharpless mechanism would be favoured, leading to the formation of the epoxide as the major product. This corroborates experimental findings, as has been discussed above in the previous section. For the H_2O_2 case, the epoxide would not be formed in the first step, but the formation of the species CpMo(O)(OOH)(OOH) (**b-11**) would be preferred. As the later section will show, this will lead to the formation of the *cis*-1, 2-diol as the preferred major product.
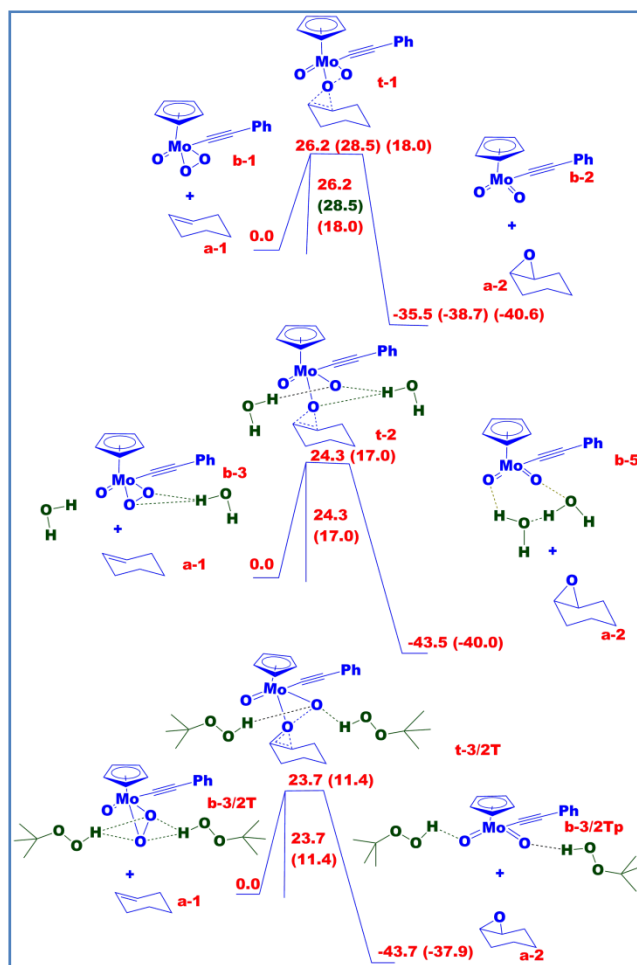
Fig 4.4: The potential energy surfaces for the first step of the "Sharpless mechanism" for the molybdenum catalyst CpMo(O)(OO)(CCPh) – the influence of hydrogen bonding by water and TBHP is considered; energy values outside the parentheses are ΔG values; values inside the parentheses are the corresponding ΔH values, all values are in kcal/mol; (the value in green parentheses is the ΔG value in 1,2-dichloroethane)

Activation of the Mo=O bond. Apart from the two mechanisms considered: Sharpless and Thiel, a third possibility, proposed earlier by Poli *et al.*[23], [39] has also been considered. In this mechanism, as in the Thiel mechanism, the oxidant: H_2O_2 or TBHP, approaches the molybdenum catalyst, but unlike in the Thiel mechanism, the oxidant transfers a hydrogen atom to the oxygen coordinating with a double bond to the molybdenum centre. As shown in Fig. 4.7 (a) (ts-3) and Fig. 4.6 (c) (t-7-H), such a reaction has a barrier of 29.6 kcal/mol for the H_2O_2 oxidant and 35.5 kcal/mol for the TBHP oxidant respectively. The presence of two H_2O molecules (for the case of the aqueous H_2O_2 oxidant) and two extra TBHP molecules (for the case of the TBHP oxidant) reduces the barriers to 23.6 kcal/mol and 27.6 kcal/mol respectively. For the

H_2O_2 case, the barrier (23.6 kcal/mol) is higher than for the first step of the Thiel Mechanism, while for the TBHP case, the barrier (27.6 kcal/mol) (See Fig. 4.6 (t-5/2T) is higher than the first step of both the Sharpless and the Thiel mechanisms. This indicates that the activation of the Mo=O bond would not be a favoured pathway during the oxidation reaction for both the H_2O_2 and TBHP oxidants.
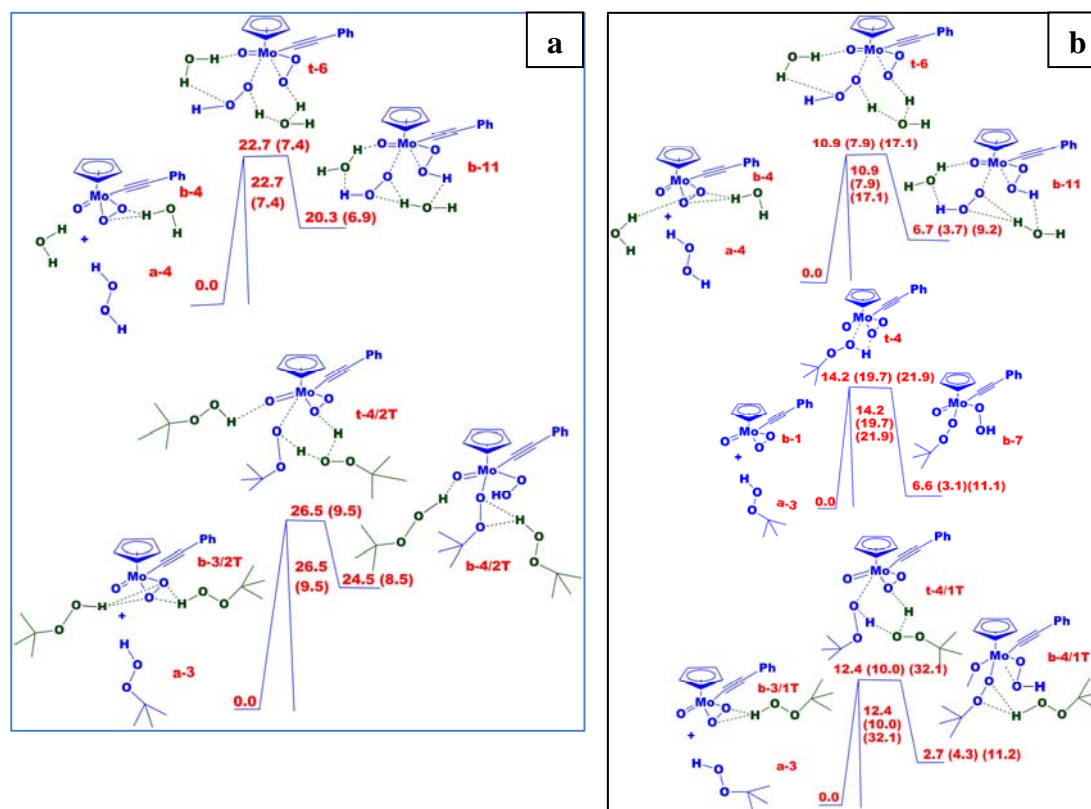

Fig 4.5: (a) The potential energy surfaces for the first step of the Thiels' mechanism: approach of the oxidants TBHP and H_2O_2 towards the molybdenum catalyst;energy values outside the parentheses are ΔG values; values inside the parentheses are the corresponding ΔH values; all values are in kcal/mol; (b) Probability for H_2O_2 and TBHP attack at Mo centre with the assistance of water molecule in the case first case and TBHP attack in the third case the values shown in the Fig are the electronic energies calculated using the BP-86, PBE and B3LYP functionals respectively – the BP-86 values are shown outside the parenthesis, while the PBE and the B3LYP energies are shown (in that order), inside the parenthesis.
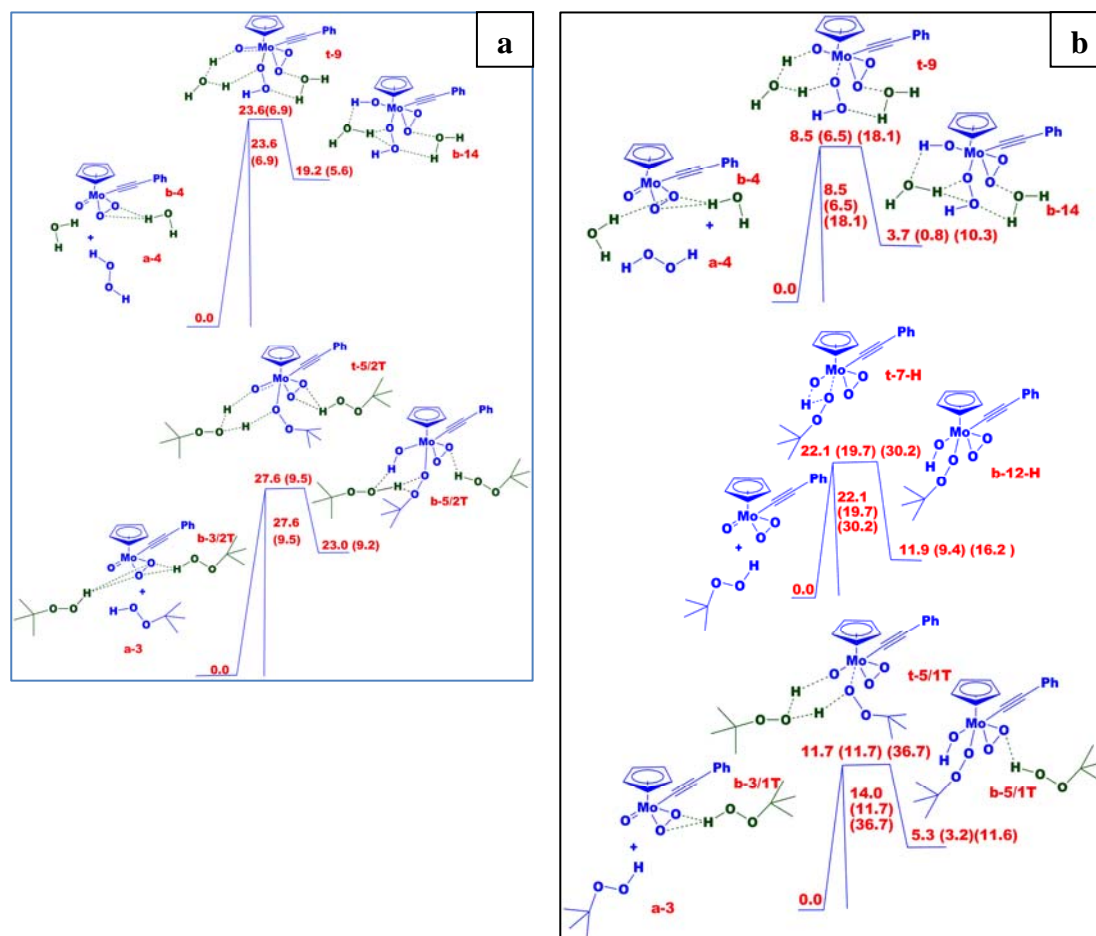
Fig 4.6: (a) The potential energy surfaces for the alternative reaction pathway for the reaction of the Mo centre with the two oxidants (TBHP and H_2O_2); energy values outside the parentheses are ΔG values; values inside the parentheses are the corresponding ΔH values; all values are in kcal/mol; (b) shows the potential energy surface for M=O activation of peroxo and dioxo molybdenum species, the values in case of (b) shown in the Fig. are the electronic energies calculated using the BP-86, PBE and B3LYP functionals respectively – the BP-86 values are shown outside the parenthesis, while the PBE and the B3LYP energies are shown (in that order), inside the parenthesis; energy values outside the parentheses are ΔG values.
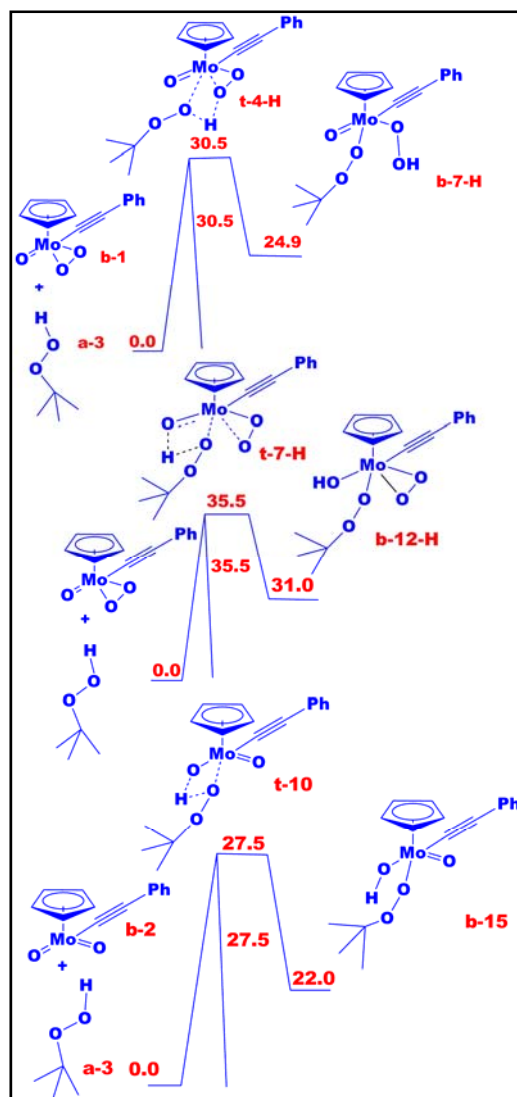
Fig 4.6: (c) The potential energy surfaces for the reaction pathway for the Mo centre with the one TBHP for Theils' mechanism, activation of Mo=O and activation of Mo=O of dioxo at Mo centre; energy values outside the parentheses are Δ G values; all values are in kcal/mol.
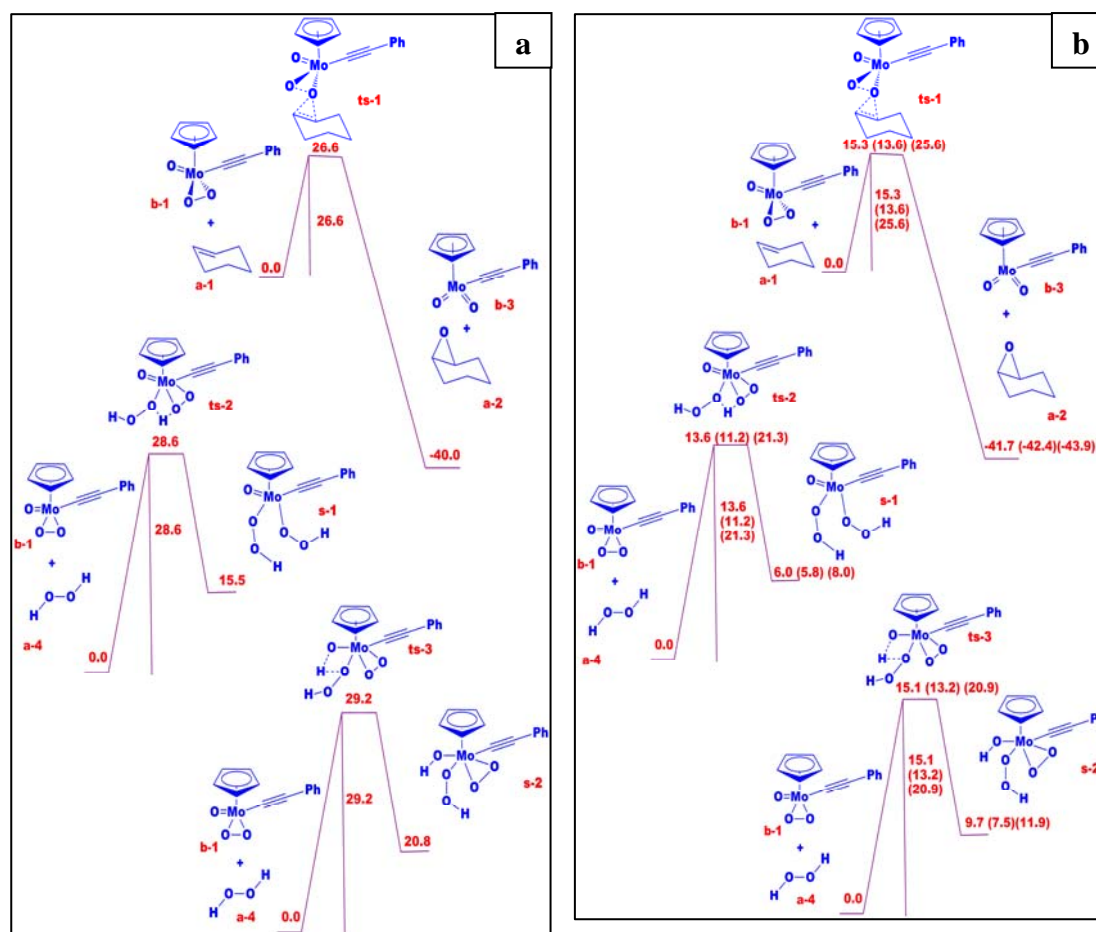
Fig. 4.7: (a) The potential energy surface of the "Sharpless mechanism", "Thiels' mechanism" and Mo=O activation without water molecule; all the ΔG (solvent corrected) values are in kcal/mol;(b) the values shown in the Fig. are the electronic energies calculated using the BP-86, PBE and B3LYP functionals respectively − the BP-86 values are shown outside the parenthesis, while the PBE and the B3LYP energies are shown (in that order), inside the parenthesis.

Completion of the Epoxidation Cycle. The previous sections have established that the first step of the Sharpless Mechanism is preferred when organic TBHP is considered as the oxidant, and that the first step of the Thiel mechanism is preferred when aqueous H_2O_2 is employed as the oxidant. Discussed in this section is the completion of the catalytic cycle for the Sharpless Mechanism. Only the TBHP oxidant case is considered here, because the catalyst will prefer the Thiel pathway when the aqueous H_2O_2 is used. Shown in Fig. 4.12 (t-3/2T) is the free energy pathway for the conversion of the molybdenum dioxo species, formed at the end of the first step of the Sharpless mechanism, to the CpMo(C-CPh)(O)(OH)(OO-*tert*-butyl) species. The aid of an extra *tert*-butyl species as a hydrogen relay agent has also been considered for this conversion. The next step of the cycle, the step that

would convert the CpMo(C-CPh)(O)(OH)(OO-*tert*-butyl) species to the original catalyst, CpMo(O)(O-O)(C-C≡Ph), and also form *tert*-butanol (one of the observed products of the reaction) is shown in Fig. 4.13. This intermolecular rearrangement reaction (See Fig. 4.13) is made more facile through the aid of a hydrogen bonded TBHP species. The barriers of the two steps shown in the Figs 4.12 and 4.13 are 24.5 kcal/mol and 23.0 kcal/mol respectively (See Figs 4.12 and 4.13) respectively. It is to be noted that the species CpMo(C-CPh)(O)(OH)(OO-*tert*-butyl) (b-16) formed as shown in Fig. 4.12 can also undergo attack by a cyclohexene species leading to further epoxidation, as has been speculated in the past.[33], [43] As shown in Fig 4.14 (ts-4) such an attack will be less favored (barrier of 33.8 kcal/mol) than the intramolecular pathway shown in Fig. 4.13 below. Hence, the most likely outcome of the oxidation process when using TBHP as an oxidant, will be the Sharpless mechanism, yielding the epoxide as the major product.
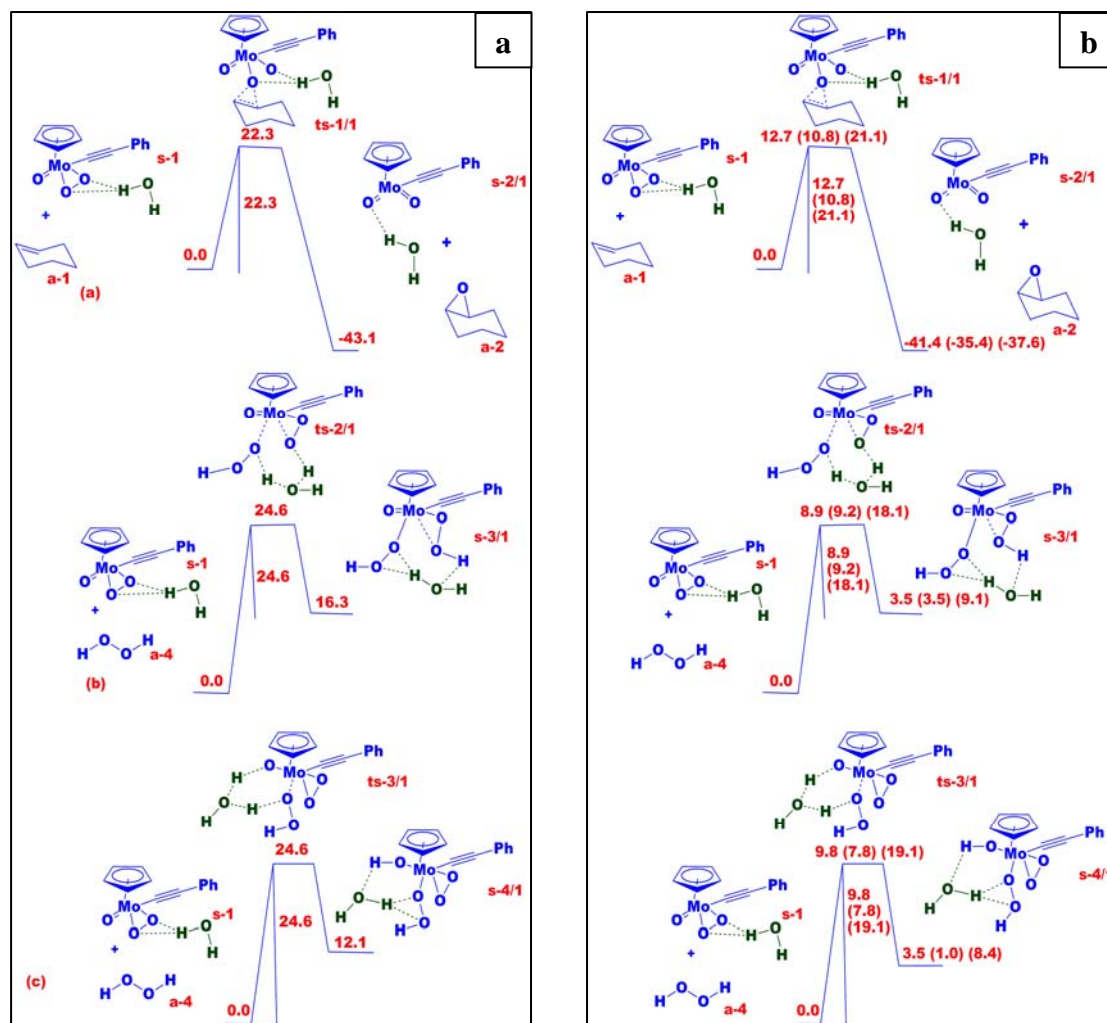
Fig. 4.8: (a) The potential energy surface of the "Sharpless mechanism" and the "Thiels' mechanism" with the inclusion of water molecules, all the ΔG (solvent corrected) values are in kcal/mol; (b) the values shown in the Fig are the electronic energies calculated using the BP-86, PBE and B3LYP functionals respectively – the BP-86 values are shown outside the parenthesis, while the PBE and the B3LYP energies are shown (in that order), inside the parenthesis.
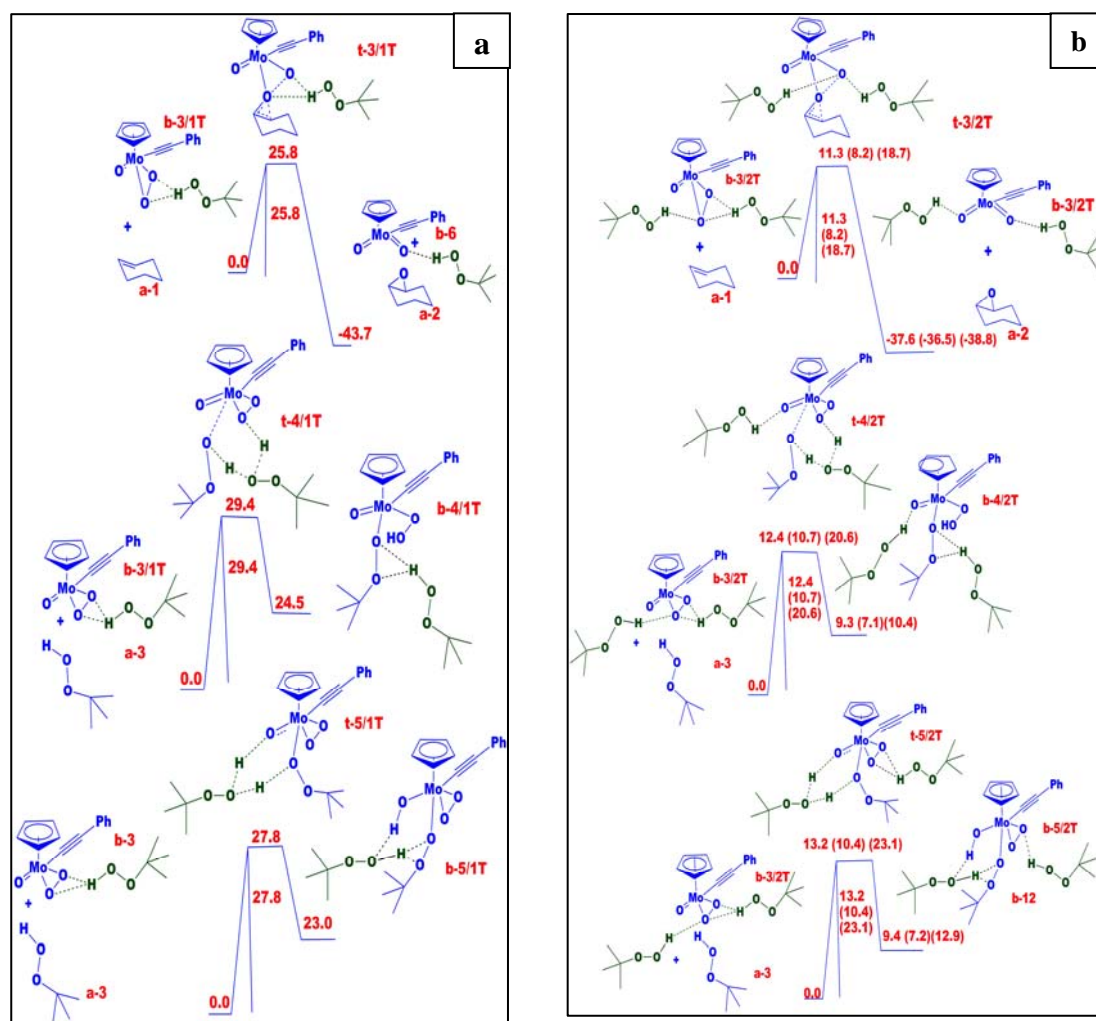
Fig. 4.9: (a) The potential energy surface for the "Thiels' mechanism" and double bond activation by TBHP molecules showing the role played by one TBHP molecule in peroxide ring breaking and epoxide formation, peroxo ring opening (Thiels' mechanism) and activation of double bonds; all the values shown in Fig are free energy Δ G (solvent corrected) in kcal/mol) ;(b) The potential energy surface for the "Thiels' mechanism" and double bond activation by TBHP molecules showing the role played by two TBHP molecules in peroxide ring breaking and epoxide formation, peroxo ring opening (Thiels' mechanism) and the activation of double bonds; the values shown in the Fig are the electronic energies calculated using the BP-86, PBE and B3LYP functionals respectively – the BP-86 values are shown outside the parenthesis, while the PBE and the B3LYP energies are shown (in that order), inside the parenthesis.

Fig. 4.10: (a) The potential energy surface for the "Sharpless mechanism" **t-4/1,** Theils mechanism and double bond activation, showing the role played by H$_2$O$_2$ molecule in peroxide ring breaking and epoxide formation ; all the values shown in Fig are free energies in ΔG (solvent corrected) in kcal/mol;(b) Theils mechanism **ts-2/2** ans double bond activation **ts-3/3** with H$_2$O$_2$; the values shown in the Fig are the electronic energies calculated using the BP-86, PBE and B3LYP functionals respectively – the BP-86 values are shown outside the parenthesis, while the PBE and the B3LYP energies are shown (in that order), inside the parenthesis.
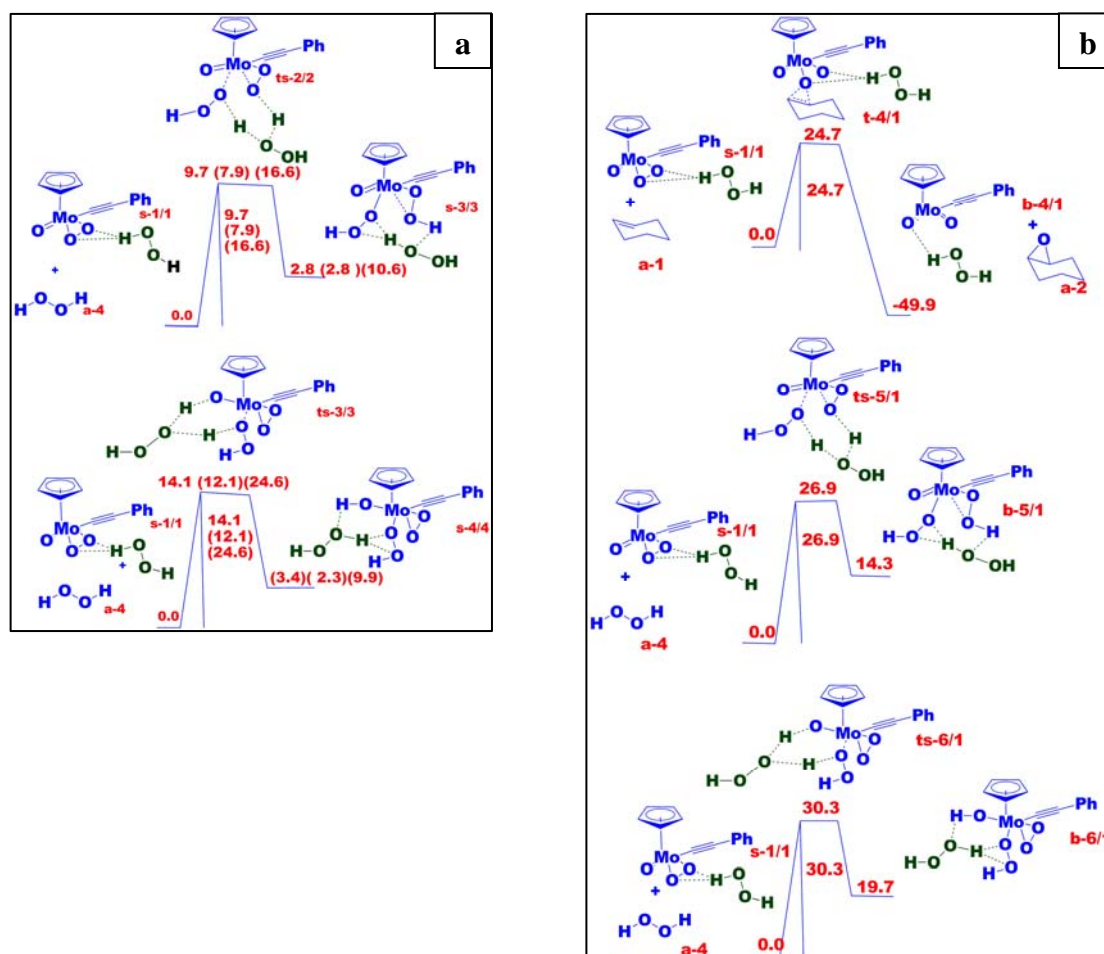
Fig. 4.11: The potential energy surface for different conditions of "Sharpless mechanism" **t-2** and **ts-5/1** and **t-3/1T**; the values shown in the Fig are the electronic energies calculated using the BP-86, PBE and B3LYP functionals respectively – the BP-86 values are shown outside the parenthesis, while the PBE and the B3LYP energies are shown (in that order), inside the parenthesis.
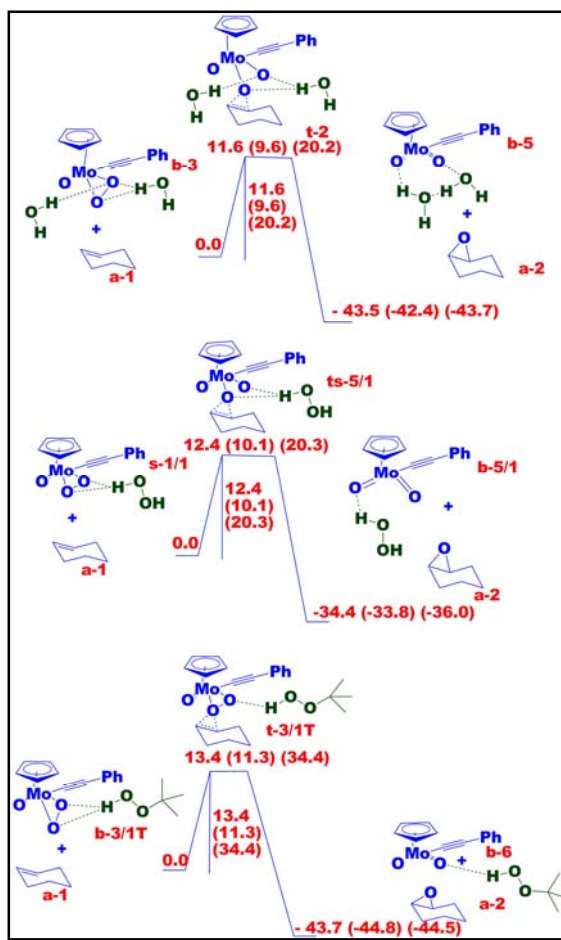

Fig. 4.12: The potential energy surface for the conversion of the molybdenum dioxo species, CpMo(O)(O)(-C≡CPh), to CpMo(O)(OH)(OO-*tert*-butyl)(-C≡CPh; energy values outside the parentheses are ΔG values; values inside the parentheses are the corresponding ΔH values; all values are in kcal/mol.

Fig. 4.13: (a) The potential energy surface for the regeneration of the catalyst from the intermediate CpMo(O)(OH)(OO-*tert*-butyl)(-C≡CPh);energy values outside the parentheses are Δ G values; values inside the parentheses are the corresponding Δ H values; all values are in kcal/mol; The potential energy surface represents the formation of peroxo species formed *via* intramolecular rearrangement and regeneration of catalyst; (b) the values shown in the Fig are the electronic energies calculated using the BP-86, PBE and B3LYP functionals respectively – the BP-86 values are shown outside the parenthesis, while the PBE and the B3LYP energies are shown (in that order), inside the parenthesis
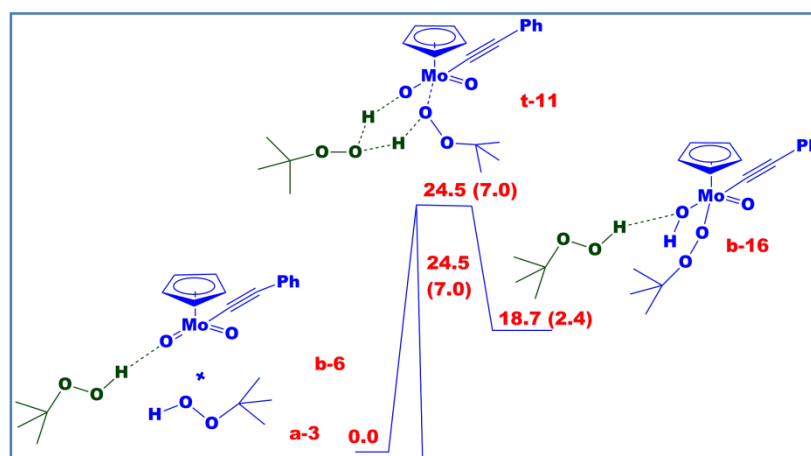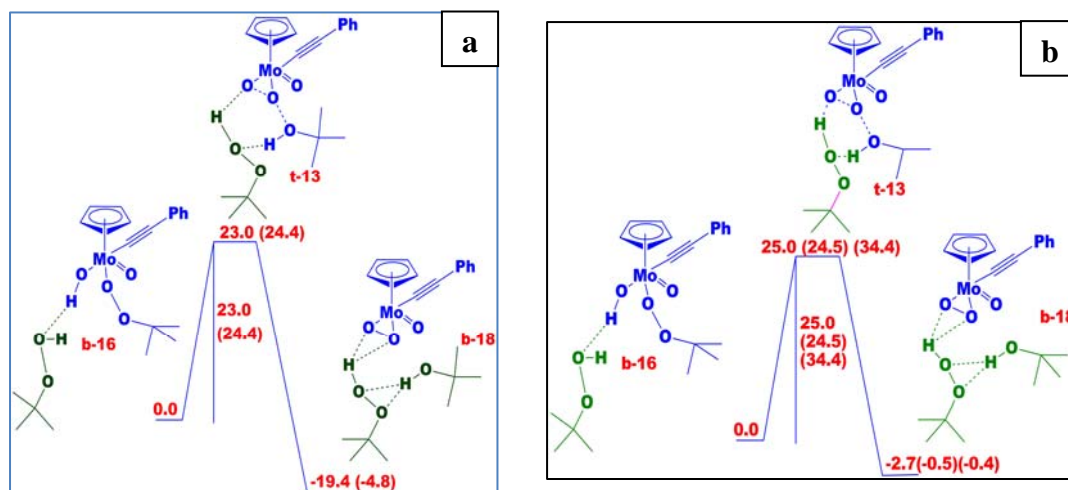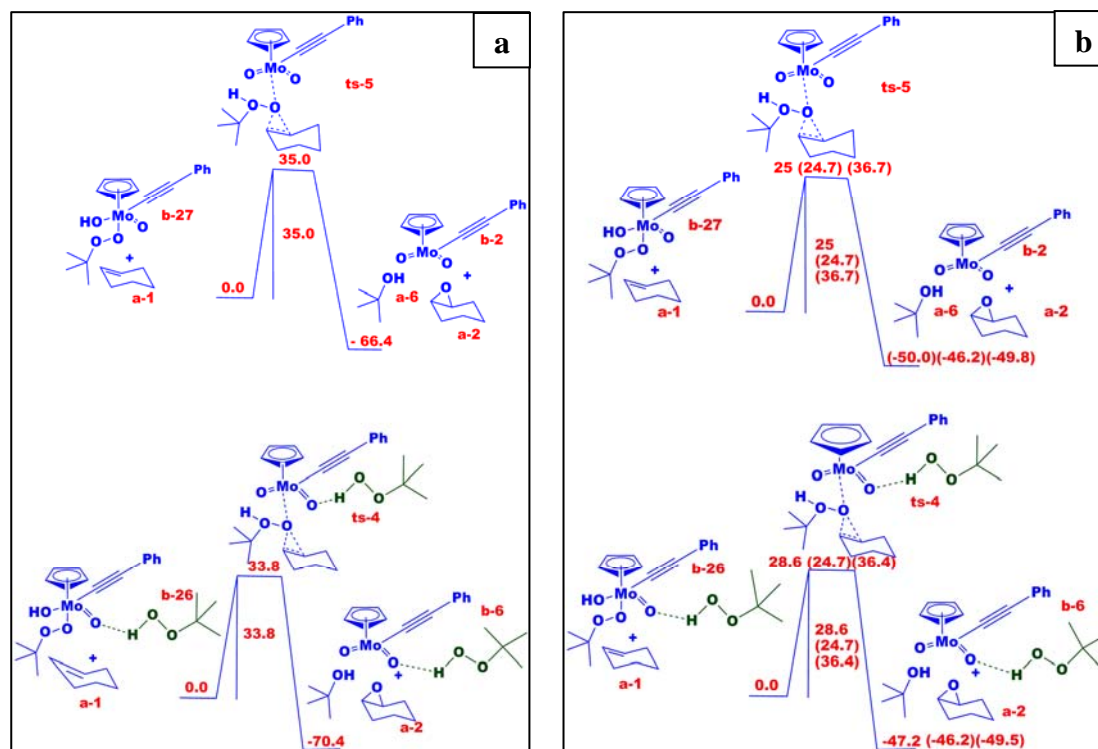
Fig. 4.14: (a) The potential energy surface for epoxide formation from the CpMo(O)(OH)(OOTBHP)-C≡CPh species; The values in parenthesis denote the energies calculated from the calculations with the PBE functional; all the values represents free energy Δ G (solvent corrected) in kcal/mol. (b) the values shown in the Fig are the electronic energies calculated using the BP-86, PBE and B3LYP functionals respectively – the BP-86 values are shown outside the parenthesis, while the PBE and the B3LYP energies are shown (in that order), inside the parenthesis.

Fig. 4.15: (a) The potential energy surface for the alternative pathway for breakdown of alkyperoxo bond and epoxide formation; all free energy values are in ΔG (solvent corrected) in kcal/mol;(b) the values shown in the Fig are the electronic energies calculated using the BP-86, PBE and B3LYP functionals respectively – the BP-86 values are shown outside the parenthesis, while the PBE and the B3LYP energies are shown (in that order), inside the parenthesis.
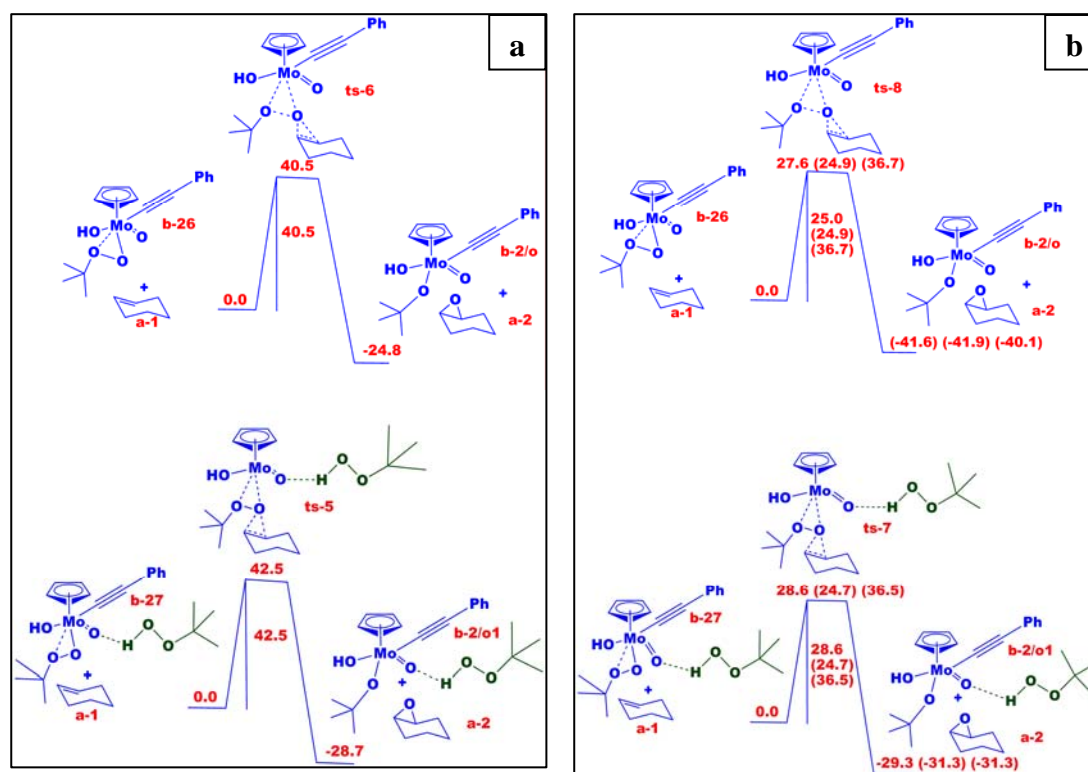
Further Reactions for the Cp(Mo)(-C≡CPh)(OOH)(OOH) Intermediate. The previous sections have shown that the molybdenum based catalyst, in conjunction with the H₂O₂ oxidant, will preferably produce the Cp(Mo)(-C≡CPh)(OOH)(OOH)(2H₂O) (**b-11**) species. Subsequent calculations (shown in Fig. 4.14 a) indicate that this species can be converted at the low barrier of 3.6 kcal/mol to the conformer CpMo(-C≡CPh)(OH)(OOH)(OO)(2H₂O) (**b-20**) which, in turn, can convert at a barrier of 6.6 kcal/mol to the conformer CpMo(-C≡CPh)(OH)(OOH)(OO)(2H₂O) (**b-14**). Hence, there are three conformers of the intermediate that can exist in solution during the catalysis process, as also further illustrated in Fig 4.17 below. Of the three, the most stable intermediate is **b-20**, lying slightly lower in energy than the other two conformers. This species, having two hydrogen bonding water molecules, can undergo further conversion to the structure referred to as **b-20(i)** in Fig. 4.18: in **b-20(i)**, where the hydrogen bonding water

molecules are at the same end (the OOH end, See Fig. 4.18), instead of the water molecules separately binding to the OOH and the OH ends, as in **b-20**. Such rearrangements of the hydrogen bonding water molecules is quite a facile process, as evidenced by the small difference in the energies of the structures **b-20** and **b-20(i)**, calculated to be 1.1 kcal/mol, with **b-20(i)** being the slightly higher in energy. Such a rearrangement of the water molecules has been considered in order to consider the reaction shown in Fig. 4.19: where a cyclohexene can approach the peroxo group of the species **b-20(i)** and be oxidized to the corresponding *cis*-1, 2-diol through a two-step process (See Fig. 4.19). This is a facile process, with the barriers for the two reactions being 16.8 kcal/mol and 10.5 kcal/mol respectively. Hence, for the case of the molybdenum catalyst with aqueous H_2O_2 as the oxidant, the first step: approach and attack of the H_2O_2 moiety, is the slowest step of the reaction, having a barrier of 22.7 kcal/mol. It is also to be noted that the *cis*-1, 2-diol can also be formed by the approach and attack of the cyclohexene species on the intermediate conformers **b-14** and **b-11**. As the potential energy surfaces shown in the Figs. 4.19 and 4.20 indicate, the reactions in each of these cases leading to the eventual formation of the *cis*-1, 2-diol were also found to have low barriers, lower than the first step of the catalytic cycle: the approach and attack of the hydrogen peroxide species.

It may also be possible for the intermediates **b-11**, **b-14** or **b-20** to form the epoxide from the approach and attack of the cyclohexene. For each of the cases **b-11** and **b-14** and **b-20** the barriers are 18.7 kcal/mol, 17.2 kcal/mol and 22.6 kcal/mol respectively. See Fig. 4.24) All the energy barriers discussed for epoxide are found to be higher than the corresponding barriers for the formation of the *cis*-1, 2-diol by the approach and attack of the cyclohexene on **b-11**, **b-14** and **b-20** (See the barrier heights in the Figs. 13, 12 and 11 respectively). Thus, overall, for the molybdenum catalyst complex with aqueous H_2O_2 as the oxidant, the calculations predict that the preferred product formed would be the *cis*-1, 2-diol, thus corroborating the experimental findings, discussed earlier. We also note here that the other mechanism possible after the formation of the Cp(Mo)(-C≡CPh)(OOH)(OOH)(2H₂O) species: the "Calhorda" mechanism (See Fig. 4.24), which would lead to the formation of epoxide, was also studied and found to have a high barrier of 27.9 kcal/mol. Hence the calculations indicate that the two operative competing mechanisms during the cyclohexene oxidation processes would be the Sharpless mechanism and our proposed mechanism which can be considered a modified Thiels'-type mechanism, with the

Sharpless mechanism being favored in the case where TBHP is used as the oxidant and the mechanism with features common with the Thiels' mechanism being preferred when H_2O_2 is employed as the oxidant.
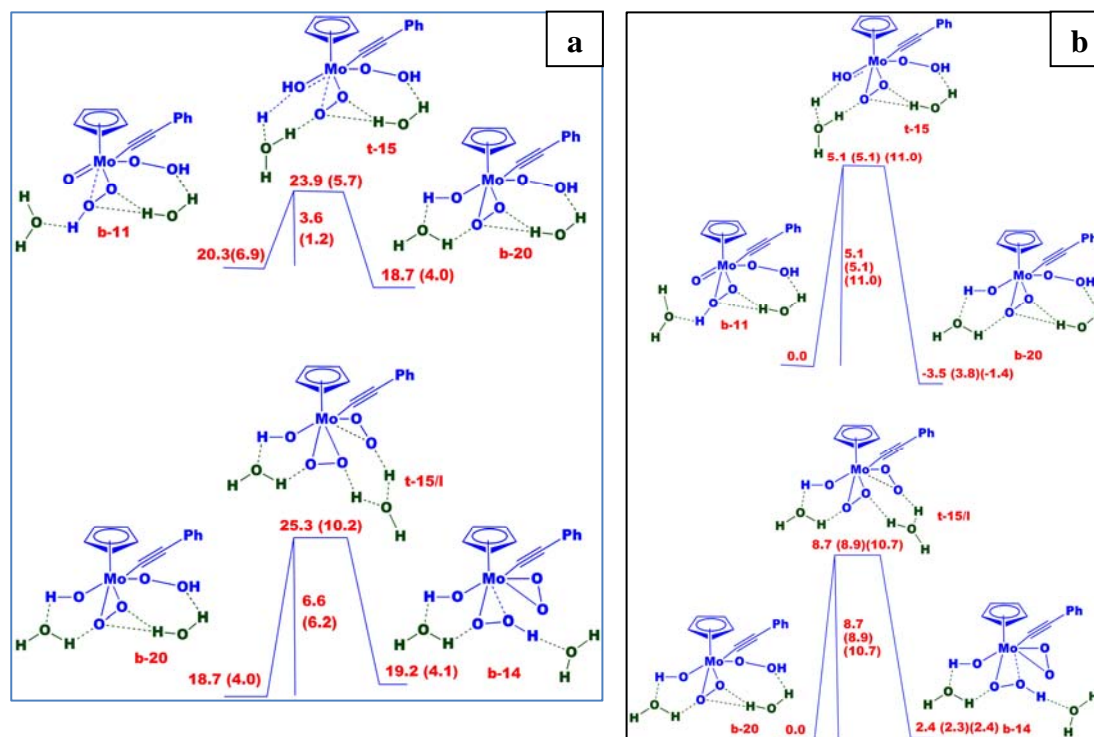
Fig 4.16: (a) The facile interconversion between the different conformers possible for the intermediates formed from the reaction of hydrogen peroxide with the acetylide coordinated molybdenum catalyst; energy values outside the parentheses are Δ G values; values inside the parentheses are the corresponding Δ H values; all values are in kcal/mol; (b) the values shown in the Fig are the electronic energies calculated using the BP-86, PBE and B3LYP functionals respectively – the BP-86 values are shown outside the parenthesis, while the PBE and the B3LYP energies are shown (in that order), inside the parenthesis.

Fig. 4.17: Interconversions between different isomers of the molybdenum catalyst after coordination of the molybdenum catalyst

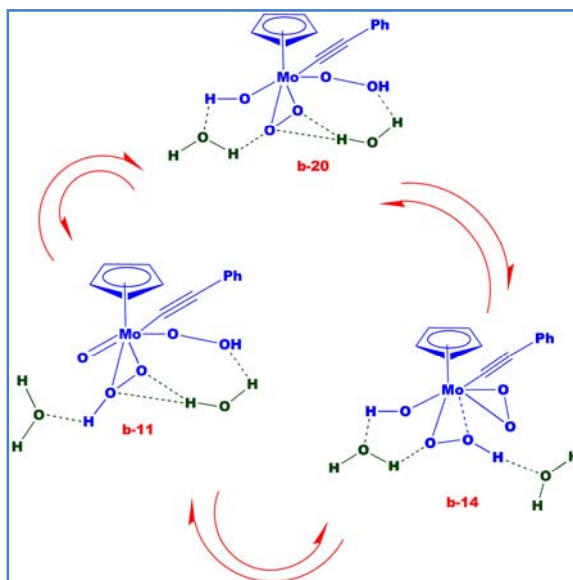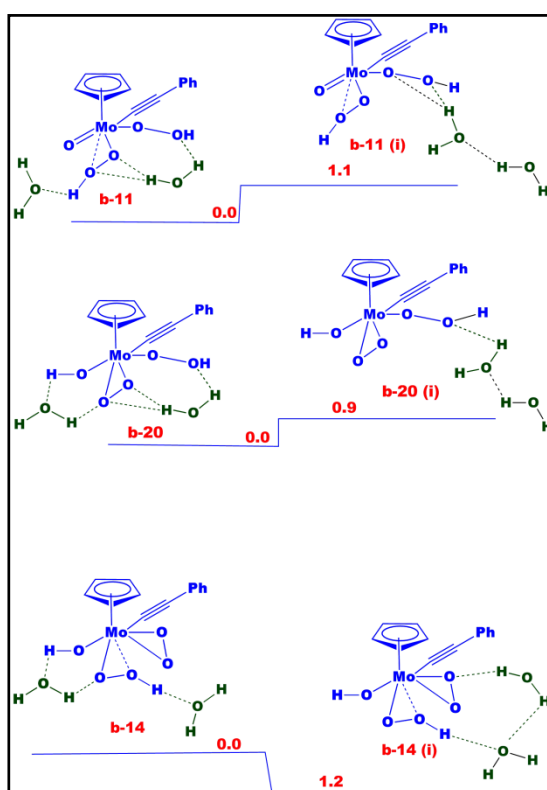**Fig. 4.18:** The optimized geometry of the various possible isomers showing hydrogen-bonded structures with water**,** at different positions in the some molecule**.**

Fig. 4.19: The potential energy surface for the formation of the *cis*-1, 2-diol from the reaction of cyclohexene with **b-20(i)–** the most stable of the three conformers of the intermediate of the reaction of hydrogen peroxide with the acetylide coordinated molybdenum catalyst; energy values outside the parentheses are ΔG values; values inside the parentheses are the corresponding Δ H values; all values are in kcal/mol;

Fig. 4.20: The potential energy surface for the formation of the *cis*-1, 2-diol from the reaction of cyclohexene with **b-11(i)–** one of the three conformers of the intermediate of the reaction of hydrogen peroxide with the acetylide coordinated molybdenum catalyst; energy values outside the parentheses are Δ G values; values inside the parentheses are the corresponding Δ H values; all values are in kcal/mol.

Fig. 4.21: (a) The potential energy surface for the formation of the *cis*-1,2-diol from the reaction of cyclohexene with **b-14(i)**–one of the three conformers of the intermediate of the reaction of hydrogen peroxide with the acetylide coordinated molybdenum catalyst; energy values outside the parentheses are ΔG values; values inside the parentheses are the corresponding ΔH values; all values are in kcal/mol;(b) the values shown in the Fig are the electronic energies calculated using the BP-86, PBE and B3LYP functionals respectively – the BP-86 values are shown outside the parenthesis, while the PBE and the B3LYP energies are shown (in that order), inside the parenthesis
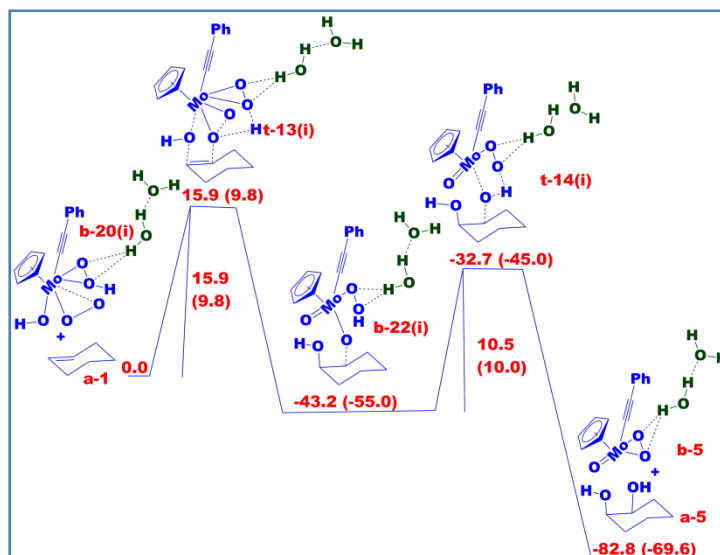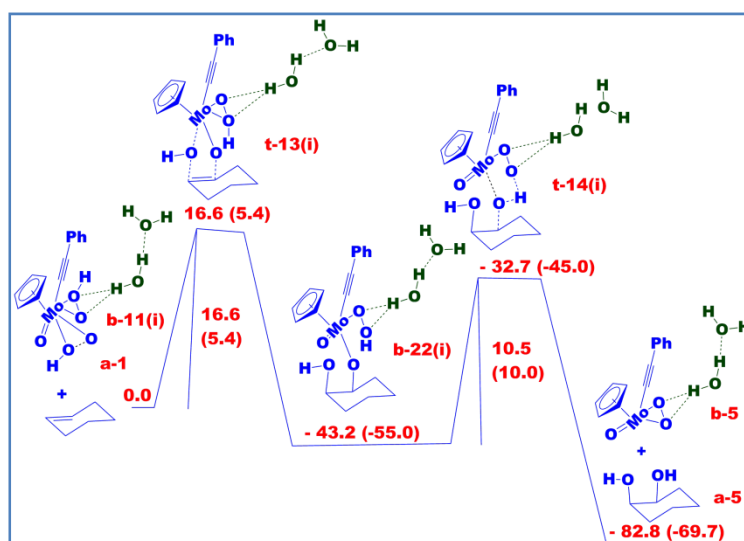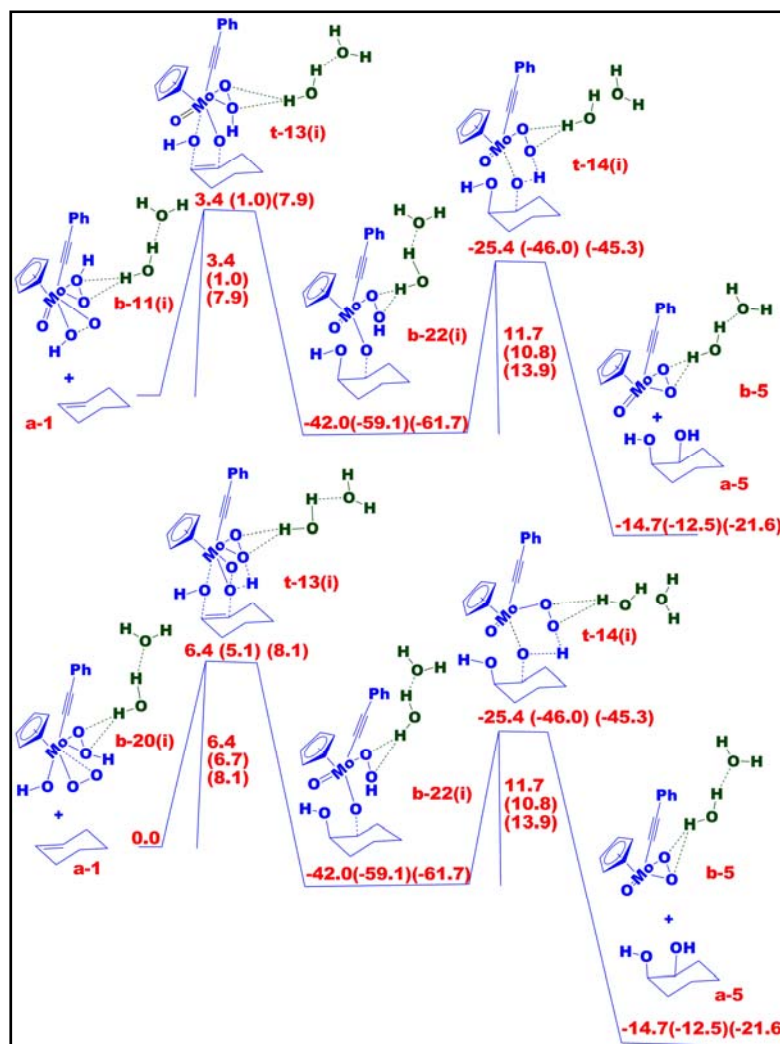
Fig. 4.22: The potential energy surface for the formation of the *cis-1,*2-diol from the reaction of cyclohexene with (**b-11**) and (**b-20)-** conformers of the intermediate of the reaction of hydrogen peroxide with the acetylide coordinated molybdenum catalyst; the values shown in the Fig are the electronic energies calculated using the BP-86, PBE and B3LYP functionals respectively – the BP-86 values are shown outside the parenthesis, while the PBE and the B3LYP energies are shown (in that order), inside the parenthesis
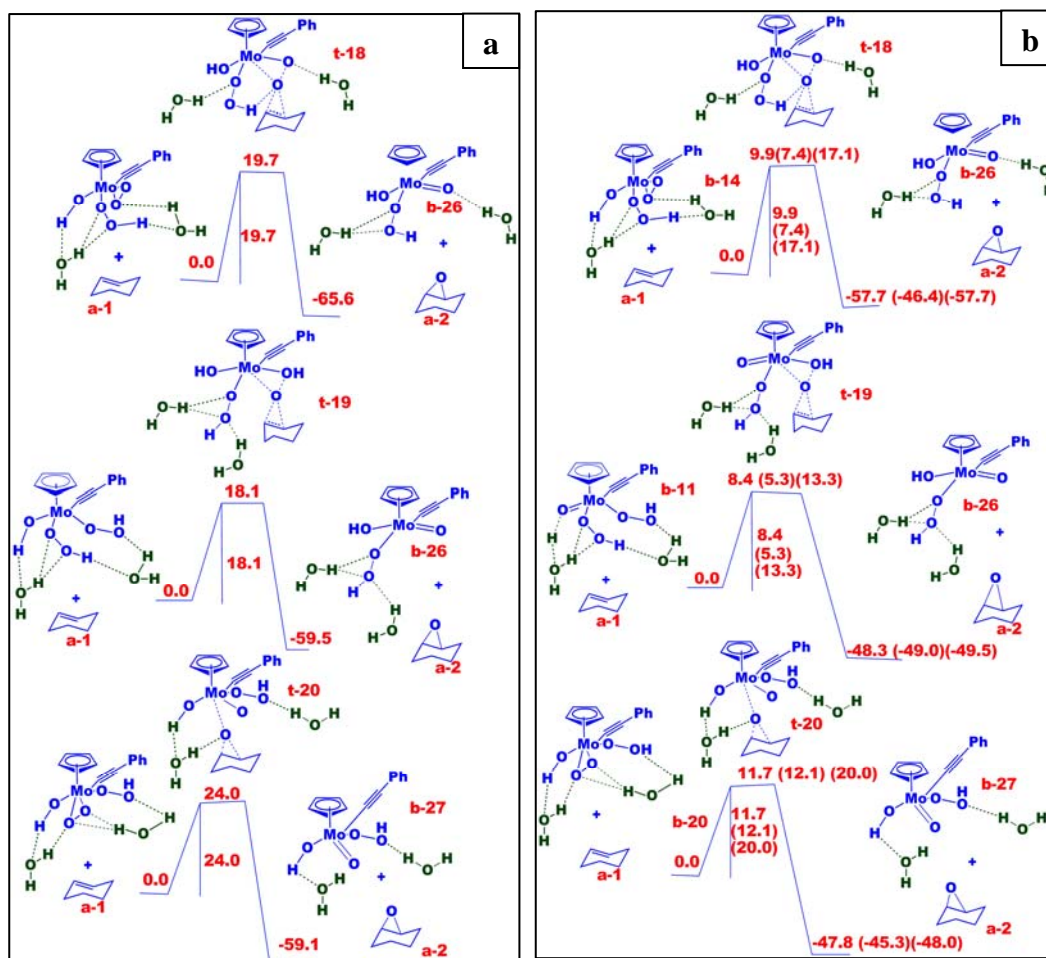
Fig.4.23: (a) The potential energy surface for the formation of the cyclohexene epoxidation with (**b-14, b-11** and **b-20-** three conformers of the intermediate of the reaction of hydrogen peroxide with the acetylide coordinated molybdenum catalyst; all energies, Δ G values G (solvent corrected), in kcal/mol; **(b)** the values shown in the Fig are the electronic energies calculated using the BP-86, PBE and B3LYP functionals respectively – the BP-86 values are shown outside the parenthesis, while the PBE and the B3LYP energies are shown (in that order), inside the parenthesis
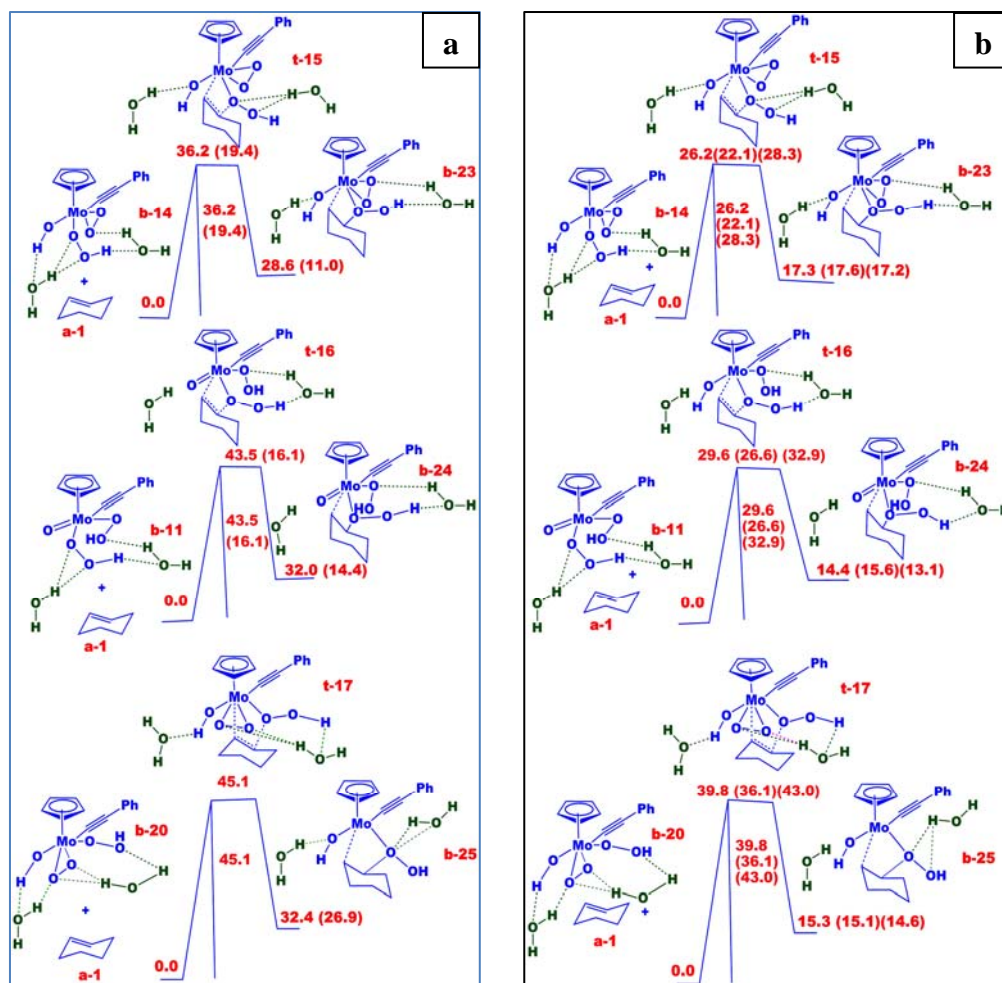
Fig. 4.24: (a) Potential energy surface for the Calhorda mechanism for epoxide formation for **b-14**, **b-11** and **b-20**; energy values outside the parentheses are ΔG values; values inside the parentheses are the correspond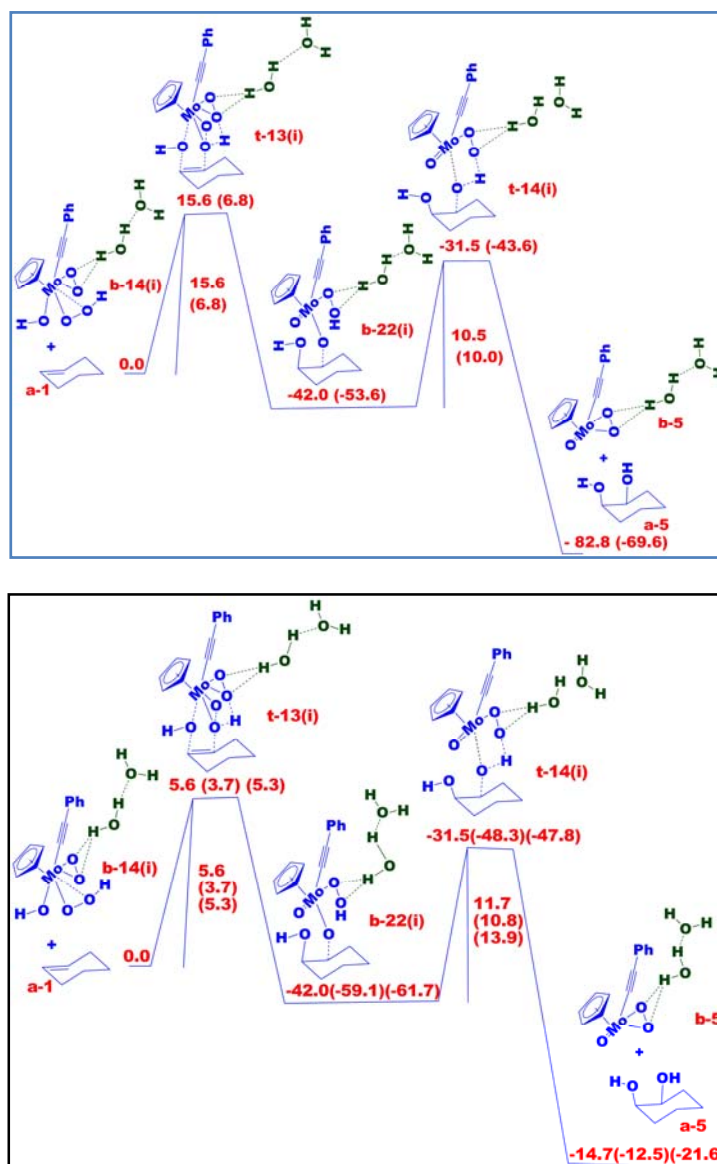ing ΔH values; all values are in kcal/mol; (b) the values shown in the Fig are the electronic energies calculated using the BP-86, PBE and B3LYP functionals respectively – the BP-86 values are shown outside the parenthesis, while the PBE and the B3LYP energies are shown (in that order), inside the parenthesis.

4.2.3. Summation of the Mechanistic Studies

The calculations discussed in the preceding sections show the complete reaction cycle for the formation of the epoxide in the case of the molybdenum catalyst CpMo(O)(OO)-C≡CPh when organic TBHP is employed as the oxidant, as well as the formation of the *cis*-1, 2-diol when aqueous H_2O_2 is used as the oxidant. Fig. 4.25 encapsulates the essential features of the two different catalytic cycles. As Fig. 4.25 indicates, the principal difference between the two cycles lies in the sequence in which the two species: cyclohexene and the oxidant (TBHP or H_2O_2), approach the molybdenum catalyst centre. For the case where the oxidant is TBHP, the preferred

order is cyclohexene followed by the TBHP species, whereas for the case where the oxidant is H_2O_2, the preferred order is H_2O_2 followed by cyclohexene. This difference in the order in which the substrates attack the catalyst centre determines the difference in the selectivity in the two cases.
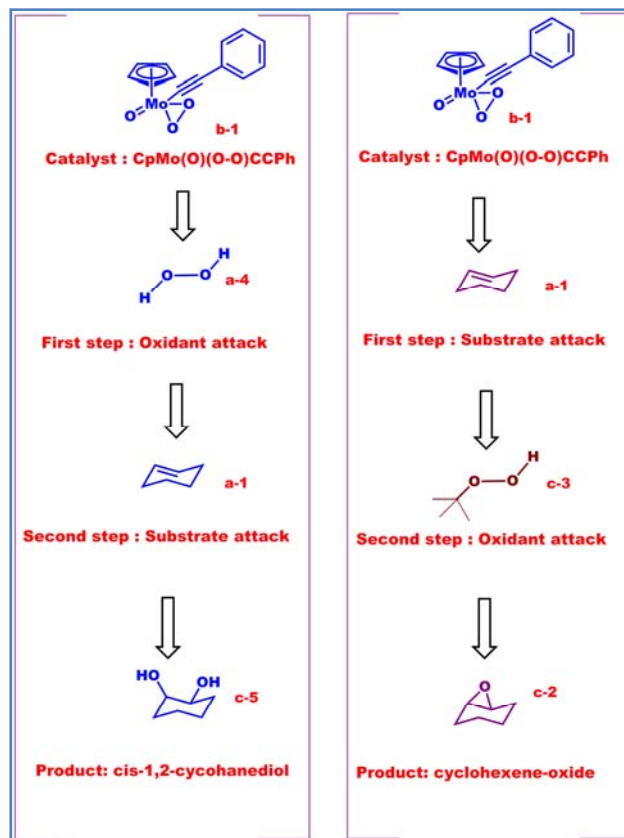
Fig.4.25: The trend in reactivity for the competitive reactions between the catalyst and the other species present in the solution: when TBHP is the oxidant, cyclohexene is seen to approach first followed by the TBHP molecule, but when H_2O_2 is used as the oxidant, the order of approach is reversed.

4.5. Computational Details

The computational procedure adopted is as follows: all the structures reported in the present work have been optimized using density functional theory (DFT) with the TURBOMOLE suite of programs, using TURBOMOLE Version 6.0.[43] The geometry optimizations were performed using the BP-86 functional.[44] The electronic configuration of the atoms was described by a triple-zeta basis set augmented by a polarization function (TURBOMOLE basis set TZVP).[45] Since it is possible that the geometry optimization procedure with DFT may be sensitive to the nature of the functional, a further test has been done to ensure the reliability of the obtained geometry optimized structures: all the structures were also optimized with the

Perdew, Burke, and Erzenhof density functional (PBE)[46], as well as with the B3LYP functional[47-48] and the TZVP basis set. The resolution of identity (RI), [49] along with the multipole accelerated resolution of identity (marij)[50] approximations were employed for an accurate and efficient treatment of the electronic Coulomb term for both of the sets of the density functional calculations. A comparison was then done between the corresponding structures obtained with the BP-86 and the PBE and B3LYP functionals. The comparison showed very little difference in bond lengths, angles and dihedral values between the corresponding structures for all the cases. A further corroboration of the smallness of the difference between the structures obtained from the two functional came from the comparison of the potential energy surfaces for the different reactions discussed in the present chapter. The ΔE values for the insertion and termination barriers for the oligomerization mechanism, obtained from the three separate set of calculations, were compared and the results indicate that there is only slight difference between the corresponding values for almost all the cases for the energies obtained with the BP-86 and the PBE functionals. The energies obtained from the B3LYP functional was found to be different by 8-10 kcal/mol from the corresponding BP-86 and PBE values, but the trends discussed in the chapter with regard to the preference for the Sharpless and the Thiels' Mechanism were found to remain unchanged for the set of calculations with the B3LYP functional. This suggests that changing the functional may result in a change of the absolute values of the barriers in the different mechanisms, but also that the essential conclusions reached in the present chapter will remain unchanged. With regard to the transition states obtained from the three sets of calculations, care was taken to ensure that the obtained transition state structures possessed only one imaginary frequency corresponding to the correct normal mode.

The contributions of internal energy and entropy were further obtained from frequency calculations done on the DFT structures at 298.15 K: thus, the energies reported in the Figs of the paper are the ΔG values. In order to account for the fact that all the species are in solution, the translational entropy term in all the calculated structures was corrected through a free volume correction introduced by Mammen *et al.*[51] and the was used for all the atoms. Solvent effects were incorporated using the COSMO model, [52] with *tert*-butanol ($\varepsilon = 12.4$) as the solvent for the cases with H_2O_2

as the oxidant, and 1,2-dichloroethane (ε = 10.4) as the solvent for the cases with TBHP as the oxidant.

It is pertinent to note that the different conformational possibilities have been considered for the structures reported for the different reactants, intermediates and products in the paper. The structures that have been reported and employed for evaluating the free energies and enthalpies for the different reactions were the ones that were the most stable conformers. It is possible that a very exhaustive conformational search, using search algorithms looking at hundreds or thousands of conformations could have been employed in order to locate unequivocally the lowest energy conformer – the "global minima" in each case, but such an approach is currently beyond the scope of full quantum chemical methods. It is also to be noted that the difference in energy between competing pathways is sometimes quite small – about 2.0 kcal/mol in some cases – but, given (a) that the relative difference is obtained at the same level of theory in these cases and (b) that the calculations have been done with three separate functionals, and have yielded the same conclusions in each case, it is believed that the results obtained, even for cases where the competing mechanisms have small barrier differences, are reliable.

4.6. Conclusion

It has been experimentally observed that the olefin oxidation using molybdenum peroxo acetylide with TBHP in decane and 50% H_2O_2 as the oxidant can lead to different oxidation products. For cyclohexene oxidation, when TBHP in decane was used as the oxidant, the epoxide was formed as the major product and when 50% H_2O_2 was used as the oxidant, the *cis*-1, 2-diol is formed as the major product. This indicates that there are competing mechanisms at work during the catalytic oxidation process in these systems. Calculations, using density functional theory (DFT), have been done in order to elucidate the nature of these competing mechanisms, with a new mechanism being proposed to explain the formation of the *cis*-1, 2-diol when aqueous H_2O_2 is used as the oxidant. DFT studies have shown that the order in which the two substrates, the olefin and the oxidant, attack the molybdenum centre is crucial in determining the eventual final oxidation product formed. For the case when TBHP in decane was used as oxidant, it was found that the preferred order of attack is that of cyclohexene followed by TBHP, leading to the preference for the epoxide product in this case. In contrast, for 50 % H_2O_2, it is seen that the preferred order of attack was

that of H_2O_2 followed by cyclohexene, leading to the preference for the *cis*-1, 2-diol product for this particular case. What is of crucial importance in determining the selectivity of the catalyst with the different oxidants is the hydrogen bonding that is seen to occur at the catalyst site between the water or oxidant molecules with the oxygen atoms of the catalyst.

The calculations thus provide insight into the nature of the olefin oxidation processes happening at the catalytic centre, and can act as a guide for the choice of oxidant necessary to obtain desired product with significant selectivity for olefin oxidation.

4.7. References

[1]   G. Sienel, R. Rieth, K. T. Rowbottom, Wiley-VCH, Weinheim, **1999**.

[2]   K. Bauer, D. Garbe, H. Surburg, *Common fragrance and flavor materials*, Wiley Online Library, **1985**.

[3]   K. Kamata, K. Yonehara, Y. Sumida, K. Yamaguchi, S. Hikichi, N. Mizuno, *Science* **2003**, *300*, 964.

[4]   X. Zuwei, Z. Ning, S. Yu, L. Kunlan, *Science* **2001**, *292*, 1139.

[5]   B. Van Duuren, B. Goldschmidt, *J. Med. Chem.* **1966**, *9*, 77-79.

[6]   A. Y. H. Lu, G. T. Miwa, *Annu. Rev. Pharmacol. Toxicol.* **1980**, *20*, 513-531.

[7]   A. W. Wood, R. L. Chang, W. Levin, R. E. Lehr, M. Schaefer-Ridder, J. M. Karle, D. M. Jerina, A. H. Conney, *Proc. Natl. Acad. Sci. U.S.A.* **1977**, *74*, 2746.

[8]   J. Schwesinger, T. Bauer, *Stereoselective Synthesis* **1995**, *21*, 4599.

[9]   B. S. Lane, K. Burgess, *Chem. Rev.* **2003**, *103*, 2457-2474.

[10]   W. Nam, R. Ho, J. S. Valentine, *J. Am. Chem. Soc.* **1991**, *113*, 7052-7054.

[11]   Y. Naruta, F. Tani, N. Ishihara, K. Maruyama, *J. Am. Chem. Soc.* **1991**, *113*, 6865-6872.

[12]   J. F. Hull, D. Balcells, E. L. O. Sauer, C. Raynaud, G. W. Brudvig, R. H. Crabtree, O. Eisenstein, *J. Am. Chem. Soc.* **2010**, *132*, 7605-7616.

[13]   D. E. De Vos, J. L. Meinershagen, T. Bein, *Angew. Chem. Int. Ed.* **1996**, *35*, 2211-2213.

[14]   A. Raith, P. Altmann, M. Cokoja, W. A. Herrmann, F. E. Kühn, *Coord. Chem. Rev.* **2010**, *254*, 608-634.

[15]   M. Herbert, E. Álvarez, D. J. Cole-Hamilton, F. Montilla, A. Galindo, *Chem. Commun.* **2010**, *46*, 5933-5935.

[16]   D. V. Deubel, G. Frenking, P. Gisdakis, W. A. Herrmann, N. Rösch, J. Sundermeyer, *Acc. Chem. Res.* **2004**, *37*, 645-652.

[17]   H. Mimoun, I. Seree de Roch, L. Sajus, *Tetrahedron* **1970**, *26*, 37-50.

[18]   K. Sharpless, J. Townsend, D. Williams, *J. Am. Chem. Soc.* **1972**, *94*, 295-296.

[19]   C. Di Valentin, P. Gisdakis, I. V. Yudanov, N. Rösch, *J. Org. Chem.* **2000**, *65*, 2996-3004.

[20]   I. V. Yudanov, C. Di Valentin, P. Gisdakis, N. Rosch, *J. Mol. Catal. A: Chem.* **2000**, *158*, 189-197.

[21]   D. V. Deubel, J. Sundermeyer, G. Frenking, *J. Am. Chem. Soc.* **2000**, *122*, 10101-10108.

[22]   D. V. Deubel, J. Sundermeyer, G. Frenking, *Inorg. Chem.* **2000**, *39*, 2314-2320.

[23]   A. Comas-Vives, A. Lledós, R. Poli, *Chem. Eur. J.* **2010**, *16*, 2147-2158.

[24]   D. V. Deubel, *J. Phys. Chem. A* **2001**, *105*, 4765-4772.

[25]   D. V. Deubel, J. Sundermeyer, G. Frenking, *Eur. J. Inorg. Chem.* **2001**, *2001*, 1819-1827.

[26]   D. V. Deubel, J. Sundermeyer, G. Frenking, *Org. Lett.* **2001**, *3*, 329-332.

[27]   M. Bühl, R. Schurhammer, P. Imhof, *J. Am. Chem. Soc.* **2004**, *126*, 3310-3320.

[28]   P. Gisdakis, I. V. Yudanov, N. Rösch, *Inorg. Chem.* **2001**, *40*, 3755-3765.

[29]   L. Salles, J. Y. Piquemal, R. Thouvenot, C. Minot, J. M. Brégeault, *J. Mol. Catal. A: Chem.* **1997**, *117*, 375-387.

[30]   D. Chakraborty, M. Bhattacharjee, R. Krätzner, R. Siefken, H. W. Roesky, I. Usón, H. G. Schmidt, *Organometallics* **1999**, *18*, 106-108.

[31]   aW. R. Thiels', T. Priermeier, *Angew. Chem. Int. Ed.* **1995**, *34*, 1737-1738; bW. R. Thiels', J. Eppinger, *Chem. Eur. J.* **1997**, *3*, 696-705.

[32]   W. R. Thiels', *J. Mol. Catal. A: Chem.* **1997**, *117*, 449-454.

[33]   P. J. Costa, M. J. Calhorda, F. E. Ku hn, *Organometallics* **2009**, *29*, 303-311.

[34]   A. V. Biradar, B. R. Sathe, S. B. Umbarkar, M. K. Dongare, *J. Mol. Catal. A: Chem.* **2008**, *285*, 111-119.

[35]   C. Bolm, J. P. Hildebrand, K. Muñiz, N. Hermanns, *Angew. Chem. Int. Ed.* **2001**, *40*, 3284-3308.

[36]   H. C. Kolb, M. S. VanNieuwenhze, K. B. Sharpless, *Chem. Rev.* **1994**, *94*, 2483-2547.

[37]   M. Schroeder, *Chem. Rev.* **1980**, *80*, 187-213.

[38]   J. Albert, A. Hamilton, John Wiley & Sons, New York, **1995**.

[39]   C. Dinoi, M. Ciclosi, E. Manoury, L. Maron, L. Perrin, R. Poli, *Chem. Eur. J.* **2010**, *16*, 9572-9584.

[40]   M. Bruce, M. Humphrey, J. Matisons, S. Roy, A. Swincer, *Aust. J. Chem.* **1984**, *37*, 1955-1961.

[41]   a) T. Fujihara, K. Hoshiba, Y. Sasaki, T. Imamura, *Bull. Chem. Soc. Jpn.* **2000**, *73*, 383-390; b) C. Bianchi, F. Porta, *Vacuum* **1996**, *47*, 179-182.

[42]   A. M. Al-Ajlouni, D. Veljanovski, A. Capapé, J. Zhao, E. Herdtweck, M. J. Calhorda, F. E. Ku hn, *Organometallics* **2008**, *28*, 639-645.

[43]   R. Ahlrichs, M. Bar, M. Haser, H. Horn, C. Kolmel, *Chem. Phys. Lett.* **1989**, *162*, 165-169.

[44]   a) A. D. Becke, *Phys. Rev. A Gen. Phys.* **1988**, *38*, 3098-3100; b) J. P. Perdew, *Phys. Rev. B* **1986**, *33*, 8822-8824.

[45]   a) F. Weigend, *Phys. Chem. Chem. Phys.* **2002**, *4*, 4285-4291; b) F. Weigend, R. Ahlrichs, *Phys. Chem. Chem. Phys.* **2005**, *7*, 3297-3305; c) A. Schaefer, H. Horn, R. Ahlrichs, *J. Chem. Phys.* **1992**, *97*, 2571-2577; d) A. Schaefer, C. Huber, R. Ahlrichs, *J. Chem. Phys.* **1994**, *100*, 5829-5835.

[46]   J. P. Perdew, K. Burke, M. Ernzerhof, *Phys. Rev. Lett.* **1996**, *77*, 3865-3868.

[47]   A. D. Becke, *J. Chem. Phys.* **1993**, *98*, 5648.

[48]   P. Stephens, F. Devlin, C. Chabalowski, M. J. Frisch, *J. Phys. Chem.* **1994**, *98*, 11623-11627.

[49]   K. Eichkorn, O. Treutler, H. Oehm, M. Haeser, R. Ahlrichs, *Chem. Phys. Lett.* **1995**, *240*, 283-290.

[50]   M. Sierka, A. Hogekamp, R. Ahlrichs, *J. Chem. Phys.* **2003**, *118*, 9136-9148.

[51]   M. Mammen, E. I. Shakhnovich, G. M. Whitesides, *J. Org. Chem.* **1998**, *63*, 3168-3175.

[52] A. Klamt, Andreas, *J. Phys. Chem.* **1995**, 99, 2224 –2235.

5

Summary, Conclusions and Future Plans

This chapter brings out the overall summary and highlights the major outcomes of the research work done. This chapter also describes the scope for the future potential developments in this field.

The present studies have proven the potential of molybdena catalyst both homogeneous as well as heterogeneous as expedient in olefin oxidation reactions. Supported molybdena catalysts (heterogeneous) were found to be selective for epoxidation and were recycled successfully without leaching from catalyst surface. Reverse micelle micro-emulsion proved to be efficient method for the synthesis of ultrasmall molybdenum oxide nanoparticles with definite structure and uniform distribution over the SiO_2, TiO_2 and ZrO_2 nanosphers. These MoO_3 nanoparticles were found to be excellent olefin epoxidation catalysts and gave exclusive epoxide products

Alternatively, molybdenum supported on silica microspheres was synthesized by HC and IHC methods. SEM images showed the silica microspheres were of uniform shapes and size and EDAX analysis showed that the Mo content was lower as compared to added metal. The prepared catalysts showed excellent activity for olefin epoxidation. Molybdenum silica synthesized by hydrolysis-condensation (HC) method was more effective as compared to molybdenum silica synthesized by impregnation-hydrolysis-condensation (IHC) method for cyclohexene oxidation in terms of catalytic activity as well as selectivity for epoxide.

Finally, detailed mechanistic investigation of olefin oxidation was done using homogeneous molybdenum based catalysts. The olefin oxidation using molybdenum peroxo acetylide with TBHP in decane or 50% H_2O_2 as the oxidant led to different oxidation products. When TBHP in decane was used as the oxidant, the epoxide was formed as the major product and when 50% H_2O_2 was used as the oxidant, the *cis*-1, 2-diol is formed as the major product. This indicated that there are competing mechanisms at work during the catalytic oxidation process in these systems. Calculations, using density functional theory (DFT) were done in order to elucidate the nature of these competing mechanisms, with a new mechanism being proposed to explain the formation of the *cis*-1, 2-diol when aqueous H_2O_2 is used as the oxidant. DFT studies have shown that the order in which the two substrates, the olefin and the oxidant, attack the molybdenum centre is crucial in determining the eventual final oxidation product formed. For the case when TBHP in decane was used as oxidant, it was found that the preferred order of attack is that of cyclohexene followed by TBHP, leading to the preference for the epoxide product in this case. In contrast, for 50% H_2O_2, the preferred order of attack was that of H_2O_2 followed by cyclohexene, leading to the preference for the *cis*-1, 2-diol as major product for this particular case. What is

of crucial importance in determining the selectivity of the catalyst with the different oxidants is the hydrogen bonding that is seen to occur at the catalyst site between the water or oxidant molecules with the oxygen atoms of the catalyst. The calculations thus provide insight into the nature of the olefin oxidation processes happening at the catalytic centre, and can act as a guide for the choice of oxidant necessary to obtain desired product with significant selectivity for olefin oxidation. Overall the present thesis work focuses on effect of various structural environments on molybdenum based catalysis. The major outcome of the present thesis work is discussed below.

Present study for catalytic applications molybdenum peroxo under various environments in oxidation reaction can help in the future to design a catalyst that is, both homogeneous as well as heterogeneous, and analyze its reaction mechanism with the help of DFT calculation. Transition metals such as molybdenum, vanadium, copper, zinc, nickel, cobalt, tungsten, etc. on inorganic materials such as silica, zirconia, titania, alumina, ceria meso, micro or nanoparticles can be utilized in catalytic reactions such as oxidation, epoxidation, esterification, hydroamination, olefin metathesis, oxidative coupling reactions, condensation reactions etc. Numerous such synthetic methods such as colloidal and reverse micelle method, sol-gel solid growth method, atomic layer deposition (ALD) method, making of dumb-bell, core@shell, yolk@shell, related nanoarchitectures, and silylation and other surface derivatization, tethering, and immobilization can be used for synthesizing novel catalytic material.

Not only heterogeneous, homogeneous transition metal complexes in various structural environments for example Os, Fe, Mo, Re, V, W, Co Ni, Co and Cu, Rh, Pd, Pt, Ir etc. can be efficiently used in oxidation, hydrogenation, oxidative coupling reactions, hydroamination, C-H activation etc. These transition metal when surrounded by appropriate ligands environment enhance the activity, selectivity i.e., chemo-selctivity, regio-selectivity and sterio-selectivity The role of theory and computation has changed dramatically as computers, software, and algorithms have enhanced the understanding of known systems, providing both qualitative and quantitative insights into experimental measurements and guiding the selection of experimental systems that are most worthy of study or enabling the design of new systems. Computational calculations help us to predict the transition state involved in the given catalytic reaction which was impossible to study with the help of currently available experimental tool and techniques. Theoretical predictions also help us to

designing the ligand for a given chemical reaction for better chemo-, regio- and sterio-selectivity. To conclude, computational calculations will aid our research and help us to explain our experimental observations.

List of Publications and Patents

[1] Mechanistic Studies on the Roles of the Oxidant and Hydrogen Bonding in Determining the Selectivity in Alkene Oxidation in the Presence of Molybdenum Catalysts.

P. Chandra, S. L. Pandhare, S. B. Umbarkar, M. K. Dongare, K. Vanka, *Chem. Eur. J.* **2013**, *19*, 2030-2040.

[2] Synthesis, Characterization and Catalytic Activity of Molybdenum S-Propargyl and S-Allyl Mercaptobenzothiazole Carbonyl Complexes. (Submitted to *Organometallics*)

Rajesh R. Jadhao, **P. Chandra**, Swati L. Pandhare, Sumeet Kale, Anjali P. Likhite, Shailaja P. Maybhate, Pranaya V. Joshi, Vedavati G. Puranik, Mohan K. Dongare, and Kumar Vanka*, Shubhangi B. Umbarkar*

[3] Synthesis and Catalytic Activity of Molybdenum oxide Supported on Silica Microspheres

P. Chandra,[a] Shubhangi B. Umbarkar,[a] and Ankush V. Biradar[a*]

[4] One Pot Synthesis of MoO₃ Nanoparticles Supported on Metal Oxides Nanospher : An Efficient Epoxidation Catalyst (Submitted to *J. Mater. Chem. A*)

P. Chandra,[a] Ankush V. Biradar [a*], Mohan K Dongare,[a*] and Shubhangi B. Umbarkar [a*]

[5] Managing High Densicity Hydroxyl Groups onto Self Assembled Silica Microsphres and Their Use in effiecient Oxygen Trasfer Olefin Epoxidation Reaction (Under prepration)

P. Chandra and Ankush V. Biradar*

Patents

[1] Corrugated silica nanosphers for metal free epoxidation of olefins and process thereof

Dr. Ankush V. Biradar, Dr. Shubhangi B. Umbarkar, **P. Chandra**, Dr. Mohan K. Dongare (Disclosure number **INV-2013-12**)

Poster and Oral Presentations

[1]   Oral presentation in the University of Lille, France on the topic "*Mechanistic Studies on the Roles of the Oxidant and Hydrogen Bonding in Determining the Selectivity in Alkene Oxidation*" in the Presence of Molybdenum Catalysts.

[2]   Poster presentation in 16th National workshop on Catalysis for sustainable development on the topic "*Synthesis, characterization and catalytic activity of molybdenum S-propargyl and S-allyl mercaptobenzothiazole carbonyl complexes*"

[3]   Poster presentation in National science day in NCL-Pune on the topic "*Synthesis, characterization and catalytic activity of molybdenum S-propargyl and S-allyl mercaptobenzothiazole carbonyl complexes*"